Scuola Normale Superiore di Pisa

CLASSE DI SCIENZE

CORSO DI PERFEZIONAMENTO IN CHIMICA

Interpretation and prediction of optical properties of medium-to-large systems by computational approaches

Relatore:
Prof. Vincenzo Barone

Correlatore:
Dott.ssa Malgorzata Biczysko

Tesi di Perfezionamento di:
Luciano Carta

Anno Accademico 2012/2013

A mamma e babbo

A madrina e padrino

CONTENTS

PREFACE

In recent years computational chemistry has became a valuable and useful tool that can be employed to study molecular properties. The contemporary widespread diffusion of computational chemistry as a support tool in many areas of molecular sciences is a direct consequence of the latest growth of computational power along with the parallel improvement of theoretical models. In fact, most of this progresses were achieved in the last decade. In this Ph.D. thesis the recently developed computational models are applied to the interpretation and the prediction of properties of selected dye molecules that are of a direct technological interest. First of all we focus on the analysis and interpretation of experimental resuls, when discussing optical properties of coumarin dyes in solution and in biological environment and of Alizarin and Alizarin-Mg/Al-complexes. Coumarins are known to be effective as polarity-dependent fluorescent probes for live high-resolution cell imaging applications and can be considered as a potentially promising photoactivatable linkers. In this thesis the study has been focused on a dual fluorescence spectra of some coumarins observed in solution, which can be considered as an effect of the photoreaction or the transition from two excited electronic states. The possibility of photoreaction is of outmost importance for the nanodiagnosis suggesting that therapeutic and diagnostic agents can be linked to the coumarin and released upon irradiation, with the concomitant fluorescent signal marking therapeutic action. In order to extend study

toward biological environments the interaction between the coumarins and some proteins of biological relevance have been investigated showing that environment introduce sensible modifications of some important properties of the coumarin core such as geometrical parameters and the maximum absoption wavelegth in the UV-VIS spectra. Alizarin dye is a constituent of the Madder Lake, a pigment commonly used by artist in the past centuries; our computational study on Alizarin has pointed out how the changes in the external conditions (that is pH, metal coordination etc...) are related to the modifications in the madder lake electronic spectra, and in turn its colour. In reality, artworks are affected over the years by the environmental changes which are responsible for the ageing and the subsequent modulations of the paint colour in the old madder lake pigments. Computational investigations have permitted to dissect the role of each of this factors in tuning optical properties.

In a second part of this the same computational tools used for coumarin and Alizarin investigations have been applied to predict the molecular properties of a series of dyes molecules, possible candidate components of a smart material; computational screening have been applied in order to select the best one target with the desired properties (i.e. large Stokes Shift, emission in the visible range, etc...). The cost-effective combination of several computational models has permitted us to finally set up a computational procedure that opens the way to the construction of a mechanoresponsive material with the desired properties; the application of the computational screening has been very beneficial since the selection of the best final target based solely on the chemical intuition is rather cumbersome. From a general point of view in the test cases selected for this Ph.D thesis have been chosen in order to highlight the capabilities and advantages of contemporary computational chemistry and recently developed theoretical models for the interpretation and prediction of spectroscopic properties of medium-to-large molecular systems of direct biological, technological or cultural heritage interest.

Part I

Introduction, state-of-the-art and operative protocols

CHAPTER 1

INTRODUCTION AND STATE-OF-THE-ART

The determination and the understanding of structure and properties of already known or a new chemical compounds, and also of the knowledge of the behaviour of large and flexible molecules in solution, or embedded in different type of environments, is now one of the central challenge in the chemical sciences. These studies are nowadays encouraged by the number of important applications that may derive in many technological fields, making the applied chemistry and the chemical engineering a very important tools for both comprehension of molecular phenomena and also, most important, in the design of new types of materials for new tailored applications (1; 2; 3; 4; 5; 6; 7; 8). For instance, the study of the interaction of a drug with its receptor and the discovery of a new ones or delivery pathways in medicinal chemistry (2; 4; 5), the design of new chemical products (1; 6; 7; 8; 9) and also the understanding of the composition of chemical abundances as a function of environment in interstellar medium(10; 11; 12) as well as the application of chemistry to investigate in cultural heritage (13; 14; 15) are only a few examples. In the last decades various kinds of instrumental techniques have been used for the analysis

and the description of the structural and dynamical properties of molecular systems that are embedded in complex environment such liquid and/or solid solvents and/or polymeric matrices. In this respect all the spectroscopic techniques, such as electronic (UV-vis) spectroscopies (16; 17; 18; 19; 20; 21; 22; 23; 24) , vibrational (IR,Raman, VCD) spectroscopies (24; 25; 26; 27; 28; 29; 30; 31), and Nuclear Magnetic Resonance (NMR) (32; 33) or Electron Spin Resonance (ESR)(34; 35; 36), are now considered a valuable and very powerful tools for the understanding of the properties of all kinds of molecular systems. Generally speaking, the point of force of spectroscopy is that it provide very detailed informations about the intimate molecular mechanisms that occurs on a microscopical level and are responsible of the final observed properties of a molecular system. Spectroscopic techniques are the most powerful tool widely applied to the studies which require non-destructive analysis of complex sample (eg. medicine, heritage, technology etc) leading to better understanding of matter morphology, properties and underlying processes. Furthermore, spectroscopical analysis of the sample of already known composition provides detailed information about its molecular function and structural parameters. This studies opens the way to a wealth of exciting opportunities, since they may lead to the engineering of new types of compounds for emerging applications. The possibility of exploiting the characteristics of supramolecular architectures in order to design and synthesize novel class of materials with, for example specific properties, has recently attracted a lot of attention in view of their numerous technological applications in material engineering (7; 8) and in bio-technological field (2; 6), making spectroscopy one of the most important investigating tools. It is the reason why modern laboratories (non only chemical ones) are often well equipped with different spectrophotometers, used not only for the analytical chemistry purposes but also for more complex studies. However, the interpretation of the rich information that can be inferred from an instrumental analysis makes the corresponding collected data (usually known as *spectra*) seldom straightforward to interpret due to the concomitant interplay of different factors as thermal or environmental effects, intrinsic properties of studied systems (e.g. vibrational effects) followed by further complications related to the presence of noise signals, instrumental errors etc., acting together at different

length and time scales on the sample. If all this factors affects the samples under investigation at the same time, the correct interpretation of spectrophotometric signals can be a very difficult task. For example when analyzing a powder of a dye coming from an artwork, the inherent complexity of the materials employed, the low quantity needed for micro-invasive analysis, together with the often unknown qualitative composition of the samples makes the pure experimental spectroscopical analysis a very difficult task, because the specific role of each effect is not so easy to separate and evaluate properly. The in general low-invasivity and low-distructivity of spectroscopy with respect to the other instrumental techniques is another important advantage not only in cultural heritage field but also when analyzing powder coming from nanomaterials or medicine and in general when a low quantity of materials is available and/or when we cannot reconstruct the sample after an analysis, this fact has been crucial for example in microspectroscopy, such as micro-raman spectroscopy (37) a low-invasive analysis that uses only a small quantity of samples. Additional complications arises when the observed spectroscopic signal emerges from structural/conformational fluctuations of a large molecule (e.g. a protein) or when many co-existing equilibrium structures are present, at the same time, under the same experimental conditions (e.g. keto-enol or amino-imino tautomerism). This complications add further difficulty to proper interpretation the corresponding registered spectra in terms of structural features and the assignment of a specific structure to a specific absorption peak at a given frequency and wavelength making an analysis even more cumbersome and sometimes misleading. Part of these difficulties can be overcome with the aid of integrated computational approaches that can allow an in-depth comprehension and rationalization of the corresponding experimental data (38; 39; 40; 41; 42; 43; 44; 45; 46; 47; 48; 49). Then, computational studies are also faster, cheaper and pollution free in comparison to the experimental techniques, thus in silico screening of new molecular systems, performed prior to their synthesis directly impacts the progress in drug design, material science, nanotechnology etc... In the last years, state-of-the-art computational studies can provide simulated spectra (50; 51; 21; 35; 29; 28; 52), with an accuracy sufficient for a meaningful comparison with their experimental counterparts. This is the reason why computational

chemistry is rapidly evolving from a highly specialized research field into a versatile and fundamental tool for the interpretation of the experimetal observations in terms of basis chemical physical processes. Therefore, the availability of theoretical tools can be used for supporting and complementing experimental results, and renders the experimental analysis much easier to interpret. Today, thanks also to the growth of computational power together with the improvement of accuracy and the increasing number of reliable and powerful theoretical chemistry models, such types of computational simulations can be applied also for medium-to-large systems, that is, those of direct biological and/or technological interest (53; 41; 42; 43; 44; 17; 54; 55; 45; 46; 47; 48; 56; 50), permitting to complete and interpret many critical experimental data. But, as stated above, the potentiality of computational approaches can be not only interpretative but also can be predictive (57). For example the choice of the best candidate among a set of novel similar target molecules may results rather difficult, since the accurate prediction of the spectral features can become very cumbersome if solely based on the simple chemical intuition. In this framework, the availability of reliable and predictive computational methods can be very beneficial, since the results of an *in silico screening*, that is the calculation of the properties of a large number of molecules at the same time, can effectively guide a synthetical work toward the molecule with the desired final properties (58). This fact has obvious benefits, in terms of costs and time in a synthetical chemistry laboratory, since the number of compounds to effective synthesize, from the suggestions given from the computational outcomes taken from the screening, is limited to a smaller number of molecules. In this respect, computational spectroscopy is becoming a needful and versatile tool for the assignment and interpretation of experimental spectra but also for determining the structure of a target molecule starting from its desired final properties. In the last years the number of studies where such an integrated experimental-computational approach is applied to spectroscopical investigations, both for prediction and for interpretation of experimental data (55; 59; 60; 54; 61; 50; 62; 56; 63; 51; 64; 65; 66; 67; 68; 69), is growing very fast and it can be foreseen that will continue even faster in the next decades. It can be also predicted that the availability of reliable and user-friendly computational

tools combined with the continuous growth of processor performance and computational power that makes possible to describe larger and more complex molecular systems at a reasonable computational cost, will increase the use of such computational models in the next years, extending their applicability to many other fields such as technology, sensing, computing, medical areas, solid state physics and, in general, from organic chemistry to inorganic one. However, it can be immediately recognized that to apply theoretical modeling for a broad range of real life problems, further extension toward fully integrated, general and automatized tools are inevitable. Of particular importance is the development of user-friendly software packages which makes computational studies easy accessible also to non-specialist. Additionally the usefullness of any theoretical/computational approach is directly related to its ability to describe system and processes of size and complexity comparable to that studied by experiments with an accuracy close to the chemical one. In this respect the space- and time-scale of interest often span such a wide range that the availability of true multiscale approaches become crucial.

In the studies performed during my Ph.D. course and here presented, recently developed and implemented computational spectroscopy tools are exploited to investigate the optical properties of several organic dyes. The main focus of my works is the fully *ab-initio* simulation of the electronic UV-VIS spectra line-shapes as resulting from the underlying vibronic transitions (53; 60; 70). Such type of approach can allow a direct comparison with its experimental counterpart, and then, to make a detailed analysis of experimentally observed contributions.In a last part we exploit also the predictive role of computational chemistry, in fact, the availability of reliable computational methods was found very beneficial also in predicting the spectral behavior of a set of investigated class of chromophores, allowing in the final part of this thesis to select the best candidate among a rather large set of homologues, and to finally guide a real synthetic work (done in collaboration with Dipartimento di Chimica of the University of Pisa) toward a precursor of a polymeric material, with the desired final properties, that is a *smart* behavior. Before to present and discuss the results, a brief introduction of the state-of-the-art in computational chemistry is performed, whereas the computational outcomes are presented and discussed in the

chapters 3, 4 and 5.

1.1 Models in computational chemistry

If we want to employ computational chemistry as a predicting and interpreting tool, first of all, the models applied should be reliable and effective at the same time, in order to give us results that can be directly used for the interpretation of the corresponding experimental data. Since recently the main limitations to the evolution of such an approach was dual and, related both to the limited power of the computational instruments available in the last century with the contemporaneous limitations of theoretical models applicable to large systems. This two main limitations made the theoretical chemistry a branch reserved only for specialists and not diffuse as it is now, where, thanks to the growth of computational power and to the development of reliable computational methods has received much attention in the scientific community. Computational chemistry is now a very important tool in both interpreting the experimental results and also in predicting molecular properties of real systems departing from the molecular structure and/or the final desired properties. In the following of this section we describe very brief the computational models available, where in the second chapter we describe this models in a more detailed point of view, with special regards to the simulations of electronic spectra.
Among the models available (classical, semi-empirical, ab-initio etc) (71; 72; 73; 74; 75), the quantum-mechanical (QM) calculations are the methods of choice for computational spectroscopy as they can account for the matter-light interactions. Within QM, the choice of method and basis set is related to the balance between the desired accuracy and the cost of the simulation; generally the latter (i.e. the time to carry out the computation) is linked to the size of the system that we want to study. In this way, due to its favorable cost-to-performance ratio, the QM Kohn-Sham density-functional theory (KS-DFT) (76; 77) has become the most popular electronic structure theory for large scale ground state systems (78). Its extension for treating excited states systems, that is the time

dependent density functional theory (TD-DFT) (79; 80; 81), has also been developed to the stage where it is now, very widely used. The essential ingredient of KS-DFT is the exchange-correlation energy functional E_{xc}, that remains unknown and needs to be approximated in some way.

There are many modalities to approximate this energy which lead to the developments of several different density functionals. Generally, in DFT the hybrid functional B3LYP(82; 83) appears to be one of the most successful over the years if measured by the numbers of its applications. However despite it provides accurate results in most cases, in particular, for ground state structure and properties it is unsuccessful in a number of important applications such as the computation of polarizability of long chains, or excited state computations using TD-DFT for Rydberg states (84; 85; 86) and also for the charge transfer (CT) excitations (87; 88; 89). The reason for these failures is understood, at long-range the exchange potential behaves as -0.2r^{-1}, instead of the $-r^{-1}$. Part of these problems can be overcome by the use of the so called long-range-corrected (LC) functionals. These LC functionals (e.g. CAM-B3LYP (90), ω-B97X...) combines the hybrid qualities of B3LYP with the long-range correction of the potential yielding satisfactory results with a computational cost comparable with the standard hybrid functionals; however LC functionals have tended to be inferior to the best hybrids for some properties such as thermochemistry (91) or vibrational properties (92). Recently, re-optimization of a LC hybrid functional (93) to include empirical atom-atom dispersion yield to a functional, ω-B97X-D (94), that provides satisfactory accuracy also for termochemistry, kinetics, and non covalent interactions, yet still remain unsatisfactory for the vibrational properties. Regarding simulation of spectra the selection of the best method in terms of DFT functional and basis set is not easy and strongly depends on the problem under study, with larger differences related to the choice of functional than to the basis set. Generally TD-DFT studies with B3LYP, sometime (e.g. for CT transition) underestimate the transition energies, while its long-range corrected counterpart, CAM-B3LYP has been shown to provide improvements for the the description of Rydberg and charge transfer states (95), and recently it has been included (along with M06-2X and ω-B97XD) into the set of the eight best performing

density functionals (96) recommended for excited electronic state studies. In a recent work Jacquemin et al (97) reports a benchmark study of vibrationally-resolved-absoption UV-VIS spectra of a series of antraquinonic dyes, showing that the B3LYP and PBE0 functionals provide accurate positions in term of wavelength for the absorption peaks but are less efficient than CAM-B3LYP and ωB97XD (two range separated hybrids) in determining the shapes of the absorption bands, that is the relative intensities. Generally speaking the choice of the functional is still rather arbitrary, and there is not a systematic procedure to select *a priori* the best one for a specific study, in particular with reference to electronic spectra simulations over a large energy range. It might be recommended to always start from some benchmark test, and comparison with experiment or reference computations at the higher level of theory. Such strategy is followed within these Ph.D. thesis: a fast benchmark is performed in the first step in order to specify and to discuss the performance of the actually employed functional and basis set.

The works here presented have been devoted to studies of spectroscopic properties of dye systems in a solution, in the following we present briefly the models employed to simulate UV-VIS spectra and the solvent enviroment. From a general point of view, various approaches are now used to simulate electronic UV-Vis spectra. In the most simple approximation the resulting absorption and/or emission vertical electronic spectra described as energies and transition intensities (collected for example form a TD-DFT calculation) from one initial state (S_i) to a final state (S_f) can be simply convoluted with Gaussian or Lorentzian functions in order to obtain a broad convoluted band that can be compared with the corresponding experimental spectra line-shape. This approach can be useful, in particular if large number of electronic transitions need to be considered, but it stay in the frame of the so called *pure electronic* picture, that is, neglect the other factors (e.g. dynamic effects) that are manifested in a UV-Vis band, such as for example the vibronic structure, that may have a very important influence on the finally observed band-shape. The neglecting of the dynamical effects can have significant influence of the final theoretical results that can be unsatisfactory or in many cases incomplete. To overcome this limitation, methods to calculate the *vibrationally-resolved* electronic spectra have been

developed and implemented (See Ref. (70) and references therein). From a general point of view, starting from Franck-Condon principle they evaluate the intensities of the transition between two vibronic states by computing the so-called Franck-Condon overlaps (98; 99; 100) considering that the nuclear positions are mostly unaltered by the electron jump, which, considering this model, takes place during the electronic transition very rapidly. More details about the electronic spectra line-shape computations employed in this work will be presented in the second (2) chapter of this thesis and in the works by Barone, Bloino et al. (101; 102)

Another important factor is the description of the environment surrounding the system under study (e.g. liquid solvent or polymeric matrices) that can modify the structure and the observed properties. In order to take into account these effects, several theoretical models have been developed and implemented in widely available quantum chemical packages (e.g. GAUSSIAN). The cost-effective schemes are represented by the continuum models, taking into account non-specific solute-solvent interactions, where the solute, that is the molecular system under study, is placed in a cavity within the so called *solvent reaction field* (SCRF). Among these methods the Polarizable Continuum Model (PCM), initially devised by Tomasi et al (103), and its variations, where a solute cavity is created via a set of overlapping spheres are the most used SCRF approaches. In particular, here, in our calculation we have used the (Conductor-like) C-PCM model (104), a variant where the solvent is described as a conductor-like continuum environment. But, the continuum model sometime can not be sufficient to correct describe the whole surrounding of a system, in these cases explicit solvent molecules can be added to the solvation sphere of a system in those positions where the so called *specific* (e.g. hydrogen bonding, metal coordination etc) interactions can occur. The contemporary use of the specific solvent models and the PCM defines a mixed discreet-continuum scheme, which leads to more accurate results respect to the use of only explicit solvent model in vacuo, because the specific interaction are well described by the explicit molecules included in the system whereas the non-specific interaction (i.e. the electrostatic ones) are well described contemporarily by the continuum model.

1.2 Challenges and perspectives in computational chemistry

Many theoretical models have been developed so-far and can be used today in computational chemistry experiments. We can state that the predictive and interpretative power of computational chemistry has been clearly demonstrated nowadays for small and medium-sized systems; today one of the main challenge of the theoretical chemistry is related to the development and validation of the effective and yet reliable methods that are applicable also for larger molecular systems embedded in complex molecular environment (i.e. real systems); It is important also to stress that an effective use of most recent computational chemistry and computational spectroscopy techniques, also by non-experts, so the experimentally oriented scientists requires that the methodologies and the software packages employed in the laboratory must to be implemented within a easy-to-use interface; this is in general the actual trend of computational and theoretical chemistry, where a number of softwares permits nowadays to obtain information on structure, spectra or properties of the system studied, within a black-box procedure. The ease of use opens the computational chemistry towards new fields of application and at the same time extends the use of QM softwares also to the non-specialist community.

In the following, we present few examples of how theoretical models can be applied for simulation, analysis and prediction of spectroscopic properties of molecular systems of direct bio-technological interest. In this respect we can recall, as first example, two integrated computational approaches, which are expected to significantly reduce the synthetic and characterization time required for design of systems with pre-determined electronic and optical properties (105), or improvement of industrial synthesis reaction rates (106), respectively. In the first case pilot applications, allowed to account in the vibronic structure of electronic spectra(101; 107) which is particularly important as the electronic spectra band shape ultimately determines the colour perceived by the human eye. Apparently, computational studies have been able to reproduce quantitatively the difference in emitting colour between two Ir(III) cyclometallated complexes, highlighting the predictive

capability of applied integrated theoretical approach. In the latter case qualitative agreement between computed and observed overall rates of ammonia production on ruthenium catalysts has been achieved integrating various theoretical approaches applied to a range of relevant elementary reaction steps determined input for a complete macroscopic kinetic model. In the latter the most relevant elementary reaction steps, have been integrated to determine the industrial reactor yield. Above mentioned pilot applications witness success of first principle studies in modelling of real-world process of vital interest: design of novel optically active materials or improvements of industrial ammonia production, reaction which account more than 1% of the entire global energy consumption. Futhermore, spectroscopies, both optical and magnetic, are the non-invasive experimental techniques able to probe molecular systems at their real life environmental conditions for any static and dynamic properties of molecular systems. For such reason, spectroscopic techniques are the most powerful tools widely applied to in vivo studies, medicine, heritage, technology etc... leading to better understanding of matter morphology, properties of the underlying processes. Moreover, the level of detail of spectroscopic techniques can in principle offer reinforces their role in drug design or construction of new superior materials of relevant technological interest. For example in determining specific optical properties (108; 109; 110; 111) of nanomaterials or molecular devices, for the use in optical communication technology, sensing, computing, medical areas etc... (110; 112; 113; 114) which allows them to act as oscillators, amplifiers, frequency converters, modulators, switches and so on. Today, thanks to the development of theoretical models, computational spectroscopy can provide spectra in a completely independent way and the integration between computational and experimental spectroscopy can give us interesting results in both interpreting and predicting the optical properties of systems. Additionally, spectroscopy techniques can also play an active role, for example modern lasers are able to control characteristics of light at a level that approaches molecular lenght and time scales. Thus the carefully in silico designed optically responsive biomolecules can be used in various fields of application, for example to transfer optical control to molecular structure or function (115). In fact, it has been already shown how the optical signal can be trans-

ferrred into a mechanical work (116). The ingration of experimental and computational spectroscopic techniques can be very beneficial, impressive progress in material science has been inspired in the last few decades by the impelling need for new intelligent materials endowed with unique megnetic, electric, optical or mechanical properties that can be tuned and controlled by external stimuli such as light, heat, magnetic and/or electric field etc. for application in such diverse fields as aerospace, electronics, ceramics, packaging, drug delivery and targeting (117; 118; 119). The category of soft smart materials, which includes among others synthetic polymers, liposomes, nanoparticles, hydrogels photocatalysts, presents many instances of spectacular effects, e.g. DNA-programmed lipids (120), metal oxide nanoparticles displaying temperature-induced reversible size/shape changes (121); pH and temperature responsive hydrogels (122) can be designed through the employ of accurate predictions caming from a previous computational analysis. All these materials, characterized by remarkable specificity, good biocompatibility and biodegradability, are extremely promising in a broad range of applications, including phase-change triggered drug delivery, morphology controlled pharmacokinetics, soft biotemplating material design for nanoelectronics, etc. Another important application of computational chemistry is the field of solar technology within the design of the Dye Sensitized Solar Cells (DSSC) (123; 124), a new type of solar cell designed first from Graetzel and that have attracted a lot of attention in the recent years due to its possible substitution of the silicon-based classical solar cell, the last type of cells, in fact, present a lot of drawbacks one of this is the higher cost. This new type of dye solar cells are based essentially on transition metal derivatives or organic dye molecules adsorbed on a semiconductor bed, formed between a photosensitized anode and an electrolyte. In this context the photochemical properties of different sensitizers have been investigated both experimentally and computationally in an integrated approach with the attempt to design new dyes with maximal visible light absorption coupled to long-lived excited states. Computational chemistry can be very helpfull to in-depth study the electron injection mechanisms and also to design new types of dyes that can be used as sensitizers for the DSSC. Computational design procedure of novel protein in bio-technological field, has recent emerged as a useful technique to study

biomolecular recognition and generate molecules for use in biotechnology research and biomedicine. For example in silico screening (125; 126; 127) has emerged as an important tool also in identifying bioactive compounds though computational means, by employing knowledge about the protein target or already known bioactive ligands. Virtual screening has appeared as an adaptive response to the massive throughput synthesis and as stated above this necessity has forced the computational chemistry community to develop tools that screen againist any given target and/or property million perhaps billions of molecules in a more and more short period of time. For this reason the screening procedure is nowadays one of the most effective tools in drug discovery process increasing the probability of finding novel hit and compounds in terms of cost-effectivness and commitment in time and material. Despite the inherent limitations, the screening procedure in medicinal chemistry is still the best option now available to explore a large chemical space and molecule-to-ligand response space.

Up to very recently, computational chemistry is important also in the field of cultural heritage restoration and conservation (13), here the non- or micro-invasive and non destructive analytical tools need to be employed. The role of computational chemistry can help to overcome this limitation facilitating the study of experimental spectra and also to dissect the role among concomitant effects (that is coordination, pH effects etc etc) that brings, in a long time scale, to the ageing of an artwork. The inherent complexity of such materials will require researchers to devise new methodologies and strategies integrating methods of variable accuracy levels into a unique multiscale computational protocol, this is the way followed nowadays by the researchers in this field.

In general, we can state that the number of examples where computational chemistry can help the chemical community is growing very fast and today, computational chemistry is applied to simulating the properties of the systems of direct technological and biological interest and, more important, where the interpretation of the corresponding experimental data is not easy due to the complexity of the materials; here the aid of computational chemistry is to dissect the role of this much concomitant effects that brings to the final observed properties. Another important application is seen when a new molecular system

must to be designed and it is important to select, among a rather large set of molecules the best candidate that brings to the final desired properties.

The work done in this Ph.D. thesis exploits essentially this dual interpretative and predictive role of the computational chemistry. First, we study optical properties of coumarin dyes in solution and in biological environment and the structure and the electronic properties of Alizarin dye in different conditions (i.e. pH conditions and different coordination with Mg and Al) with an emphasis on the simulation of optical spectra line-shape directly comparable with their experimental counterparts. Then, in a second step we guide a synthetical work trough the *in silico* design of the best compound with the desired properties, in this context our computational protocol was found to be very beneficial since it was show capable of predicting with good accuracy the spectral behaviour of the investigated class of chromophores, allowing us to select the best candidate among a rather large set of homologues and to finally produce a polymer with the desired smart behaviour. This report is organized as follows: in the following chaper (2) we describe from a more theoretical point of view the theory underlying computations employed in the following of the report with a particular emphasis on the theory under the simulation of the vibrationally-resolved electronic spectra, in the chapters 3,4 and 5 we describe the results obtained in the main three applications related to to the biochemistry, cultural heritage and material sciences, respectively: optical properties of coumarin dyes (3), electronic spectra of alizarin and its Mg al Al-complexes (4), and the in silico design of mechanoresponsive materials (5). Finally, in the chapter (6) we make our conclusion and we point out some perspective departing from the results obtained in this thesis.

Bibliography

[1] Sanchez, C.; Julian, B.; Belleville, P.; Popall, M. *Journal of Materials Chemistry* **2005**, *15*(35-36), 3559–3592.

[2] Klostranec, J. M.; Chan, W. C. W. *Adv. Materials* **2006**, *18*(15), 1953–1964.

[3] Tian, H.; Wang, Q. *Chem. Soc. Rev.* **2006**, *35*(4), 361–374.

[4] Hajduk, P. J.; Greer, J. *Nature Reviews Drug Discovery* **2007**, *6*(3), 211–219.

[5] Jun, Y.-W.; Lee, J.-H.; Cheon, J. *Angew. Chem. Int. Ed.* **2008**, *47*(28), 5122–5135.

[6] Nel, A. E.; Maedler, L.; Velegol, D.; Xia, T.; Hoek, E. M. V.; Somasundaran, P.; Klaessig, F.; Castranova, V.; Thompson, M. *NATURE MATERIALS* **2009**, *8*(7), 543–557.

[7] Eliseeva, S. V.; Buenzli, J.-C. G. *Chem. Soc. Rev.* **2010**, *39*(1), 189–227.

[8] Kim, H. N.; Guo, Z.; Zhu, W.; Yoon, J.; Tian, H. *Chem. Soc. Rev.* **2011**, *40*(1), 79–93.

[9] Hill, M. *Computer & Chemical Engineering* **2009**, *33*(5), 947.

[10] Kaiser, R.; Asvany, O.; Lee, Y. *Planetary and Space Science* **2000**, *48*(5), 483 – 492.

[11] Herbst, E.; van Dishoeck, E. F. In *Annual Review of Astronomy and Astrophysics, Vol. 47*; Blandford, R and Kormendy, J and VanDishoeck, E., Ed., Vol. 47 of *Annual Review of Astronomy and Astrophysics;* 2009; pages 427–480.

[12] Chela-Flores, J. *International Journal of Astobiology* **2013**, *12*(1), 8–16.

[13] Fantacci, S.; Amat, A.; Sgamellotti, A. *Acc. Chem. Res.* **2010**, *43*, 802–813.

[14] Creagh, D. C. *Radiat. Phys. Chem.* **2005**, *74*, 426–442.

[15] Capitani, D.; Di-Tullio, V.; Proietti, N. *Progress in Nuclear Magnetic Resonance Spectroscopy* **2012**, *64*, 29–69.

[16] Berova, N., Polavarapu, P. L., Nakanishi, K., Woody, R. W., Eds. *Comprehensive Chiroptical Spectroscopy: Applications in Stereochemical Analysis of Synthetic Compounds, Natural Products, and Biomolecules, Volume 2;* John Wiley & Sons, Inc. Hoboken: New Jersey, 2012.

[17] Grimme, S. In *Reviews in Computational Chemistry;* John Wiley & Sons, Inc., 2004; chapter Calculation of the Electronic Spectra of Large Molecules, pages 153–218.

[18] Berova, N.; Di Bari, L.; Pescitelli, G. *Chem. Soc. Rev.* **2007**, *36*(6), 914–931.

[19] Barbara, P. F.; Gesquiere, A. J.; Park, S.-J.; Lee, Y. J. *Acc. Chem. Research* **2005**, *38*(7), 602–610.

[20] Roy, R.; Hohng, S.; Ha, T. *Nature Methods* **2008**, *5*(6), 507–516.

[21] Zhuang, W.; Hayashi, T.; Mukamel, S. *Angew. Chem. Int. Ed.* **2009**, *48*(21), 3750–3781.

[22] Lichtman, J.; Conchello, J. DEC **2005**, *2*(12), 910–919.

[23] Cho, M. *Chem. Rev.* **2008**, *108*, 1331.

[24] Quack, M.; Merkt, F. *Handbook of High-Resolution Spectroscopy;* John Wiley & Sons, 2011.

[25] Siebert, F., Hildebrandt, P., Eds. *Vibrational Spectroscopy in Life Science;* Wiley-VCH Verlag GmbH and Co. KGaA, 2008.

[26] Barth, A.; Zscherp, C. *Quarterly Reviews of Biophysics* **2002**, *35*(4), 369–430.

[27] Laane, J., Ed. *Frontiers of Molecular Spectroscopy;* Elsevier: Amsterdam, 2009.

[28] Nafie, L. A. *Vibrational Optical Activity: Principles and Applications;* John Wiley & Sons: Chichester, UK, 2011.

[29] Berova, N., Polavarapu, P. L., Nakanishi, K., Woody, R. W., Eds. *Comprehensive Chiroptical Spectroscopy: Instrumentation, Methodologies, and Theoretical Simulations, Volume 1;* John Wiley & Sons, Inc. Hoboken: New Jersey, 2012.

[30] Astrid, G., Rudolf, R., Jerker, W., Eds. *Single Molecule Spectroscopy in Chemistry, Physics and Biology: Nobel Symposium;* Springer-Verlag: Berlin Heilderberg, 2010.

[31] Dresselhaus, M.; Dresselhaus, G.; Saito, R.; Jorio, A. *Physics Reports* **2005**, *409*(2), 47 – 99.

[32] Cohen, Y.; Avram, L.; Frish, L. *Angew. Chem. Int. Ed.* **2005**, *44*(4), 520–554.

[33] Mittermaier, A.; Kay, L. *Science* **2006**, *312*(5771), 224–228.

[34] Borbat, P.; Costa-Filho, A.; Earle, K.; Moscicki, J.; Freed, J. *Science* **2001**, *291*(5502), 266–269.

[35] Barone, V.; Polimeno, A. *Phys. Chem. Chem. Phys.* **2006**, *8*, 4609–4629.

[36] Schiemann, O.; Prisner, T. F. *Quarterly Reviews of Biophysics* **2007**, *40*(1), 1–53.

[37] Meier, R. *International Journal of Electronics* **1995**, *78*(2), 285–288.

[38] Clary, D. *Science* **2006**, *314*, 5797.

[39] Truhlar, D. G. *J. Am. Chem. Soc.* **2008**, *130*, 16824–16827.

[40] Visscher, L.; Bolhuis, P.; Bickelhaupt, F. M. *Phys. Chem. Chem. Phys.* **2011**, *13*, 10399–10400.

[41] Gao, J. *Acc. Chem. Research* **1996**, *29*, 298–305.

[42] Cui, Q.; Karplus, M. *J. Chem. Phys.* **2000**, *112*, 1133–1149.

[43] Canuto, S.; Coutinho, K.; Trzesniak, D. In *Advances in Quantum Chemistry*; Sabin, J. R., Brandas, E., Eds., Vol. 41; Academic Press, 2002; chapter New developments in Monte Carlo/quantum mechanics methodology. The solvatochromism of carotene in different solvents, pages 161 – 183.

[44] Gao, J.; Truhlar, D. G. *Annual Review of Physical Chemistry* **2002**, *53*, 467–505.

[45] Ramos, M. J., Ed. *Computational Proteomics;* Transworld Research Network, 2008.

[46] Grotendorst, J., Attig, N., Blügel, S., Marx, D., Eds. *Multiscale Simulation Methods in Molecular Sciences. Lecture Notes*, Vol. 42 of *NIC Series;* Forschungszentrum Julich, 2009.

[47] Senn, H. M.; Thiel, W. *Angew. Chem. Ind. Ed. Engl.* **2009**, *48*, 1198–1229.

[48] Sabin, J. R., Brandas, E., Eds. *Combining Quantum Mechanics and Molecular Mechanics. Some Recent Progresses in QM/MM Methods*, Vol. 59 of *Advances in Quantum Chemistry;* Academic Press, 2010.

[49] Kamerlin, S. C. L.; Warshel, A. *Phys. Chem. Chem. Phys.* **2011**, *13*, 10401–10411.

[50] Barone, V., Ed. *Computational Strategies for Spectroscopy, from Small Molecules to Nano Systems.;* John Wiley & Sons, Inc. Hoboken: New Jersey, 2011.

[51] Barone, V.; Baiardi, A.; Biczysko, M.; Bloino, J.; Cappelli, C.; Lipparini, F. *Phys. Chem. Chem. Phys.* **2012**, *14*, 12404–12422.

[52] Pedone, A.; Biczysko, M.; Barone, V. *Chem. Phys. Chem.* **2010**, *11*, 1812–1832.

[53] Warshel, A.; Karplus, M. *Journal of the American Chemical Society* **1974**, *96*(18), 5677–5689.

[54] Aidas, K.; Mikkelsen, K. V.; Kongsted, J. *J. Comp. Methods in Sci. and Eng.* **2007**, *7*, 135–158.

[55] Barone, V.; Polimeno, A. *Chem. Soc. Rev.* **2007**, *36*, 1724–1731.

[56] Arul Murugan, N.; Kongsted, J.; Rinkevicius, Z.; Aidas, K.; Ågren, H. *J. Phys. Chem. B* **2010**, *114*, 13349–13357.

[57] Marshall, K.L.and Noto, A.; Painter, G.; Tabiryan, N. *Proceedings of the SPIE - The International Society for Optical Engineering* **2006**, *6332*, 63320C–1–10.

[58] Prampolini, G.; Bellina, F.; Biczysko, M.; Cappelli, C.; Carta, L.; Lessi, M.; Pucci, A.; Ruggeri, G.; Barone, V. *Chemistry* **2013**, *19*(6), 1996–2004.

[59] Barone, V.; Improta, R.; Rega, N. *Acc. Chem. Res.* **2008**, *41*(5), 605–616.

[60] Grimme, S. *Rev. Comput. Chem.* **2004**, *20*, 153.

[61] Pedone, A.; Biczysko, M.; Barone, V. *Comp. Phys. Comm.* **2010**, *11*, 1812–1832.

[62] Grunenberg, J., Ed. *Computational Spectroscopy;* Wiley-VCH Verlag GmbH & Co. KGaA, 2010.

[63] Pedone, A.; Prampolini, G.; Monti, S.; Barone, V. *Chem. Mater.* **2011**, *23*, 5016–5023.

[64] Herrmann, C.; Reiher, M. In *Atomistic Approaches in Modern Biology: from Quantum Chemistry to Molecular Simulations*; Reiher, M., Ed., Vol. 268 of *Topics in Current Chemistry;* Springer-Verlag: Berlin, Germany, 2007; pages 85–132.

[65] Barone, V.; Biczysko, M.; Brancato, G. *Adv. Quantum Chem.* **2010**, *59*, 17.

[66] Barone, V.; Biczysko, M.; Bloino, J.; Borkowska-Panek, M.; Carnimeo, I.; Panek, P. *Int. J. Quantum Chem.* **2012**, *112*, 2185–2200.

[67] Neugebauer, J.; Reiher, M.; Kind, C.; Hess, B. A. *J. Comput. Chem.* **2002**, *23*(9), 895–910.

[68] Herrmann, C.; Neugebauer, J.; Reiher, M. *New J. Chem.* **2007**, *31*(6), 818–831.

[69] Jacob, C. R.; Luber, S.; Reiher, M. *J. Phys. Chem. B* **2009**, *113*(18), 6558–6573.

[70] Biczysko, M.; Bloino, J.; Santoro, F.; Barone, V.; Wiley: Chichester, 2011; chapter Time Independent approaches to simulate electronic spectra lineshapes: from small molecules to macrosystems., pages 361–443.

[71] Cramer, C. *Essentials of Computational Chemistry: Theories and Models;* John Wiley & Sons Ltd., Chichester, UK, 2005.

[72] Young, D. *Computational Chemistry: A Practical Guide for Applying Techniques to Real World Problems;* John Wiley & Sons Inc, New York, US, 2004.

[73] Jensen, F. *Introduction to Computational Chemistry;* John Wiley & Sons: Chichester, UK, 2006.

[74] Leach, A. R. *Molecular Modelling: Principles And Applications, 2nd Edition;* Pearson Education, Harlow, England, 2009.

[75] Hinchliffe, A. *Molecular Modelling for Beginners;* John Wiley & Sons Ltd., Chichester, UK, 2011.

[76] Hohenberg, P.; Kohn, W. *Phys. Rev.* **1964**, *136*, B864.

[77] Kohn, W.; Sham, L. J. *Phys. Rev.* **1965**, *140*, A1133.

[78] Kohn, W.; Becke, A. D.; Parr, R. G. *J. Phys. Chem.* **1996**, *100*, 12974.

[79] Burke, K.; Werschnik, J.; Gross, E. K. U. *J. Chem. Phys.* **2005**, *123*, 062206.

[80] Casida, M. E. *Journal of Molecular Structure: THEOCHEM* **2009**, *914*(1-3), 3–18.

[81] Scalmani, G.; Frisch, M. J.; Mennucci, B.; Tomasi, J.; Cammi, R.; Barone, V. *J. Chem. Phys.* **2006**, *124*, 094107.

[82] Becke, A. D. *J. Chem. Phys* **1993**, *98*, 5648.

[83] Stephens, P.; Devlin, F.; Chabalowski, C.; Frisch, M. *J. Phys. Chem.* **1994**, *98*, 11623.

[84] Casida, M. *Recent advances in Density Functional Methods (vol.1) World Scientific - Singapore*.

[85] Bauernschmitt, R.; Ahlrichs, R. *Chem. Phys. Lett.* **1996**, *256*, 454.

[86] Tozer, D.; Handy, N. *J. Chem. Phys.* **1998**, *109*, 10180.

[87] Tozer, D.; Amos, R.; Handy, N.; Roos, B.; Serrano-Andres, L. *Mol. Phys.* **1999**, *97*, 859.

[88] Dreuw, A.; Weisman, J.; Head-Gordon, M. *J. Chem. Phys.* **2003**, *119*, 2943.

[89] Bernasconi, L.; Sprik, M.; Hutter, J. *J. Chem. Phys.* **2003**, *119*, 12417.

[90] Yanai, T.; Tew, D.; Handy, N. *Chem. Phys. Lett.* **2004**, *393*, 51–57.

[91] Chai, J.-D.; Head-Gordon, M. *Physical Chemistry Chemical Physics* **2008**, *10*, 6615.

[92] Biczysko, M.; Panek, P.; Scalmani, G.; Bloino, J.; Barone, V. *J. Chem. Theory Comput.* **2010**, *6*, 2115–2125.

[93] Chai, J.; Head-Gordon, M. *J. Chem. Phys.* **2008**, *128*, 084106.

[94] Chai, J.; Head-Gordon, M. *Phys. Chem. Chem. Phys.* **2008**, *10*, 6615–6620.

[95] Peach, M. J. G.; Helgaker, T.; Salek, P.; Keal, T. W.; Lutnaes, O. B.; Tozer, D. J.; Handy, N. C. *Phys. Chem. Chem. Phys.* **2006**, *8*, 558–562.

[96] Isegawa, M.; Peverati, R.; Truhlar, D. G. *J. Chem. Phys.* **2012**, *137*(24), 244104.

[97] Jacquemin, D.; Bremond, E.; Planchat, A.; Ciofini, I.; Adamo, C. *J. Chem. Theory Comput.* **2011**, *7*, 1882–1892.

[98] Franck, J. *Transactions of the Faraday Society* **1926**, *21*(3), 536.

[99] Condon, E. *Physical Review* **1926**, *28*, 1182.

[100] Condon, E. December **1928**, *32*, 858.

[101] Barone, V.; Bloino, J.; Biczysko, M.; Santoro, F. *J. Chem. Theory Comput.* **2009**, *5*, 540–554.

[102] Bloino, J.; Biczysko, M.; Santoro, F.; Barone, V. *J. Chem. Theory Comput.* **2010**, *6*, 1256–1274.

[103] Tomasi, J.; Mennucci, B.; Cammi, R. *Chem. Rev.* **2005**, *105*, 2999–3093.

[104] Cossi, M.; Scalmani, G.; Rega, N.; Barone, V. *Journal of Computational Chemistry* **2003**, *24*, 669.

[105] De-Angelis, F.; Santoro, F.; Nazeruddin, M.; Barone, V. *J. Phys. Chem. B* **2008**, *112*, 13181–13183.

[106] Hellman, A.; Baerends, E.; Biczysko, M.; Bligaard, T.; Christensen, C.; Clary, D.; Dahl, S.; Harrevelt, R.; Honkala, K.; Jonsson, H.; Kroes, G.; Luppi, M.; Manthe, U.; Norskov, J.; Olsen, R.; Rossmeisl, J.; Skulason, E.; Tautermann, C.; Varandas, A.; Vincent, J. K. *J. Phys. Chem. B* **2006**, *110*, 17719–17735.

[107] Santoro, F.; Improta, R.; Lami, A.; Barone, V. *J. Chem. Phys.* **2007**, *126*, 184102.

[108] Suzuki, M.; Husimi, Y.; Komatsu, H.; Suzuki, K.; Douglas, K. *J. Am. Chem. Soc.* **2008**, *130*, 5720.

[109] Escribano, P.; Julian-Lopez, B.; Planelles-Arago, J.; Cordoncillo, E.; Viana, B.; Sanchez, C. *J. Matter. Chem.* **2008**, *18*, 23.

[110] Willner, I.; Baron, E.; Willner, B. *Biosensor and Bioelectronics* **2007**, *22*, 1841.

[111] Fu, Y.; Hellstrom, S.; Agren, H. *Journal of non linear optical physics and materials* **2009**, *18*(2), 195–226.

[112] Sotiropoulou, S.; Sierra-Sastre, Y.; MArks, S.; Batt, C. *Chem.Matter* **2008**, *20*, 821.

[113] N.Ma.; Sargent, E.; Kelley, S. *L. Matter. Chem.* **2008**, *18*, 954.

[114] Gill, R.; Polsky, R.; Willner, I. *Small2* **2006**, page 1037.

[115] Martinez, T. *Acc. Chem. Res.* **2006**, *39*, 119.

[116] Barret, C. J.; Mamiya, J.; Yagerc, K. G.; Ikeda, T. *Soft Matter* **2007**, *3*, 1249–1261.

[117] Amato, I. *Science News* **1990**, *137*, 152.

[118] Port, O. *Business Week* **1990**, *3224*, 48.

[119] et al., C. *J. Am. Chem. Soc.* **2009**, *131*, 13297.

[120] et al., M. T. *Nano Lett.* **2010**, *10*, 2690.

[121] et al., M. C. *Angew. Chem. Int. Ed.* **2010**, *49*, 5076.

[122] et al., T. M. *Adv. Drug Delivery Rev.* **2002**, *54*, 79.

[123] Jiao, Y.; Zhang, F.; Gratzel, M.; Meng, S. *Advanced functional materials* **2013**, *23*(4), 424–429.

[124] Cai, L.; Tsao, H.; Zhang, W.; Wang, L.; Xue, Z.; Gratzel, M.; Liu, B. *Advanced functional materials* **2013**, *3*(2), 200–205.

[125] Phatak, S.; Stephan, C.; Cavasotto, C. *Expert opinion on drug discovery* **2009**, *4*(9), 947–959.

[126] Pauli, I.; Timmers, L.; Caceres, R.; Soares, M.; de Azevedo, W. *Current Drug Targets* **2008**, *9*(12), 1054–1061.

[127] Gombar, V.; Alberts, J.; Cassidy, K.; Mohutsky, B. M. M. *Current Computer-aided drug design* **2006**, *2*(2), 177–188.

CHAPTER 2

OPERATIVE PROTOCOLS AND METHODOLOGIES

In the introductive chapter we have discussed about the state-of-the-art in computational chemistry pointing out also the power and the limits of the computational protocols when applied to study molecular properties of medium-to-large systems. In this second chapter we want, after a brief description of our computational protocol and the methodologies, to describe shortly the theory under the models employed to compute the vibrationally-resolved electronic spectra.

2.1 Computational protocol

Fist, we want to state that all the calculations made and here presented, are done using, as computational softwares, the locally modified GAUSSIAN suite of programs. While the GAUSSVIEW graphical interface is used to construct and visualise molecular structures, generate molecular orbitals and make electronic density difference plots. Then, also a locally developed program by D. Licari, VSL (Virtual Spectroscopy Laboratory) (1) was

used to analyze the resulting electronic spectra line shapes, further information about this program can be found in the corresponding reference (2). All QM computations have been performed using models rooted into the Density Functional Theory (DFT) and its time-dependent extension (TD-DFT), considering their reliability in the description of ground and excited state properties for medium-to-large molecular systems, at a reasonable computational cost. All high performance computations (HPC) have been performed using a dedicated and versatile infrastructure, within the DREAMS HPC center (http://dreamshpc.sns.it) fig. 2.1.
In order to proceed with all calculations, a stepwise computational protocol was defined and followed for all the molecular systems here studied. In the first step a geometry of a molecular system under study has been constructed with GAUSSVIEW, taking also into account the symmetry cosiderations, and then geometry structure in its ground (S_0) state has been optimized, using standard convergence criteria. It has been followed by the computation of the harmonic frequencies, first off all in order to check the nature of the stationary point on the Potential Energy Surface (PES), i.e. to assure that the stationary point found is a (global or local) minimum and not a saddle point. Computations of harmonic vibrational frequencies in the ground electronic state have been also an necessary ingredient in all models applied to simulate vibrationally-resolved electronic spectra (*vide infra*). The sample input (*.com*) files used in the first two steps are presented in table 2.1 where other parameters such as the DFT functional, basis set and other keywords e.g. related to the solvent description are specified and commented in the relative caption.

Then as a third step, in order to calculate absorption UV-Vis spectra we have followed essentially two ways, in the first approximation the *pure electronic* computations have been performed and then followed by the *vibronic* computations, that is the *vibrationally-resolved-electronic-spectra-computations*. In order to calculate the pure electronic absorption spectra, the resulting Vertical Energies (VE) and oscillator strengths (f) calculated using the time-dependent DFT method from the ground to the first (e.g. 10) excited

```
P Opt B3LYP/gen 6d SCRF=(CPCM,solvent=acetonitrile)

Title

Molecule specification

@link to the basis set
```

```
P Freq=(HPModes,SaveNM) B3LYP/gen 6d SCRF=(CPCM,solvent=acetonitrile)

Title

Molecule specification

@link to the basis set
```

Table 2.1: Input files for GAUSSIAN to search a minimum in the PES (optimization and frequency calculation), the keyword **Opt** stay for optimization with standard convergence criteria, **Freq** for frequency calculation after the optimization step, then in the same input we specify the methods and basis set, here, for example **B3LYP** is the functional of DFT employed and the key *gen* stay for the external basis set, in our case the N07D or SNSD basis set was used linked in an external file, then **SCRF** stay for Self Constistent Reaction Field, here we done the calculation within the **CPCM** model with a specified solvent, for example *acetonitrile*.

Figure 2.1: Instruments used to carry out computations.

states were directly convoluted with Gaussian or Lorentzian function with an appropriate Half-Width at Half-Maximum (HWHM). The number of excited state to be taken into account in the TD calculation has been chosen in order to cover the desired UV-Vis energy region, depending on the case study from 3 states (the default value of GAUSSIAN) to a maximum of 15 states have been considered. In the output of the TD calculations, the results for each excited state are summarised, including the spin and the spatial symmetry, the excitation energy (in eV), the corresponding wavelength (expressed in nm) and the transition intensities (oscillator strengths f) with also the largest coefficient for the CI expansion, this final results together with the visual inspection of the molecular orbitals (MO) and Electron density diffrerence (ELD) plots, was employed to classify the nature of the transition under study (e.g. bright or dark, and $n \rightarrow \pi^*$ or $\pi \rightarrow \pi^*$). The sample input (*.com*) file used for TD calculation is presented in table 2.2.

When calculation are done in a solvent with the use of CPCM model, an important issue to be accounted for is a distinction between *equilibrium* and *non-equilibrium* regimes; In fact the surrounding solvent can respond in two different ways to the changes in the state of our solute molecule: it can polarizes its electron distribution with a rapid process or the solvent molecules can also reorient themselves, but this second possibility is clearly

```
P TD=(nstates=10) B3LYP/gen 6d SCRF=(CPCM,solvent=acetonitrile)

Title

Molecule specification

@link to the basis set
```

Table 2.2: Input for VE calculation with TD-DFT method, the keyword **TD** invoke the TD-DFT and the **nstates=x** solve for x states, here for example to the first 10 singlet excited electronic states. For the other keywords see table 2.1.

a much slower process. From a general point of view an equilibrium calculation describes a situation where the solvent has the time to fully respond to the changes of electron density distribution of solute whereas a non-equilibrium calculation is more appropriate for those processes which are too rapid to allow solvent to fully respond to the solute modifications. For VE calculation described above, the non-equilibrium is the most appropriate situation and then, when calculating absorption spectra in a solvent we have adopted this model for PCM (which is also the default procedure in GAUSSIAN).

The calculation of emission spectra with the pure electronic picture was done optimising (here in an equilibrium regime, if CPCM was used) the molecular structure in the excied electronic state of interest (e.g. the first, second, third ... one) and then, doing a single point (SP) vertical energy calculation in order to re-asset the energy of the molecule in order to adopt the non equilibrium regime, that also for emission is the more accurate and closer to the real physical situation picture. The sample input (*.com*) file used for excited state geometry optimization is presented in table 2.3.

P Opt TD=(root=1) B3LYP/gen 6d SCRF=(CPCM,solvent=acetonitrile)
Title
Molecule specification
@link to the basis set

Table 2.3: Input for excited state optimization with TD-DFT method invoked by the keyword **TD**; The **TD=(root=n)** whit n=1 stay for optimization of the structure in its first excited electronic state. For the other keywords see table 2.1.

Regarding the vibronic computations, they are the key point of this thesis and represent improvement with respect to the standard spectra simulation within VE approach. Thus, the theory underlying the calculation of vibrationally resolved electronic spectra (in absorption and/or emission) will be described in more detail in the next section of this chapter.

2.1.1 General approach to calculate vibronic spectra

As stated above, UV-Vis spectra can be simulated by computing VE energies and then convoluting the resulting stick-spectra with Gaussian or Lorentzian function. However, such a treatment neglects all the possible dynamic effects that can be sometime very important to correctly simulate the spectra line-shape. To overcome this limitation we have choosen to adopt a recently implemented procedure to calculate the so called *vibronic* spectra, which is developed in the group of Prof. Barone and has been also recently implemented in GAUSSIAN 09. From a theoretical point of view this approach relies on the Franck-Condon principle to evaluate the intensities of the transition between two

vibronic energy levels. Within the Franck-Condon priciple, it is considered that the nuclear positions are mostly unaltered by the electron jump which takes place during the transition. This thesis has a computational character, thus the theoretical description is not intended to be exhaustive but rather to provide a basic overview of the underlying methodological background. More detailed and complete description of the methodology applied in this thesis can be found in the original references (3; 4), while more general description of models used to compute vibrationally resolved electronic spectra within the time-independent framework can be found in the recent review (5).

Line intensities in one-photon absorption and emission spectra depends on the square of the transition dipole moment integral $\langle\Psi'|\mu|\Psi''\rangle$ as well as on the frequency of the radiation $(\omega)^2$:

$$\sigma(\omega)_{absorption} = \frac{4\pi^2\omega}{3c} = \sum_{'} \rho' \sum_{''} |\langle\Psi'|\mu|\Psi''\rangle|^2 \delta(E'' - E' - \hbar\omega) \tag{2.1}$$

$$\sigma(\omega)_{emission} = \frac{4\omega^3}{3\hbar c^3} = \sum_{'} \rho' \sum_{''} |\langle\Psi'|\mu|\Psi''\rangle|^2 \delta(E'' - E' + \hbar\omega) \tag{2.2}$$

where ρ' is the is the Boltzmann population of each initial state and $\sigma(\omega)$ is the rate of photo absorption or emission per molecule an per unit of radiant energy. In the same equations Ψ' and Ψ'' represents the molecular wave functions, of the initial and final state, respectively. Within the Born-Oppenheimer approximation framework, the total molecular wave function Ψ can be splitted in two parts the electronic wave function (ψ_e) and the nuclear one (ψ_n):

$$\langle\Psi'|\mu|\Psi''\rangle| = \langle\psi'_e\psi'_n|\mu_e|\psi''_e\psi''_n\rangle| + \langle\psi'_e\psi'_n|\mu_n|\psi''_e\psi''_n\rangle| \tag{2.3}$$

and since the electronic wave functions are orthogonal to each other, the second term of the rhs in the equation above vanishes. We further assume that the Eckart conditions (6) are met, so that the nuclear wave function can be, with a good approximation, separated into a rotational and vibrational contributions where the translational part, completely separated to the other two, can be safely discarded. In the following the rotational energies

will be considered sufficiently small and will not be taken into account. Finally, using both approximation stated above, we can lead to the following simpler equation:

$$\langle \Psi' | \mu | \Psi'' \rangle \approx \langle \psi'_v | \mu_{if} | \psi''_v \rangle \tag{2.4}$$

where $\mu_{if} = \langle \psi'_e | \mu | \psi''_e \rangle$ is the electronic transition dipole moment. In the method implemented in GAUSSIAN and so used in this thesis the harmonic approximation is also adopted. As a consequence of it, it is possible to write the wave functions ψ_v as a product of monodimensional wave functions $\psi_{v_i}(Q_i)$ where Q_i is one of the N normal coordinates, describing the i-th vibration of a molecule. But, since the analytic form of the electronic transition dipole moment is unknown, these approximations are not yet sufficient to compute the dipole moment. An additional approximation is done by using the Franck-Condon principle(7; 8; 9). The underlying theory is that, during a transition, the electron jump is so fast that the relative positions and velocities of the nuclei are nearly unaltered by the molecular vibrations. Following these statement, the most intense transition will be from the chosen initial state to a final state being at a minimum of the lowest potential surface vertically upward. Since these approximation is very restrictive by assuming that the dipole moment remains constant during the transition, a more flexible approach can be adopted. Indeed since the shifts of the nuclear positions in the molecule are often fairly small during the electronic transition, it is possible with a good accuracy to expand matematically the form of the transition dipole moment in a Taylor series about the equilibrium geometry of one state respect to another. A state must be chosen as a reference, and in our case it is the final state:

$$\mu_{if} \approx \mu_{if}(Q''_0) + \sum_{k=1}^{N} (\frac{\partial \mu_{if}}{\partial Q''_k})_0 Q''_k + \frac{1}{2} \sum_{k=1}^{N} \sum_{l=1}^{N} (\frac{\partial \mu^2_{if}}{\partial Q''_k Q''_l})_0 Q''_k Q''_l \tag{2.5}$$

in this equation the term Q''_0 represents the equilibrium geometry of the final state. The zeroth order term corresponds to a static electronic transition dipole. This is a direct application of the Franck-Condon principle mentioned above. As a consequence of it, it is referred as the Franck-Condon (FC) approximation. When dealing with intense and fully

allowed transitions (i.e when the $|\mu_{if}(Q''_0)|$ term is high) this approximation generally give very goods results. However, in the case of less intense and weakly allowed transitions or dipole forbidden electronic transitions (i.e when the $|\mu_{if}(Q''_0)|$ term is near to 0) this approximation is not describing correctly the overall spectrum, missing the most intense vibronic transitions. Sometime it is necessary to include a variation of the dipole moment during the transition and a first approximation is to account for a its linear variation with respect the normal coordinates. This fact corresponds mathematically to the taking into account of the second term of the above Taylor expansion and is referred as the Herzberg-Teller approximation (10) whereas the FC approximations take into account only the first one. There is a second type of approximation, named the FCHT where both terms are considered together. So finally, the transition dipole moment can be written in terms of the Franck Condon integrals ($\langle\psi'_v|\psi''_v\rangle$) as:

$$\langle\Psi'|\mu|\Psi''\rangle = \mu_{if}(Q''_0)\langle\psi'_v|\psi''_v\rangle + \sum_{k=1}^{N}(\frac{\partial\mu_{if}}{\partial Q''_k})_0\langle\psi'_v|Q''_k|\psi''_v\rangle + \frac{1}{2}\sum_{k=1}^{N}\sum_{l=1}^{N}(\frac{\partial^2\mu_{if}}{\partial Q''_k\partial Q''_l})_0\langle\psi'_v|Q''_kQ''_l|\psi''_v\rangle \tag{2.6}$$

In addition, the vibrational wave function can be written in a different manner replacing the v_i by a vector $\vec{v}$ containing the quantum numbers v_i representing the same vibrational state described by ψ_v:

$$|\vec{v}\rangle = |\psi_v\rangle = |\prod_{i=1}^{N}\psi_{v_i}\rangle \tag{2.7}$$

A problem, to calculate the integrals $\langle\vec{v}'|\vec{v}''\rangle$ between two states arises from the fact that each vibrational state is expressed in a different set of normal coordinates. To overcome this limitation we can use the linear transformation proposed by Duschinsky (11) to express the normal coordinate of one state with respect to the normal coordinate of the other state:

$$Q' = JQ'' + K \tag{2.8}$$

where J is a matrix called the *Duschinsky Matrix* and represents, physically speaking,

Calculation	VG	AS	AH
INITIAL STATE			
equilibrium geometry	X	X	X
frequencies	X	X	X
FINAL STATE			
equilibrium geometry		X	X
forces at the equilibrium geometry of the initial state	X		
frequencies			X

Table 2.4: Types of calculation needed for the simulation of the vibrationally resolved electronic spectra with the vertical gradient (VG), adiabatic shift (AS) and adiabatic hessian (AH) models.

the mixing of the normal modes during the transition, and K is a *Shift Vector* due to the changes in geometry between the initial and final states. This model is a good approximation when the molecule does not undergo a noticeable distortion during the electronic transition. In particular, the Duschinsky matrix and the shift vector are given by the following equations:

$$J = (L')^{-1}L'' \tag{2.9}$$

$$K = (L')^{-1}M^{1/2}\Delta X \tag{2.10}$$

where, the L' and L'' are the transformation matrices from the mass-weighted Cartesian coordinates to the normal coordinates, M is the diagonal matrix of the atomic masses and ΔX is a vector representing the shift of the nuclear cartesian coordinates between the initial and the final states.

Different models to compute vibronic spectra

In order to compute the vibrationally resolved electronic spectra different models are now available, which differs by their conceptual approach to the transition, vertical or

adiabatic, as well as the level of approximation of the respective PESs of the initial and final states. Additionally, various approximation on the transition dipole moment Franck-Condon (FC), Herzberg-Teller (HT) or Franck Condon-Herzberg Teller (FCHT) can be applied. From the table 2.4 we can see that the simplest model is the VG, that is, Vertical Gradient where for the final state only the forces at the equilibrium geometry of the initial state are needed. This model is the less time-demanding and physically speaking is related to the short-term dynamics on the spectra, so it is expected to reproduce well the low resolution spectrum line-shape. On the contrary it does not account for the changes in vibrational frequencies and for the normal modes's mixing (J=1) between the excited and ground electronic states. Because of its characteristics the VG model provides the most up to date and feasible approach for the studies on the spectrum in a broad energy range and/or for macromolecules, in other words when calculation of the final state geometry and/or frequencies requires a lot of time and only a broad reproduction of the spectrum is needed. On the contrary the AS (that is the Adiabatic Shift) model requires the geometry on the final state but not the frequencies, so it might be considered as a solution for cases where the main interest is in the spectral features close to the transition origin, but not precise frequencies are required. It should taken into account that both VG and AS models constrains the total zero-point vibrational energy (ZPVE) to be the same in the initial and in the final state. At variance they evaluate differently the transition energy between the minima of the initial and the final states, which is more accurately computed within the adiabatic framework. However in both cases if ZPVE effects are introduced and excited state frequencies are computed from second derivatives of the excited-state PES, sensible differences can be found, introducing shifts of the final energy levels that are often larger than 0.1 eV. Finally the AH (Adiabatic Hessian) approach is best suited when an accurate reproduction of the excited-state frequencies, a fine structure of the spectra, and a good estimate for absolute positions of vibronic bands are necessary. However they are rather expensive in terms of computational costs since they involve the geometry optimization and frequency computations in the excited electronic states. However, for semi-rigid semi-harmonic systems both types of approaches provide similar results, while

Chk=initialstate.chk
Geom=Allcheck Frequency=(ReadFC,ReadFCHT,FC,SaveNM) NoSymm
AdiabaticShift
forcesgeometryorfrequenciesfinalstate.chk

Table 2.5: Input file for vibronic calculation: i.e. Adiabatic Shift absorption calculation. The .chk for initial state is specified in the standard section of the input then, in the part related to the vibronic computations the .chk for final state containing the optimized geometry is defined. The details of the other keywords are described in the references (13; 14)

.

anharmonic effects lead to enhanced differences between them (see for instance Ref. (12) and references therein). The procedure implemented in GAUSSIAN and used in the present work, allow to make use of QM data stored in the internal checkpoint (*.chk) files from the frequency computations for the ground state and, depending on the model employed the excited electronic state force, optimization or frequency computations if an VG, AS or AH model is applied to carry out vibronic spectra simulations respectively. This procedure, greatly facilitate computations and allow to use precise data stored with the machine precision. In practice, both checkpoint files, being source of QM data are defined in the input, along with the keyword related to the model used or computations see tab. 2.5.

Bibliography

[1] Zerbetto, M.; Licari, D.; Barone, V.; Polimeno, A. *Molecular Physics* **2013**, pages 1–11.

[2] Daniele, L. *USER'S MANUAL: Virtual Spectroscopic Laboratory (VSL).*

[3] Barone, V.; Bloino, J.; Biczysko, M.; Santoro, F. *J. Chem. Theory Comput.* **2009**, *5*, 540–554.

[4] Bloino, J.; Biczysko, M.; Santoro, F.; Barone, V. *J. Chem. Theory Comput.* **2010**, *6*, 1256–1274.

[5] Biczysko, M.; Bloino, J.; Santoro, F.; Barone, V.; Wiley: Chichester, 2011; chapter Time Independent approaches to simulate electronic spectra lineshapes: from small molecules to macrosystems., pages 361–443.

[6] Eckart, C. April **1937**, *47*(7), 552–558.

[7] Franck, J. *Transactions of the Faraday Society* **1926**, *21*(3), 536.

[8] Condon, E. December **1926**, *28*, 1182.

[9] Condon, E. December **1928**, *32*, 858.

[10] Herzberg, G.; Teller, E. February **1933**, *21*, 410–446.

[11] Duschinsky, F. *Acta Physicochimica URSS* **1937**, *7*, 551.

[12] Avila Ferrer, F. J.; Santoro, F. **2012**, *14*, 13549–13563.

[13] August **2009**, pages http://dreamslab.sns.it/sites/default/files/download/docs/vibronic_spectra_G09–A02.pdf.

[14] August **2009**, pages http://dreamslab.sns.it/sites/default/files/download/docs/vibronic_spectra_GDV–H01.pdf.

Part II

Results and discussions

CHAPTER 3

COMPUTATIONAL STUDY ON THE OPTICAL PROPERTIES OF COUMARINS

Coumarins, also known as benzopyrones, is a weel known class of naturally occurring compounds that have been applied in a variety of biotechnological applications in many important scientific areas: from solar cell technology (1; 2) to medicine (3; 4; 5). They are present in plants in remarkable amounts although their presence has also been detected in some microorganisms and animal sources (6; 7). The structural diversity found in this family of compounds lead to the division into different categories, from simple coumarins to other types of policyclic coumarins such as furocoumarins and pyranocoumarins. Simple coumarins and analogues are a large class of compounds that have attracted interest for a long time due to their biological activities: their have also been shown, for example, to be a good antitumorals (8) and good anti-HIV agents (9). Furthermore, they have been reported to have multiple biological activities such as anticoagulant (10) and anti-inflammatory effect (11), although all these properties have not been evaluated systematically. In addition their enzyme inhibition, antimicrobial and antioxidant properties, are other relevant aspects of coumarin applications in different fields of research. Coumarins

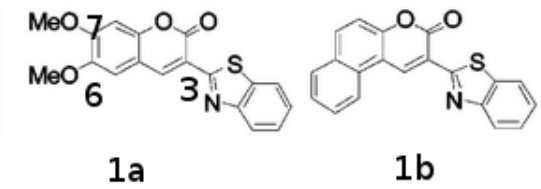

1a 1b

Figure 3.1: Stucture of the two coumarins studied in this section.

are attracting a lot of attention also in their use as a polarity-dependent fluorescent probes for live high-resolution cell imaging applications (12). In the following of this chapter an analysis of optical properties of some coumarin dyes is presented as a test-case a study of the biological applications. An extended benchmark of the DFT functionals is performed, and the choice of the most suitable one is discussed in more details. Then the same level of theory is employed to carry out calculations and is also used in the following chapters.

3.1 Methods

All our calculations have ben performed using GAUSSIAN suite of programs, with the default parameters except when noted. As a first step, the optical properties of two simple coumarins have been investigated through a large set of DFT functionals: B3LYP(13), CAM-B3LYP(14), PBE0(15), LC-ωPBE(16), M062X(17; 18), BMK(19), ωB97X(20), ωB97XD(21), whereas in all cases we have resorted to the double-ζ SNSD (22) basis set, recently developed in our group and aimed at spectroscopic studies of medium-to-large closed- and open-shell molecular systems. This basis set has been constructed from the polarized double-ζ N07D basis set (23; 24; 25; 22) by consistently including diffuse s functions on all atoms, and one set of diffuse polarized functions (d on heavy atoms and p on hydrogens). The SNSD basis set allows cost-effective prediction of a broad range of spectroscopic properties, including electron-spin resonance(ESR)(23; 24; 25; 26), vibrational (IR, Raman, VCD)(26; 27; 28; 29; 30) and electronic (absorption, emission, ECD)(26; 31; 29; 30)

spectra.

As a first step we have performed benchmark computations of both vertical energies (VE) and vibronic spectra in order to select the best functional to employ for the following calculations. The present benchmark has been performed for the two coumarins depitched in fig. 3.1 substituted in position 3 by one benzothiazene ring and in position 6 and 7 by two metoxy groups for **1A** and a pheno condensed group in positions 5 and 6 for **1B**. The geometries have been optimized by DFT and TD-DFT for ground and excited state respectively while only the ground state vibrational frequencies have been calculated. They confirmed that the structures are the minima on the ground state PES by the absence of any imaginary frequencies. For the excited electronic states it has been assumed that the stationary points found correspond to the minima, and the excited state frequency computations have been omitted due to their large computational cost, unless directly needed for the computations of vibronic spectra with adiabatic hessian model. In our calculations we have included also the bulk solvent effects by using the C-PCM(32) model that correctly interpret the major solvent effects as long as no specific solute solvent effects are present. In order to compute spectra we have followed two ways, first we have calculated the vertical excitation energies (VE) from the ground to the first excited electronic states and then the theoretical spectra are obtained by convoluting the subsequent VE by using a Gaussian distribution function with the half-width at half-maximum HWHM adapted from the corresponding experimental spectra. But, it is well known that such an approach completely neglect the dynamical effects (i.e. vibronic coupling) that may occur in real systems and for these reason we have focused in a second step on the calculation of the vibrationally-resolved-electronic spectra that, from a physical point of view are better suited for the comparison with structured experimental spectra, because they take into account also the vibronic couplings. Regarding the vibronic spectra computation we have adopted two models, that is, the vertical gradient (VG) and the adiabatic shift (AS), for the VG spectra only the forces at the equilibrium geometry of the initial state are required for each state whereas the AS requires the geometry optimized at the final state but the frequencies are supposed to be equal of those of the initial state. Finally, the temperature

effects have not been taken into account, but it is considered that simulated spectra can be compared directly to the experimental ones registered at the room temperature.

In the last part the influence of biological environment on the optical properties of coumarins have been evaluated. In the first place a most favourable docked structures have been determined with the VsLab software (33), an interface with the user and the AutoDock suite, developed in the Prof. Maria Ramos Group in Porto(33) that permits to easily study the docking between the protein (here 2V61 and 2QC6) and the ligand (the coumarin). Then the both steric and electrostatic effects of environment on the coumarin absorption electronic spectra have been evaluated by the vertical energy computations, for the latter within the ONIOM model(34), a computational procedure where the molecular system studied is divided into two or more layer which are treated with different model chemistries. In our case the, two-layer ONIOM procedure have been adopted, with the coumarin (High layer) treated at the TD-DFT level and all atoms of protein environment (Low level) described using a standard UFF force field (35) with the atomic charges determined by the QEq method (36).

3.2 Results

First of all we have considered the whole UV-VIS spectrum for compounds **1A** and **1B** in order to dissect the main contributions to the spectral bands and finally to select the most relevant transition to focus on. In fig. 3.2 spectra calculated with the VE approach for **1A**(left panel) and **1B** (right panel) are compared with the corresponding experimental ones. Experimental spectrum of **1A** presents 3 main bands, one (band I) in the 350-450 nm range, the second (band II) is present as a small shoulder at about 320-340 nm and the third (band III) is present at 260-280 nm range, the experimental spectrum of **1B** is simpler and shows one broad band between 300 and 450 nm and a second band around 250-300nm. The spectra presented in fig. 3.2 are calculated with the B3LYP functional and CPCM, within non-equilibrium description of the solvent (acetonitrile), the subsequent stick-spectrum is convoluted with gaussian functions with an HWHM of

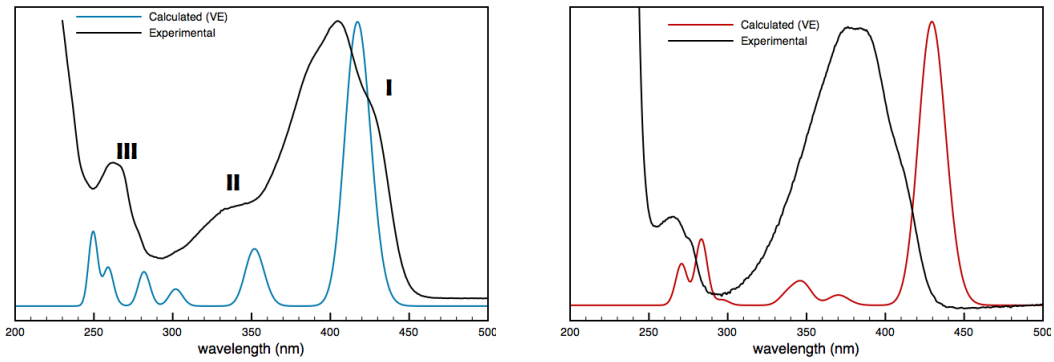

Figure 3.2: Experimental and calculated spectra for 1a (left panel) and 1b (right panel). The first intense band of the spectrum is characterized by the transition between the S_0 and S_1 electronic states. The computed spectra is calculated within vertical energy approximation by TD-B3LYP and CPCM (acetonitrile) and is convoluted with gaussian functions with an HWHM of 550 cm^{-1}

550 cm^{-1}. Both computed spectra matches fairy well the experimental one and we can see that the first intense band of the spectrum for both **1A** and **1B** compound is related to the lower energy transition between the ground state and the first one excited state. For these reasons we focus, in the following, only in these $S_1 \leftarrow S_0$ transition. The molecular orbitals involved in such a transition are the Highest Occupied Molecular Orbital (HOMO) and the Lowest Unoccupied Molecular Orbital (LUMO). The graphical representation of this frontier orbitals is presented in fig. 3.3 in the first row for **1A** and in the second row for **1B**, clearly showing that this type of orbitals are of π nature, thus the corresponding transition can be classified as $\pi \leftarrow \pi^*$ with no charge-transfer character, as we can see from the electron density difference plots presented in the lower panel of the same fig. 3.3.

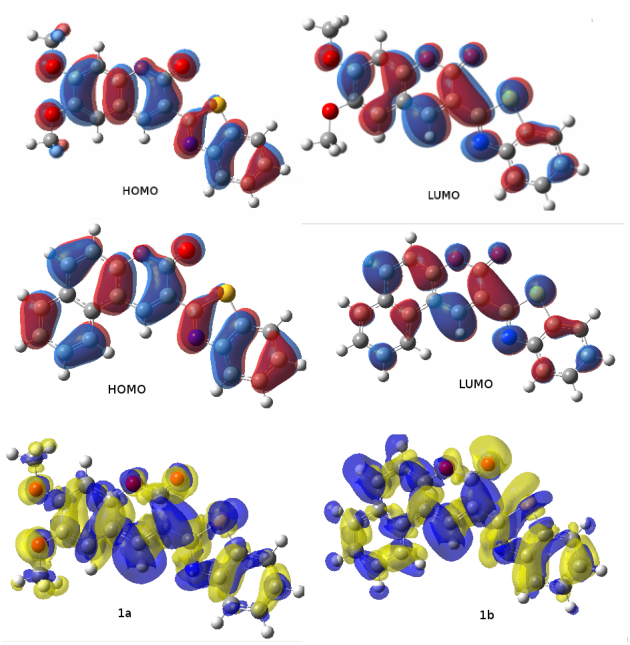

Figure 3.3: Frontier molecular orbitals (first two panels) and changes in the electronic density ELD (lower panel) during the HOMO → LUMO transition for 1a and 1b compounds. For ELD plots, the regions which have lost electron density as a result of transition are shown in bright yellow, whereas the darker blue regions gained electronic density. The transition do not show a charge transfer (CT) character for both cases.

1A	B3LYP	CAM-B3LYP	PBE0	M062X	BMK	ωB97X	ωB97XD	LCωPBE	Exp.
VE (Vac.)	402	363	391	361	367	347	359	341	
VE (Solv.)	417	376	406	375	380	360	372	353	405
1B	B3LYP	CAM-B3LYP	PBE0	M062X	BMK	ωB97X	ωB97XD	LCωPBE	Exp
VE (Vac.)	416	372	403	370	377	354	367	345	
VE (Solv.)	430	384	417	383	390	365	379	357	406

Table 3.1: Vertical Excitation Energies (VE), in nm, computed with different functionals. Experimental values measured in acetonitrile are from reference (12).

3.2.1 DFT functionals benchmark

The VE values of the $S_1 \leftarrow S_0$ electronic transition computed with the 8 functionals in both vacuum and solvent (acetonitrile described by CPCM) are compared in table 3.1 with experimental λ_{max} measured in acetonitrile solution (12). The latter are essentially the same for both derivatives, being 405 nm for **1A** and 406 nm for **1B** respectively. In all cases the value computed in solvent is higher than the one computed in vacuum leading to a bathocromic shift of the spectra due to the higher polarity of the first excited state respect to the ground state for both **1A** and **1B** compounds. The PBE0 functional yield VE in the closest agreement with the experimental λ_{max}, within of +1 and +11 nm for **1A** and **1B** respectively, B3LYP leads to VE red-shifted with respect to experiment, while all other functionals show larger discrepancies with the blue-shifts up to 50 nm. The VE computed with global hybrid M062X and the two range separated hybrids CAM-B3LYP and the ωB97XD are very similar showing blue-shift of 30 nm and 20 nm for **1A** and **1B** respectively. The comparison discussed above has shown that the value of vertical energy computed for the $S_1 \leftarrow S_0$ electronic transition is strongly dependent from the functional employed. However, computed vertical energies do not correspond to the experimental λ_{max}, which are influenced by the spectra-line shape arising from the vibronic transitions, thus the seemingly best accuracy shown by PBE0, do not necessarily need to be retained if the vibronic profile is accounted for. In the following we will analyze the spectral band-shape simulated with the different functionals as well as different approximations for the vibronic spectra computations (at the VG and AS level). Regarding the VG approach, absorption and emission vibrationally-resolved electronic spectra of compounds **1A** and **1B** calculated both in vacuum and in solvent are presented in fig. 3.5. The general trends are the same as discussed above for the VE energies (that is the solvent values are red shifted respect to the vacuum) and the absolute position of the spectra predicted by different functionals is retained, with the B3LYP being the most red-shifted and the ωB97XD the most blue-shifted. From the figure, we can see that by vibronic computations not only VE value is obtained but also the spectra line shape is reproduced. It can be

noted that the differences in the spectra line shape simulated with different functionals are less marked then what is observed for vertical energy and generally all functionals performs very well in reproducing the double shoulder of the band. Taking into account the overall comparison between computed and experimental spectra in solution we can note that B3LYP and PBE0 show a small red-shift for absorption and small blue-shift for emission for **1A** and large red-shift for absorption, with emission profile fairly well matched for **1B**. In variance, CAM-B3LYP and M06-2X show similar trends for both absorption and emission, namely a blue-shift for **1A** and good match for **1B**. These results clearly shows that taking into account not only the VE but the overall spectra line-shape, there is no functional matching accurately both absorption and emission spectra, and the choice of most suitable functional is not obvious.

In order to further investigate that issue we resort to the adiabatic shift (AS) method based on directly computed equilibrium structures in the excited states, thus allowing to avoid any ambiguities related to their approximations within the VG model, potentially influencing shape and the position of emission spectra. The spectra computed with each functional are compared with the corresponding experimental findings in figures 3.6 and 3.7, showing clearly also the relative positions of absorption and emission ones. For example the popular B3LYP functional match well the 0-0 transition (crossing point between the absorption and emission spectra) of **1A**, but for **1B** do not reproduce relative intensities of emission spectra main features and for both **1A** and **1B** clearly underestimates the Stokes-shift. Considering the overall performance the best functionals seems to be the CAM-B3LYP and the M062X that reproduces well not only the spectral line shape but also the Stokes shift even that for **1A** both spectra are blue-shifted with respect to the experiment.

Concluding this section we note that the type of DFT functional used to calculate VE energies and vibronic spectra have a strong impact on the final obtained result. In particular the major discrepancies are observed for the computed VE energies, so also the absolute position of the simulated vibrationally resolved electronic spectra. Relatively smaller differences are observed in the line-shapes, with CAM-B3LYP and M06-2X show-

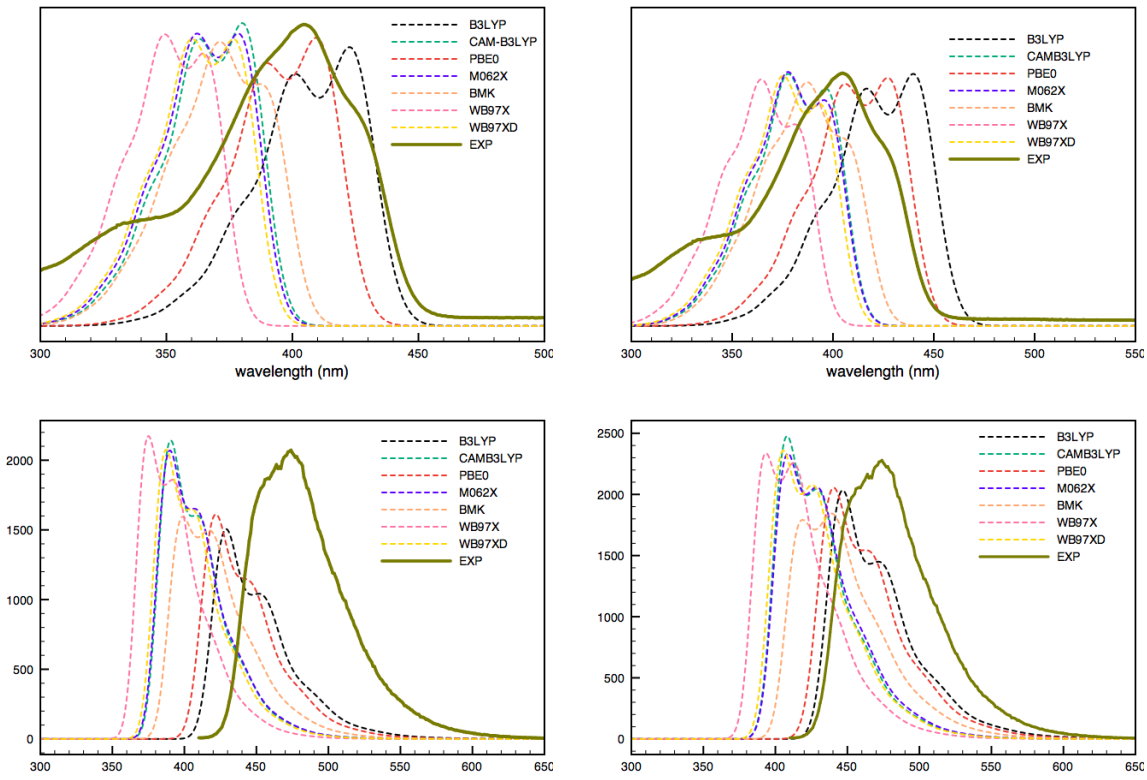

Figure 3.4: $S_0 \rightarrow S_1$ absorption (top) and $S_1 \rightarrow S_0$ emission (bottom) spectra of coumarin **1A** in vacuum (left) and in acetonitrile (right) computed with different functionals. The experimental band(12) is represented by continue green line. For calculated spectra an HWHM of 550 cm^{-1} is employed for convolution.

ing the best intensity pattern, but essentially all functionals reproducing qualitatively well the broad transitions considered in this work. These findings clearly show that the main drawback of the present DFT/TD-DFT approaches is the accurate computation of vertical electronic transitions, while excited states properties are qualitatively well described in most cases. Moreover, it is evident that the comparison of the computed VE with the experimental λ_{max} is not sufficient to asses the accuracy and validate the choice of the functional, and that vibronic computations are necessary for direct comparison with experimental results. It can be noted that the absolute position of simulated spectra can be corrected by hybrid approaches with the most expensive part of computations, related

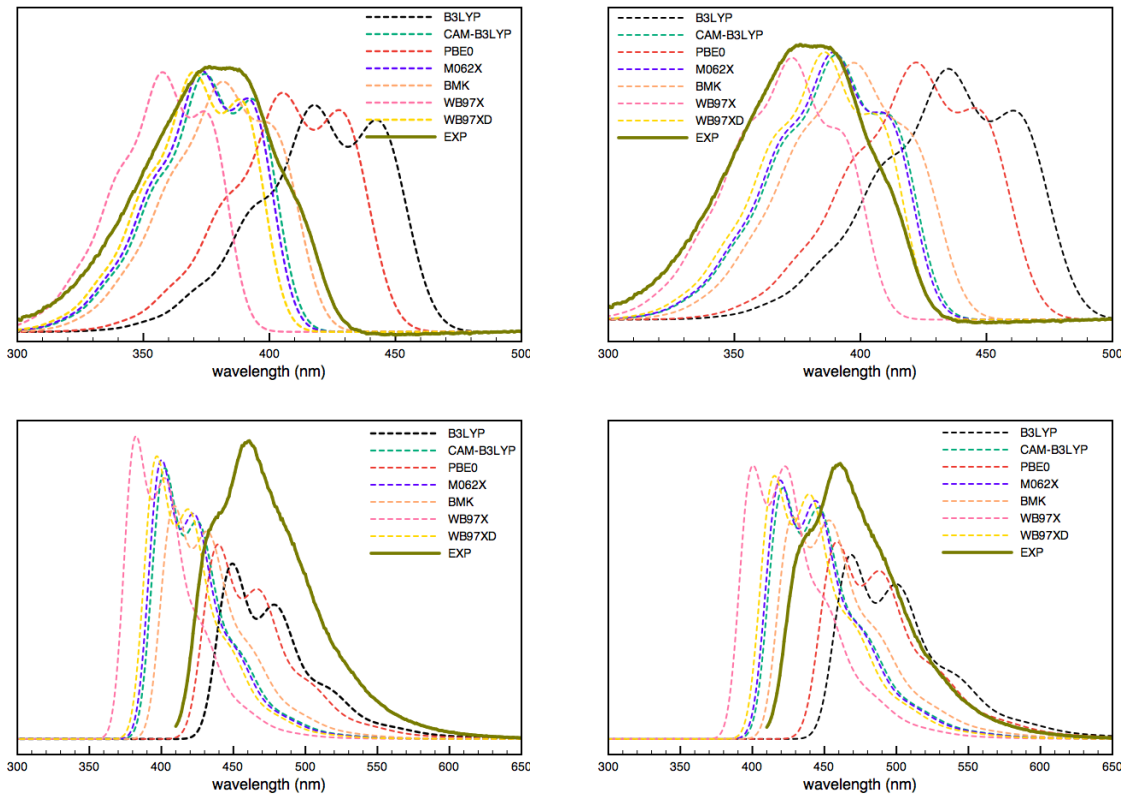

Figure 3.5: $S_0 \rightarrow S_1$ absorption (top) and $S_1 \rightarrow S_0$ emission (bottom) spectra of coumarin 1b in vacuum (left) and in acetonitrile (right) computed with different functionals. The experimental band(12) is represented by continue green line. For calculated spectra an HWHM of 550 cm^{-1} is employed for convolution.

to the excited state PES description, performed at TD-DFT level and VE adjusted on the basis of more accurate computational models (37). However, in the following we will resort mainly to the CAM-BLYP functional, due to its good accuracy and balance description in simulation of absorption and emission spectra line-shapes.

3.2.2 Vibronic models

Different approaches for the calculation of vibronic spectra, namely, Adiabatic Hessian (AH), Adiabatic Shift (AS) and Vertical Gradient (VG), have been considered for the

coumarin **1C**, an analogue of previously discussed 1A with the cyano group added at the position 4, so phenothiazene, cyano and two metoxy substituents present in the coumarin core (fig. 3.10), which will be discussed in more detail in the next section. Figure 3.8 compares the spectra line-shapes of **1C** the $S_1 \rightarrow S_0$ transition calculated in acetonitrile solution for with AH, AS and VG methods, both in absorption and in emission, and convoluted with an HWHM of 500 cm^{-1}. The direct comparison between the VG and AS inform us on the differences in the shift between the initial and the final electronic state structures along the normal modes. In the former case it is estimated from the excited state energy gradients computed at the Franck-Condon point and assuming the harmonic excited state PES, while in the latter is is directly obtained from comparison of initial and final state equilibrium structures. The similarity of the VG line-shape and position respect to AS confirms good accuracy of the former showing also validity of the harmonic approximation, in this case. Regarding adiabatic methods, the comparison between AS and AH give us information about the influence of the changes in frequency and in rotation of the normal modes between the two involved electronic states. Both spectra present very similar line-shapes but are shifted by approximately 10 nm and this difference is due to the different estimation of the 0-0 transition, which only in the latter case takes into account frequency changes upon electronic excitation. Furthermore this results suggests that the Duschinsky effect do not play a significant role, as also shown by the direct inspection of the corresponding matrix **J**, and can be safely discarded. In fig 3.9 the absorption spectra calculated with AH, AS and VG models convoluted with different HWHM: 40 cm^{-1} for the dotted lines and 123 cm^{-1} for continuous lines are compared in a relative energy scale, so the energy values with respect to the 0-0 transition. More pronounced differences between the spectra are observed only with the higher resolution i.e. at 40 cm^{-1} HWHM and are mainly related to the shifts of most pronounced vibronic transitions between VG/AS and AH due to the more accurate description of excited state frequencies in the latter. For this reason the VG and AS methods represents a good approximation for the simulation of the low-resolution spectra.

3.2.3 From the spectra analysis to excited state photophysics: the dual fluorescence of 1C coumarin

After discussion on the accuracy of DFT approaches and models used for the simulation of electronic spectra line-shape, in this section we present a case study: the fluorescence of the **1A** and **1C** coumarins. Recent fluorescence emission studies of this compounds underlined an interesting behaviour, that is, when excited on the high-energy absorption shoulder below 400 nm the emission spectra of **1C** show a minor band at 470 nm in addition to the main band at 570 nm. This dual fluorescence has been associated with a nearly constant band ratio for any excitation below 400 nm. Is demonstrated, however, that this effect is not the result of excimer formation and must be related to the photophysics of the excited state(12). In variance, no such effect has been observed for the coumarin **1A**. In this section we present how simulation of vibronic spectra can be used to analyze two possibilities to explain this dual fluorescence. First assumption is related to additional emission from the second excited state while the other to the presence of some co-products during the photoexcitation process. Moreover, easy to dissect in theoretical model both hypothesis are not exclusive and both can give rise to the overall experimental phenomena.

Regarding the first hypotesis, in fig. 3.11 and fig. 3.12 the final emission (VG) spectrum of the 1C and 1A compounds, respectively, calculated considering two emission pathways from both the first ($S_1 \rightarrow S_0$) and the second excited state ($S_2 \rightarrow S_0$) are presented. It is evident that such simulation reproduces well both the relative positions and the relative intensities of the two emission peaks for 1C, with the whole spectra blue-shifted with respect to experiment as discussed in previous sections. This result is in agreement with experimental findings, so in favour of the assignment of the shoulder at 470 nm to the emission from the second excited state. If the same assumption is applied to the second case, coumarin **1A**, again computations predicts the double-band spectra, while only a single emission band has been observed experimentally. This finding suggest, that within the first hypothesis, both coumarins behave unlike, with the particularities going beyond the model here applied and most likely related to the dynamical processes

occurring upon excitation. However, taking into account similarity of the structures such different performance seems peculiar. Another way to explain the dual fluorescence is related to the assumption that during the photoexcitation process some co-product are created and then present in the measured sample. In such case the final spectra would result from all possible contributions, so the reactants coumarin **1A** or **1C** and some most probable photoproducts. In fig. 3.13 the possible photodissociation pathways, both homolytic and heterolytic, are presented for the example of the **1C** compound. In the left part of the scheme the homolytic route: breaking of the metoxilic bonds in two following steps is presented, while in the right part refers to a possible heterolytic pathway that brings to the formation of anionic species. In both cases, the possible bond breaking has been chosen based on the the change in the electronic density during the transition, being the same for **1A** and **1C** compounds and involving the metoxilic bond. Following this hypothesis the emission spectrum of **1A** and **1C** and of some of their co-products have been computed, the comparison of all of this spectra is represented in fig. 3.14 for **1C**. As we can see from this figure the multiple peaks of emission can be ascribed to the presence of some of photoproducts which show emission blue-shifted with respect to the **1C**, leading again to the simulated spectra in a good agreement with the experimental findings and the second less intense band well reproduced. Among the co-product considered the **1CP1** is the one that leads to the best agreement with the experimental spectrum. In the case of 1A, the most probable photoproducts show emission in essentially the same energy range as the parent component, so in this case just one broad emission band is simulated, in agreement with the experimental findings. On the overall, we can conclude that the simulation of vibronic spectra, directly comparable with experimental results provides several interesting insights which may guide further studies on the photophysical behaviour of coumarin dyes.

Coumarin	VE (f) Vacuum	VE (f) in 2V61	VE (f) in 2QC6
1A	394nm (0.7222)	367nm (0.6487)	388nm (0.6208)
1B	418nm (0.6532)	394nm (0.5642)	405nm (0.6347)
1C	471nm (0.5431)	440nm (0.3539)	463nm (0.4295)
1D	391nm (0.7617)	361nm (0.5936)	385nm (0.7955)

Table 3.2: Absorption wavelengths and oscillator strengths for the coumarin 1A, 1B, 1C and 1D in vacuum and embedded in the biological environments of 2V61 and 2QC6 proteins.

3.2.4 Coumarin optical properties in a biological environment

Finally, we present a preliminary study of the interactions of coumarins with a real biological environment. Part of these work here presented was performed during my Short Term Scientific Mission at the Group of Prof. M. Ramos at University of Porto. The aim of these work is analyze how a real biological environment, for example a protein or an enzyme, can influence the final observed optical properties of a molecular system embedded into it. In particular, we have focused on the absorption maximum wavelengths and transition intensities for the coumarins 1A, 1B, 1C discussed already along with the 1D, all presented in the fig. 3.15, computed within the simplest VE approximation.

First of all, the absorption wavelengths as well as the oscillator stenghts (f) correlated to the absorption intensity have been calculated in the vacuum for the respectively optimized coumarin equilibrium structures, and are reported in table 3.2. In a second step, the interaction with the biological environment was studied in both the 2V61 and the 2QC6 environments. The acronym 2V61 stands for human monoamine oxidase B (MAO B) whereas 2QC6 stands for the subunit alpha of the Casein Kinase 2 (CK2) that is an ubiquitous, essential, and highly pleiotropic protein kinase whose abnormally high constitutive activity is suspected to underlie its pathogenic potential in neoplasia and other diseases. The study of the influence of this two type of biological environments on molecular stuctures of chromophores allowed to obtain some insights about the structure-activity

interactions. First, it has been observed that docking of coumarin into the biological environment leads to the change in the geometry of the dye, that is the interaction with the protein changes some bond lengths and dihedrals angles, so, the resulting structure in the active site has been weakly distorted respect to those found in vacuum. This is a direct result of the electrostatic and steric interactions and the distortion permits to minimize the potential energy of the whole system. In particular the changes in geometry occurs mainly in the dihedral that connect the benzothiazene with the coumarin core leading to a structure that, at variance with the vacuum situation, is not planar. In fig. 3.15 the biological environment and the distortion of the geometries for the coumarins embedded in the 2QC6 protein are represented. In a further step, the VE absorption energies was calculated for the (distorted) structures extracted from the biological environment, so considering only the steric effects of protein on the chromophore geometry, and consequent changes in the spectral properties, (table 3.2). As we can see the values for the docked structure are different from those for the vacuum situation and in particular for 2V61 and 2QC6 environment the values for the absorption VE are smaller than in the vacuum, that is, the change in the geometrical parameters causes the blue-shift of the absorption energy. In particular the extent of the change in the VE is different for the two biological environment, namely, it is larger in the 2V61 environment than in the 2QC6, whit an average shifts of -28 nm and -8 nm respectively. This fact is probably due to the different size of the active site where the coumarin molecule is linked and the corresponding steric hindrance of the residuals of the protein, this fact directly constraints the coumarin cores to be more or less distorted. Consequently a direct correspondence between the size of the active site and the change in the absorption wavelenghts can be easily found.

In a second step we have focused in more detail on the interaction of the coumarin with the 2QC6 environment. In particular we have described the interaction of the molecules with the protein within the ONIOM scheme in order to study the electrostatic effect on the changes of the absorption spectra. The results collected from the ONIOM calculations are reported in table 3.3 and compared with those found for the vacuum equilibrium structures and the docked structure for both S_1 and S_2 states. It can be observed that although steric

Coumarin	λ_{max} equilibrium (f)	λ_{max} docked (f)	λ_{max} ONIOM (f)
1A	S1 394nm (0.7222)	S1 388nm (0.6208)	S1 391nm (0.6171)
	S2 358nm (0.0393)	S2 339nm (0.0128)	S2 387nm (0.0470)
1B	S1 418nm (0.6532)	S1 405nm (0.6347)	S1 418nm (0.6153)
	S2 387nm (0.0538)	S2 366nm (0.0076)	S2 413nm (0.0037)
1C	S1 471nm (0.5431)	S1 463nm (0.4295)	S1 498nm (0.0161)
	S2 439nm (0.0569)	S2 420nm (0.0039)	S2 472nm (0.4504)
1D	S1 391nm (0.7617)	S1 385nm (0.7955)	S1 400nm (0.6710)
	S2 370nm (0.0788)	S2 354nm (0.0100)	S2 393nm (0.0335)

Table 3.3: Absorption wavelengths and oscillator strengts for the coumarin 1A, 1B, 1C, and 1D in the 2QC6 biological environment calculated at equilibrium, in docked structure and with the ONIOM scheme.

changes lead mainly to some blue-shift of VE, the electrostatic environment instead leads to some red-shifts. In general we can state that there is no clear trend as for the magnitude of the electrostatic effect which may be lower, equal or larger than the geometrical one. As a results the overall change in the absorption VE from the equilibrium structure to the fully considered protein environment can not be easily rationalized, in fact, for **1A** and **1C** the shift is minor and negative (-3nm) and positive (+1nm), respectively while **1B** show the same VE (of 418nm) for vacuum equilibrium and distorted in the protein environment, and the largest shift, of + 9 nm, is obtained for **1D**. It can be also noted that for 1C the overall effects of biological environment leads to the exchange of excited state order, strongly stabilising the dark state described in all other cases as S2, it is interesting to note that **1C** is also the coumarin showing peculiar double-fluorescence behaviour. In general, the presence of a biological environment and the corresponding specific interactions influences the properties of the molecules embedded in the active site and both geometrical and electrostatic effects needs to be taken into account together in order to obtain a reliable description of the real situation.

3.3 Conclusions

In this chapter, we have discussed several aspects related to the analysis and simulation of electronic spectra line-shapes, which will be applied in following to the more detailed studies. First of all we analyze problems related to the selection of the most appropriate DFT functional, in order to carry out reliable computations of the optical properties of medium-to-large systems performing a benchmark study of the several widely used and recently developed DFT functionals. Here we have underlined that not only the reproduction of the maximum of the bands but also the reproduction of the spectra band-shape is very important along with the balance description of absorption and emission spectra. The most reliable functionals performing in this way seems to be the CAM-B3LYP and the M062X. However, as the conclusions may not be transferable limited benchmark computations preceding study of any new type of molecular systems can be advised. Then we have addressed issue of the choice of theoretical model to be applied for spectra simulations, and have shown how the simulations of theoretical spectra can be applied to analysis or prediction of experimental results. First we have studied the dual fluorescence of **1C** compound and explained it on the basis of two different approaches all in agreement with the experimental findings, then we have studied the docking of some coumarins with a real biological environment (2QC6 and 2V61 proteins) showing how the biological environment affect changes of the finally observed optical properties (in our case the absorption wavelengths) respect to the isolated species.

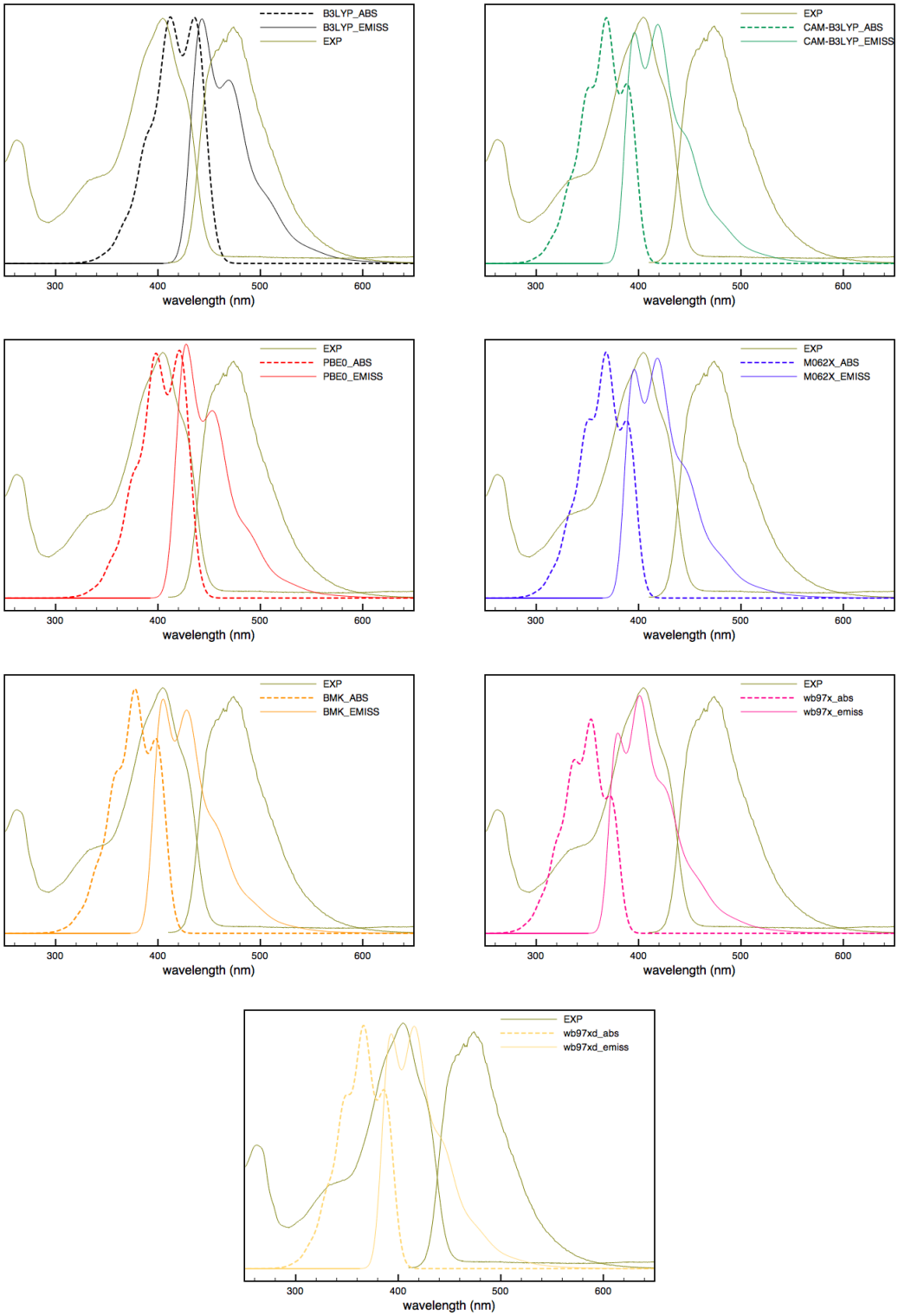

Figure 3.6: Adiabatic shift vibronic spectra for the compound **1A** calculated with different functionals.

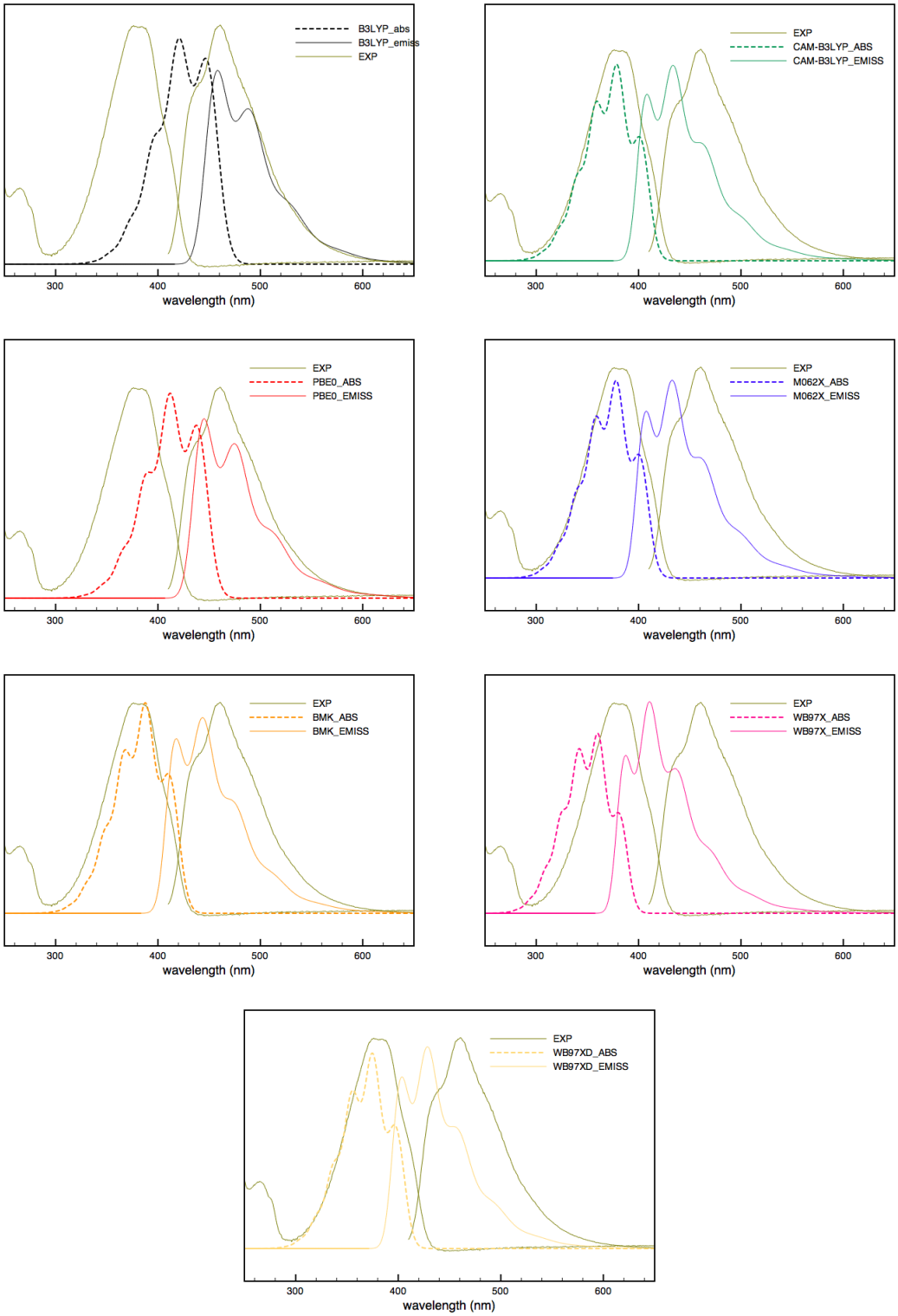

Figure 3.7: Adiabatic shift vibronic spectra for the compound **1B** calculated with different functionals.

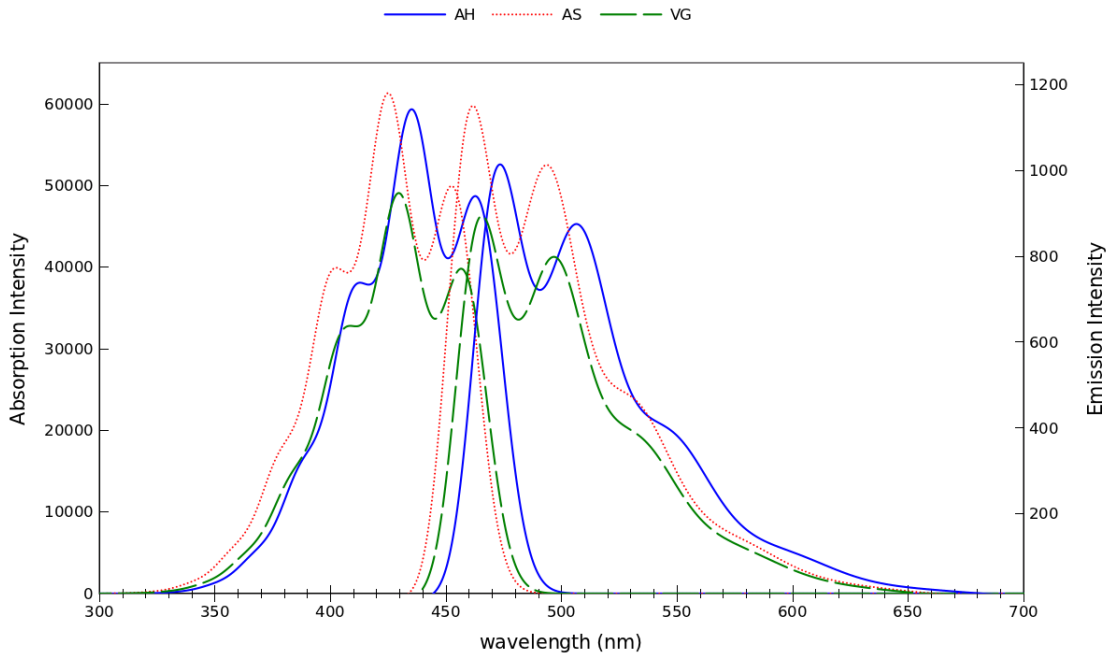

Figure 3.8: Vibrationally resolved electronic spectra for 1C molecule calculated with AH, AS and VG methods for absorption and for emission. Convolution 500cm^{-1}.

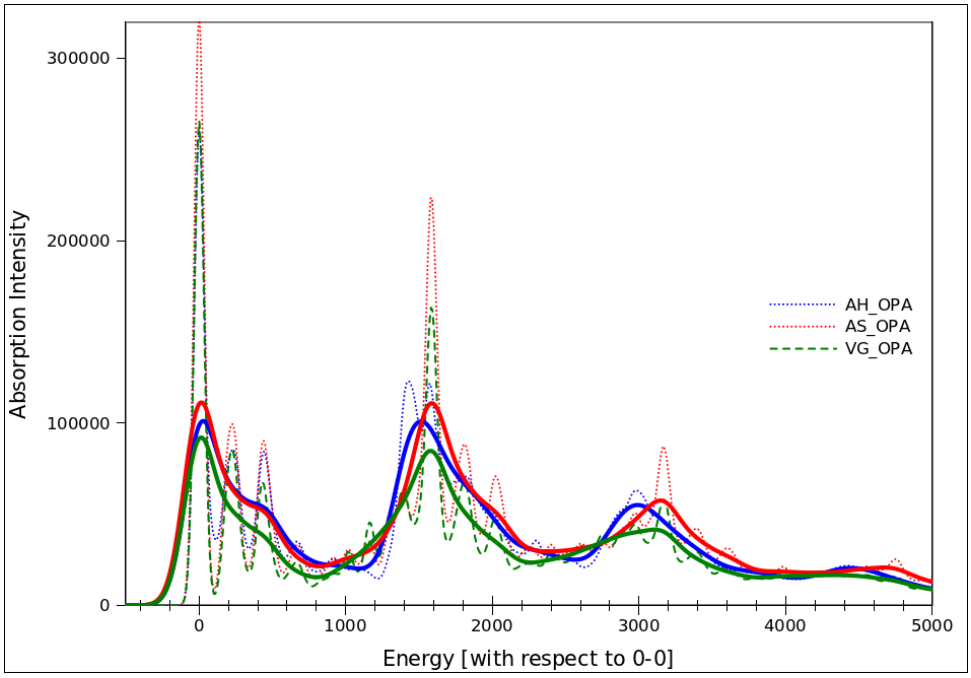

Figure 3.9: Vibrationally resolved electronic spectra for 1C molecule calculated with AH, AS and VG methods for absorption. Convolution 40cm^{-1} (dotted lines) and 123cm^{-1} (continuous lines).

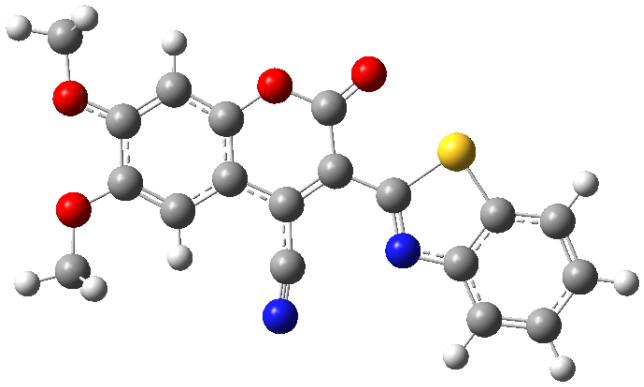

Figure 3.10: Molecular structure of compound 1C

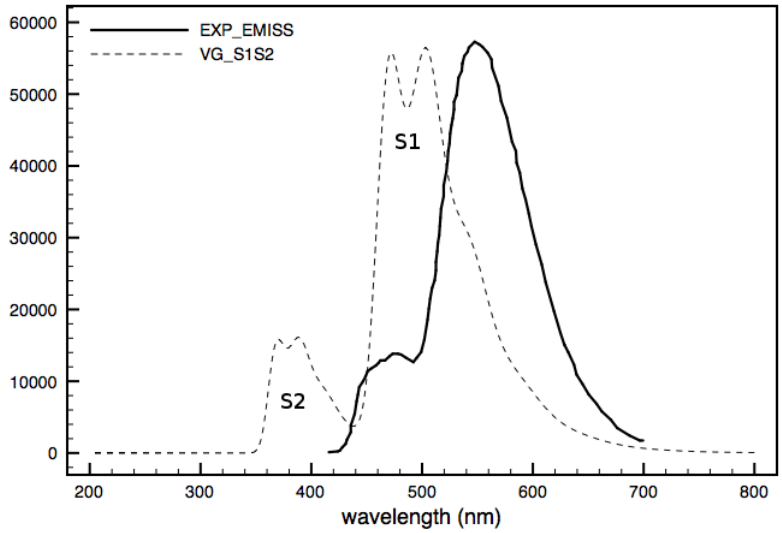

Figure 3.11: Emission spectrum of compound **1C**. The experimental band (continuous line) present two caratteristic peaks at 470nm (less intense) and 570nm (most intense). Our VG computations (dotted line) reproduces very well the experimental findings.

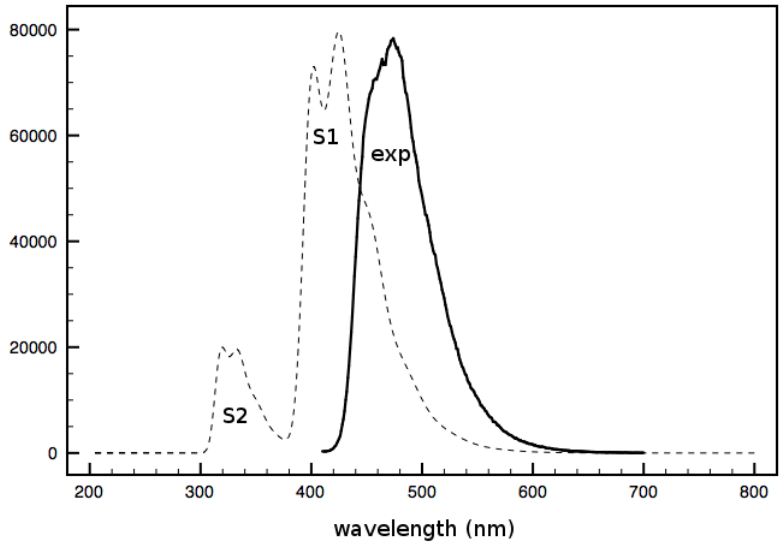

Figure 3.12: Emission spectrum of compound **1A**. The experimental band (continuous line) present only one caratteristic peak. Our VG computations (dotted line) reproduces presents two emission peaks as in the case of dual fluorescence of **1C** compound.

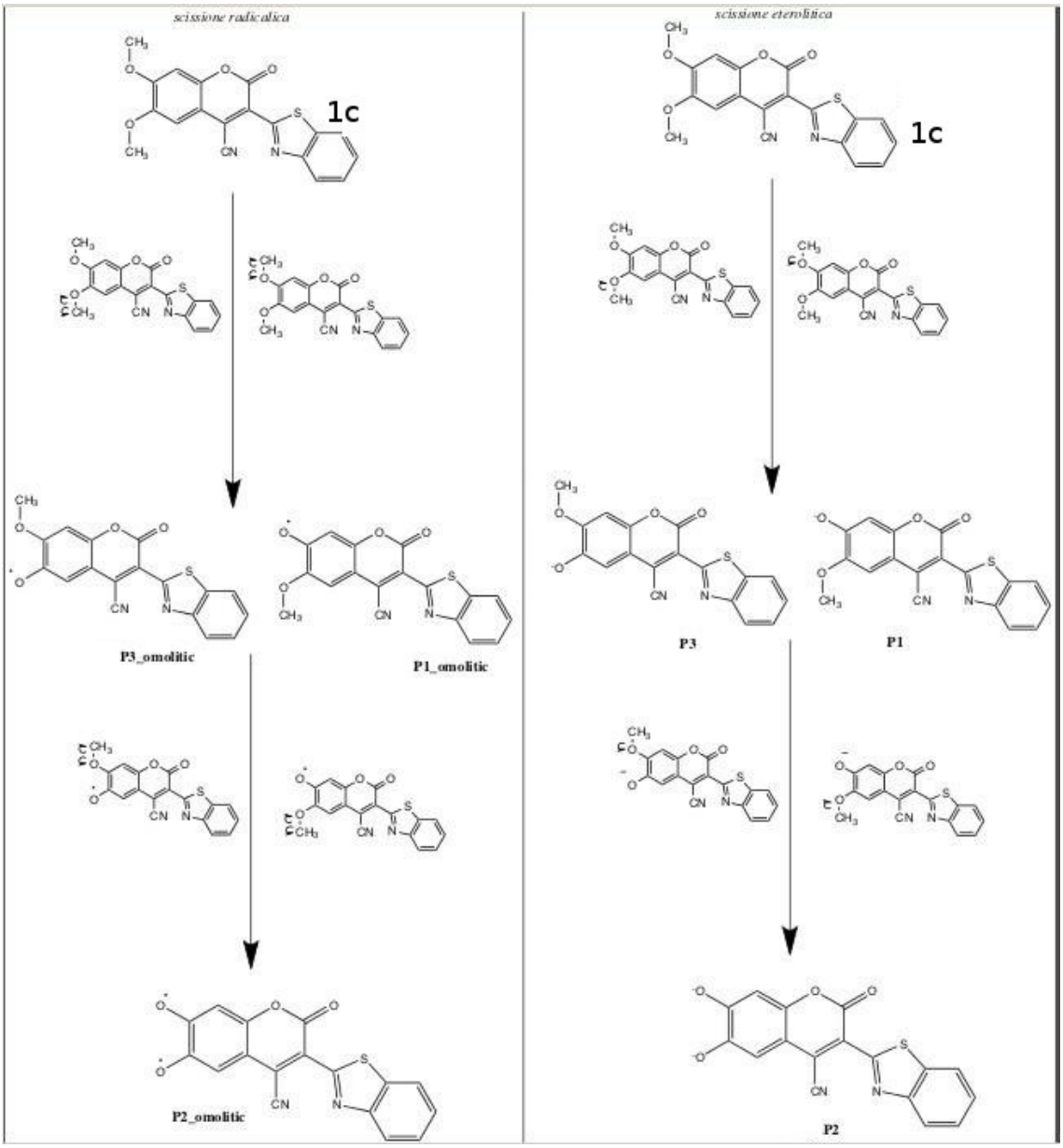

Figure 3.13: Possible pathways of dissociation of the **1C** molecule. In the left panel is represented the homolytic dissociation that brings to radicals whereas in the right part is presented the heterolytic dissociation that brings to anionic species.

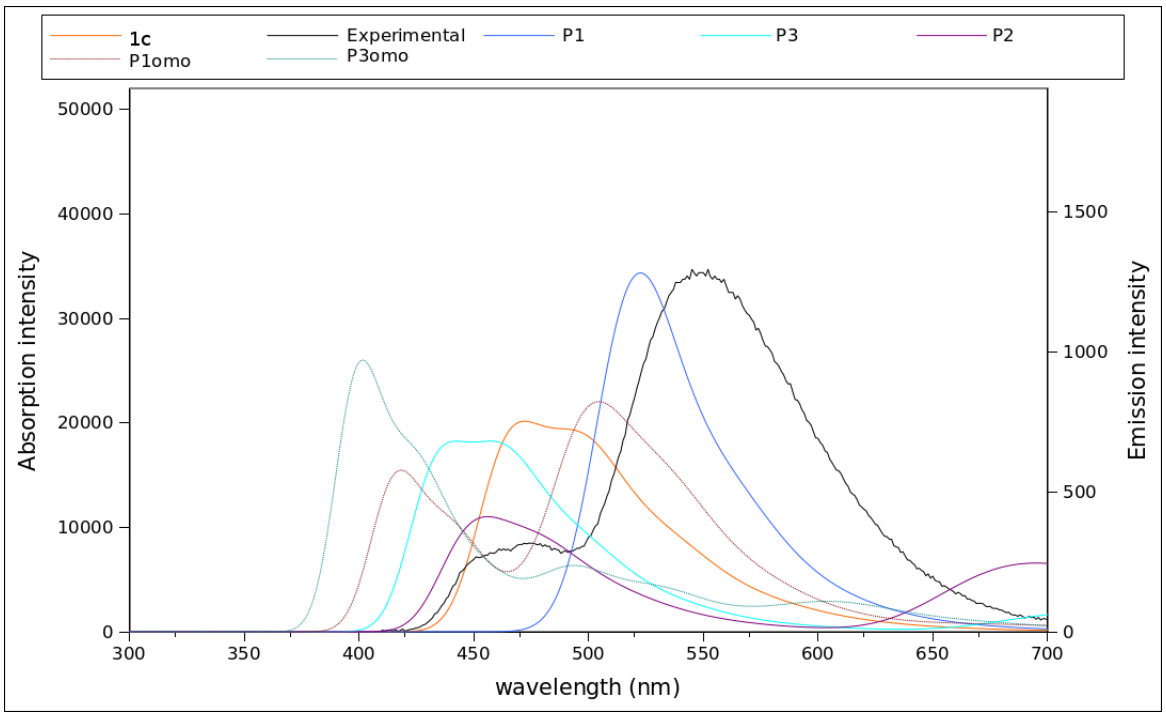

Figure 3.14: Emission spectra (VG) of **1C** and some of the radical and anionic species of fig. 3.13. Convolution 720 cm^{-1}.

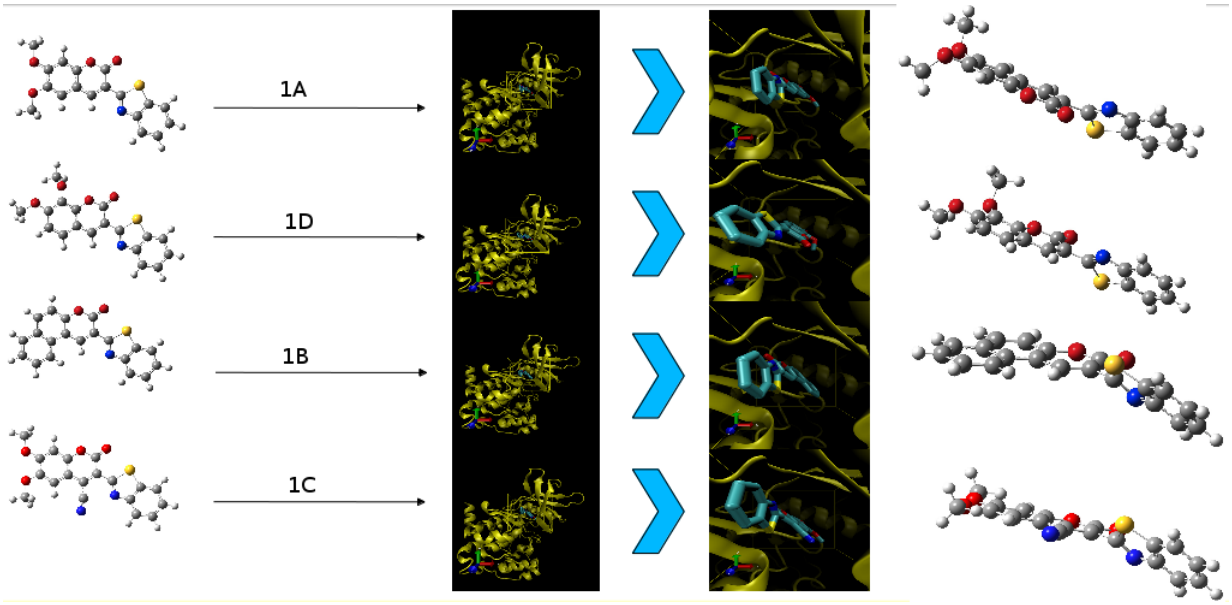

Figure 3.15: Representation of the coumarins embedded in the biological environment of 2QC6 protein.

Bibliography

[1] Hara, K.; Tachibana, Y.; Ohga, Y.; Shinpo, A.; Suga, S.; Sayama, K.; Sugihara, H.; Arakawa, H. *Solar Energy Materials and Solar Cells* **2003**, *77*(1), 89 – 103.

[2] Palmas, S.; Pozzo, A. D.; Mascia, M.; Vacca, A.; Ricci, P. *Chemical Engineering Journal* **2012**, *211*, 285 – 292.

[3] Hoult, J.; Paya, M. *General Pharmacology: The Vascular System* **1996**, *27*(4), 713 – 722.

[4] Cho, J.-Y.; Hwang, T.-L.; Chang, T.-H.; Lim, Y.-P.; Sung, P.-J.; Lee, T.-H.; Chen, J.-J. *Food Chemistry* **2012**, *135*(1), 17 – 23.

[5] Borges, F.; Roleira, F.; Milhazes, N.; Santana, L.; Uriarte, E. *Current Medicinal Chemistry* **2005**, *12*(8), 887–916.

[6] Chen, Y.; Fan, G.; Chen, B.; Xie, Y.; Wu, H.; Wu, Y.; Yan, C.; Wang, J. *Journal of Pharmaceutical and Biomedical Analysis* **2006**, *41*(1), 105 – 116.

[7] Stein, A. C.; Ãlvarez, S.; Avancini, C.; Zacchino, S.; von Poser, G. *Journal of Ethnopharmacology* **2006**, *107*(1), 95 – 98.

[8] Ito, C.; Itoigawa, M.; Onoda, S.; Hosokawa, A.; Ruangrungsi, N.; Okuda, T.; Tokuda, H.; Nishino, H.; Furukawa, H. *Phytochemistry* **2005**, *66*(5), 567 – 572.

[9] Yu, D.; Suzuki, M.; Xie, L.; Morris-Natschke, S. L.; Lee, K.-H. *Medicinal Research Reviews* **2003**, *23*(3), 322–345.

[10] Cravotto, G.; Nano, G. M.; Palmisano, G.; Tagliapietra, S. *Tetrahedron: Asymmetry* **2001**, *12*(5), 707 – 709.

[11] Fylaktakidou, K. C.; Hadjipavlou-Litina, D. J.; Litinas, K. E.; Nicolaides, D. N. *Current Pharmaceutical Design* **2004**, *10*(30), 3813–3833.

[12] Signore, G.; Nifosi, R.; Albertazzi, L.; Storti, B.; Bizzarri, R. *Journal of the American Chemical Society* **2010**, *132*(4), 1276–1288.

[13] Becke, D. *J. Chem. Phys.* **1993**, *98*, 5648–5652.

[14] Yanai, T.; Tew, D. P.; Handy, N. C. *Chem. Phys. Lett.* **2004**, *393*, 51–57.

[15] Adamo, C.; Barone, V. *J. Chem. Phys.* **1999**, *110*, 6158–6170.

[16] Jacquemin, D.; Perpète, E.; Scalmani, G.; Frisch, M. J.; Kobayashi, R.; Adamo, C. *J. Chem. Phys.* **2007**, *126*, 144105/1–12.

[17] Zhao, Y.; Schults, N. E.; Truhlar, D. G. *J. Chem. Theory Comput.* **2006**, *2*, 364–382.

[18] Zhao, Y.; Truhlar, D. G. *Theor. Chim. Acta* **2008**, *120*, 215–241.

[19] Boese, A. D.; Martin, J. M. L. *J. Chem. Phys.* **2004**, *121*(8).

[20] Chai, J.-D.; Head-Gordon, M. *J. Chem. Phys.* **2008**, *128*, 084106/1–15.

[21] Chai, J.-D.; Head-Gordon, M. *Phys. Chem. Chem. Phys.* **2008**, *10*, 6615–6620.

[22] Double and triple-ζ basis sets of sns and n07 families, are available for download. **2012**.

[23] Barone, V.; Cimino, P.; Stendardo, E. *J. Chem. Theory Comput.* **2008**, *4*, 751.

[24] Barone, V.; Cimino, P. *Chem. Phys. Lett.* **2008**, *454*, 139–143.

[25] Barone, V.; Cimino, P. *J. Chem. Theory Comput.* **2009**, *5*, 192–199.

[26] Barone, V.; Bloino, J.; Biczysko, M. *Phys. Chem. Chem. Phys.* **2010**, *12*, 1092–1101.

[27] Carnimeo, I.; Biczysko, M.; Bloino, J.; Barone, V. *Phys. Chem. Chem. Phys.* **2011**, *13*, 16713–16727.

[28] Biczysko, M.; Bloino, J.; Carnimeo, I.; Panek, P.; Barone, V. *J. Mol. Struct.* **2012**, *1009*, 74–82.

[29] Biczysko, M.; Bloino, J.; Brancato, G.; Cacelli, I.; Cappelli, C.; Ferretti, A.; Lami, A.; Monti, S.; Pedone, A.; Prampolini, G.; Puzzarini, C.; Santoro, F.; Trani, F.; Villani, G. **2012**, *131*, 1201/1–19.

[30] Barone, V.; Baiardi, A.; Biczysko, M.; Bloino, J.; Cappelli, C.; Lipparini, F. *Phys. Chem. Chem. Phys.* **2012**, *14*, 12404–12422.

[31] Bloino, J.; Biczysko, M.; Santoro, F.; Barone, V. April **2010**, *6*(4), 1256–1274.

[32] M., C.; G., S.; N., R.; V., B. *J. Comput. Chem.* **2003**, *24*, 669.

[33] N.M.F.S.A., C.; J., R.; P.A., F.; M.J., R. *International Journal of quantum chemistry* **2011**, *111*, 1208–1212.

[34] Dapprich, S.; Komaromi, I.; Byun, K. S.; Morokuma, K.; Frisch, M. J. *J. Mol. Struct. (Theochem)* **1999**, *462*, 1–21.

[35] Rappe, A. K.; Casewit, C. J.; Colwell, K. S.; III, W. A. G.; Skiff, W. M. *J. Am. Chem. Soc.* **1992**, *114*, 10024–35.

[36] Rappe, A. K.; Bormann-Rochotte, L. M.; Wiser, D. C.; Hart, J. R.; Pietsch, M. A.; Casewit, C. J.; Skiff, W. M. *Mol. Phys.* **2007**, *105*, 301.

[37] Biczysko, M.; Bloino, J.; Brancato, G.; Cacelli, I.; Cappelli, C.; Ferretti, A.; Lami, A.; Monti, S.; Pedone, A.; Prampolini, G.; Puzzarini, C.; Santoro, F.; Trani, F.; Villani, G. *Theor. Chim. Acta* **2012**, *131*, 1201.

CHAPTER 4

ENVIRONMENTAL AND COMPLEXATION EFFECTS ON OPTICAL PROPERTIES OF ALIZARIN AND ALIZARIN-MG(II)/AL(III) COMPLEXES

4.1 Introduction

Computational modeling recently received significant attention also in the cultural heritage field, in connection with restoration and conservation of art or historical objects(1; 2). From an experimental point of view, a broad range of methodologies are now employed to investigate artistic materials(1; 3), such as spectrophotometric and fluorimetric techniques in the ultraviolet-visible (UV-Vis) energy range (4), infrared (IR)(5; 6) and Raman(7) spectroscopies, as well as nuclear magnetic resonance (NMR) (8), with additional impor-

tant contributions provided by other analytical tools like mass spectrometry (MS) (9), chromatography and X-Ray diffraction (XRD) (10). Spectroscopic techniques are particularly suited for the characterisation of works of art or other unique objects such as archeological samples, since they provide very detailed information on the system under investigation by means of non-invasive studies. However, the analysis of the rich information coming from experimental studies is particularly difficult in the field of cultural heritage, due to the inherent complexity of the materials together with the often unknown composition ofthe sample. A significant aid in rationalizing experimental data is offered by computational approaches (11; 12; 13; 2), which provide also deeper insights into the nature and composition of the artistic materials and detailed descriptions of the physical and chemical changes that bring to degradation processes responsible for their modifications. It can be foreseen that the availability of reliable and user-friendly computational tools(14; 15) combined with the possibility to describe larger and more complex molecular systems (16; 17; 18; 19; 20; 21) at a reasonable cost will increase the use of computational models in the cultural heritage field. The possibility to simulate and predict the overall spectroscopic properties, has been recently demonstrated for a set of novel chromophores(22) or NIR-emitting fluorescence probes(23), for the latter taking into account both the pH-dependence and the possible coexistence of different tautomers in solution. In the present work we will focus on environmental factors responsible for the ageing and colour modification of ancient pigments exploiting recently developed and implemented computational spectroscopy approaches(24; 15) to analyse the optical properties of alizarin-based pigments. It will be shown how the simulation of the electronic band line-shape allows the direct comparison with experimental outcomes and a detailed analysis of experimentally observed vibrational contributions(25), taking also into account that the band shape is directly responsible for the colour perceived by the human eye(26).

Alizarin is one of the most known and stable organic dyes and is found as the main component, with purpurin and quinizarin, of the *madder lake* pigment, known to painters as *Rose Madder* and *Alizarin Crimson*. Extracted from *Rubia Tinctorum* roots(27) since 3.000 BC, it has been widely used in Europe during the XVI century in both artistic

painting and textiles. Although alizarin has been nowadays largely replaced by other commercial colorants, its synthetic lake pigment can be still found in contemporary works of art. Due to the availability of an abundant set of experimental data, alizarin-based systems stand as suitable cases to define and validate computational approaches, which can be further applied to the analysis of other ancient pigments, and in general for the application of computational spectroscopy in the field of cultural heritage. Moreover, alizarin as a chromophore received some attention also for technological(28; 29; 30) applications while its capability to form stable complexes with different metal atoms (31; 32), also shown by its most common derivatives has led to their use in medicine (33; 34) and chemical analysis(35; 36).

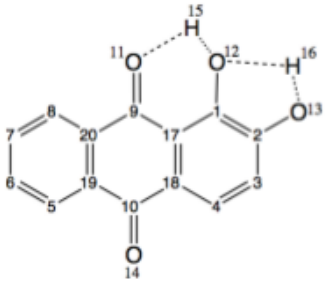

Figure 4.1: Molecular structure and atom labelling of Alizarin

The structure of alizarin is sketched in Figure 4.1, along with the atom labelling. The chromophoric functional groups (the two carbonyls at positions 9 and 10 and the two hydroxyls bound to carbons 1 and 2) are responsible for alizarin's optical properties in the visible region and, except for the carbonyl in position 10, they can also act as binding groups between the dye and the support base through an intermediate metal atom called *mordant*. Neutral free alizarin can exist in several tautomeric forms in solution while pH increase leads by subsequent deprotonation to mono-anionic and di-anionic forms (see Figure 4.2). Moreover, for alizarin complexes with metal cations, there are also different possibilities of metal-ligand complexation, namely, 1,2-dihydroxyl alizarin (1,2Aliz) or 1-hydroxy-9-keto alizarin (1,9Aliz) (see Figure 4.2). It has been postulated(37; 38) that alizarin complexes in solution are essentially mixtures of these two forms. Absorp-

tion and emission processes of free and complexed alizarin in the UV-Vis energy range have been studied both experimentally(39; 40; 41; 4; 42) and computationally(43; 44; 45), including also environmental effects on the final optical properties. In fact, the strong dependence on environmental conditions (e.g. solvation) was well-known to artists who considered alizarin-based pigments as fugitive colours. This "real life" observation of colour modifications caused by ageing and exposition to pollutants have been confirmed by UV-Vis experimental analysis to be largely related to pH changes(46; 25). However, the pH and the solvent are not the only possible factors responsible for modifying the chromatic properties of alizarin. Indeed, complexes formed with metals (Al(III), Cr(III), Ni(II), Cu(II), Zn(II), Cd(II), Fe(III)) (47; 48; 49) are reported to red-shift (from 0.34 to 1.55 eV, depending on the metal atom (47)) the visible band with respect to the isolated chromophore, leading eventually to further changes in the madder colour (50). Both environmental effects are concomitantly present and influence madder lake colour changes, while computational studies allow to dissect the specific role of pH and non-specific environmental effects from the ones related to the metal complexation. In this work we have chosen to consider coordination with magnesium Mg(II) and aluminium Al(III), in order to dissect factors leading to their different effect on alizarin spectra properties, taking also into account that both these metals may act as binding sites in complex molecular systems. Better knowledge about the composition of such ancient pigments (e.g. Maya blue) can also lead to new materials like the stable nano-composites formed by alizarin with palygorskite (component of the Maya blue pigment) which represent innovative solid pH sensors inspired by Mayas "nanotechnologies" (51). In this respect computational modeling of alizarin-metal complexes is a first, necessary, step toward modeling the hybrid nano-pigments(52). As the complexes with Al(III), the most predominant ingredient of madder lake, have been the focus of several experimental and theoretical investigations(53; 54; 55), a more detailed study will be performed on alizarin-Mg complexes, for which only some structural and thermodynamic properties(49; 47; 56) are well established, despite the improved environment-friendship of this pigment. Moreover, alizarin complexes with different metal atoms show similar structures, with an almost unaffected anthraquinonic

backbone and the metal atom placed very close the molecular plane(47). This suggests that some conclusions on the spectra line-shape and vibronic contributions can be quite general, and transferable to other alizarin-metal systems.

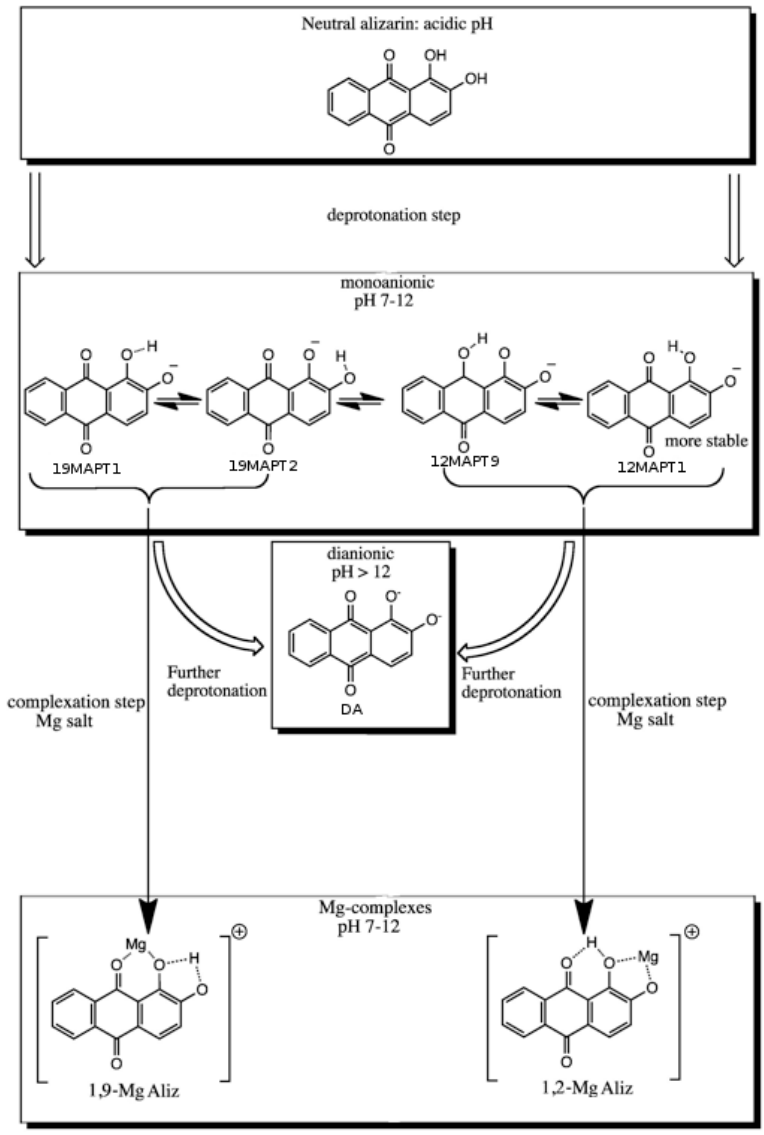

Figure 4.2: Indicative alizarin deprotonation and complexation paths in weakly alkali media.

This chapter is organised as follows: details on computational approaches including a discussion on methodological aspects of spectra simulations are gathered in section 4.2. Environmental, namely: metal complexation and pH effects, modifying electronic spectra

line-shape, and in consequence pigment colour are discussed in section 4.3. Final conclusions including the applicability of the computational approaches to studies of optical properties for complex molecular systems of relevance in the cultural heritage field are given in section 4.4.

4.2 Computational details

4.2.1 DFT and TD-DFT computations

All the electronic structure calculations have been performed using methods rooted into the density functional theory (DFT) (57; 58) and its time-dependent extension (TD-DFT) (59) for the ground and excited states, respectively. For all systems, full geometry optimisations in the electronic ground state have been performed and followed by harmonic frequency computations. Then, vertical excitation energies (VE) and energy gradients have been computed for the relevant excited electronic states, at the ground-state geometries.

The long-range corrected CAM-B3LYP Coulomb attenuated functional (60) has been applied to all computations in view of its balanced description of both ground- and excited-state properties, including also vibrational frequencies(60; 61; 62). This functional has been also shown to perform well over a large spectral range with similar molecular systems, providing, for instance, accurate vertical excitation energies for 9,10-anthraquinone dyes (63) and reliable vibrationally-resolved absorption spectra line-shapes for a series of anthraquinoidic dyes(64). All computations have been performed employing the *aug*-N07D basis set(65; 66), built from the reliable and effective N07D polarised double-zeta basis set(67; 68) (modified with respect to original formulation to include consistently diffuse s functions on all heavy atoms) by adding a set of diffuse d functions for heavy atoms.

In order to further check the reliability of adopted computational approach, the relative energies of the two tautomeric forms related to the proton transfer (PT) within the

O(11)-H(15)-O(12) frame [PT9: O(11)-H(15)$\cdots$O(12) and PT1: O(11)$\cdots$H(15)-O(12)], and corresponding excitation wavelengths computed at DFT/TD-DFT level with CAM-B3LYP/*aug*-N07D have been compared to other theoretical approaches. Table 4.1 shows clearly that the relative stabilities of the two proton-transfer minima in the ground electronic state are confirmed by all theoretical models, with CAM-B3LYP, ω-B97XD(69; 70) and M06-2X(71; 72) giving PT1 structures slightly more stable than B3LYP(73) and PBE0(74). We note that CAM-B3LYP functional slightly underestimates the proton-transfer barriers, with the Mean Signed Deviations (MSD) lower than 1.5 kJ/mol, but larger deviations, both positive and negative are found for other functionals on their respective optimized geometries(75). Moreover, for all structures, the CAM-B3LYP/*aug*-N07D excitation energies agree well with the results from M06-2X and ω-B97XD, while standard B3LYP and PBE0 functionals predict the $S_1 \leftarrow S_0$ transition energy to be lower by about 0.4 eV. We note that on the basis of vertical excitation energies only it is difficult to define the best performing functional. The seemingly better agreement between PBE0 and B3LYP vertical excitation energies and experimental λ_{max} in solution may be attributed to the lack of vibronic and solvent dynamic effects as shown by the electronic spectra line-shapes discussed in Ref.(76). Taking into account vibronic effects a good agreement with experiment for mono-anionic alizarin and its metal complexes has been obtained by computations with CAM-B3LYP *vide infra*. Moreover, CAM-B3LYP has been already shown to provide improvements over B3LYP for the the description of Rydberg and charge transfer states(77), and recently it has been included (along with M06-2X and ω-B97XD) into the set of the eight best performing density functionals(78) recommended for excited electronic state studies. On these grounds this functional has been applied in all spectra simulations. However, we note that in this work we will focus on the analysis of electronic spectra line-shapes, which facilitate a qualitative interpretation of environmental effects on dye optical properties. In fact the absolute excitation energy may be often affected by the choice of functional while the band-shape is usually qualitatively well reproduced by several functionals, at least as far as broad-band in solution are considered(79). In our opinion simulation of electronic-spectra line-shapes

facilitates analysis of experimental results and helps to overcome difficulties related to the accurate estimates of excitation energies. Finally, we note that the *aug*-N07D basis set provides results fully consistent with its larger 6-311+G(d,p) counterpart also for ground- and excited-state energies for systems with Mg(II) and Al(III) ions.

Experimental studies of free and complexed alizarin have been performed in several polar(80; 45; 25; 81; 82; 53) and non-polar(46) solvents, with all spectra recorded in polar solvents (methanol(81) and mixtures: water-methanol(80; 53), water-DMSO(45; 25) or water-dioxan(82)) showing essentially the same spectral features. In the following, the non-specific solvent effects are taken into account by means of C-PCM (*Conductor-Polarizable Continuum Model*) (83; 84; 85) using the default parameters for the cavity definition. Moreover solvent effects on the vertical excitation energies are computed with the linear response LR-PCM/TD-DFT approach within the non-equilibrium regime(86; 87; 88; 89; 59; 90). Additionally, specific solute-solvent interactions, namely the metal coordination by explicit water molecules for alizarin-Mg/Al complexes, and solvent effect on the proton transfer in the 1,2NT alizarin, have been taken into account considering up to four explicit H_2O molecules.

4.2.2 Simulation of electronic spectra line-shape

Computations of vibrationally-resolved electronic spectra have been performed through an integrated procedure (described in detail in references (15; 24)) based on the overlap integrals, also known as Franck-Condon (FC) integrals, between the vibrational wave-functions of the electronic states involved in the transition. It allows to define several computational models and levels of approximations related to the description of normal modes and electronic transition dipole moments. As a general rule, normal modes in the two electronic states are different and the resulting mode-mixing can be taken into account though a linear transformation proposed by Duschinsky (91): $\mathbf{Q} = J\mathbf{Q}' + \mathbf{K}$; where$\mathbf{Q}$ and $\mathbf{Q}'$ represent the mass-weighted normal coordinates of the initial and final electronic states, respectively; the Duschinsky matrix J describes the projection of the

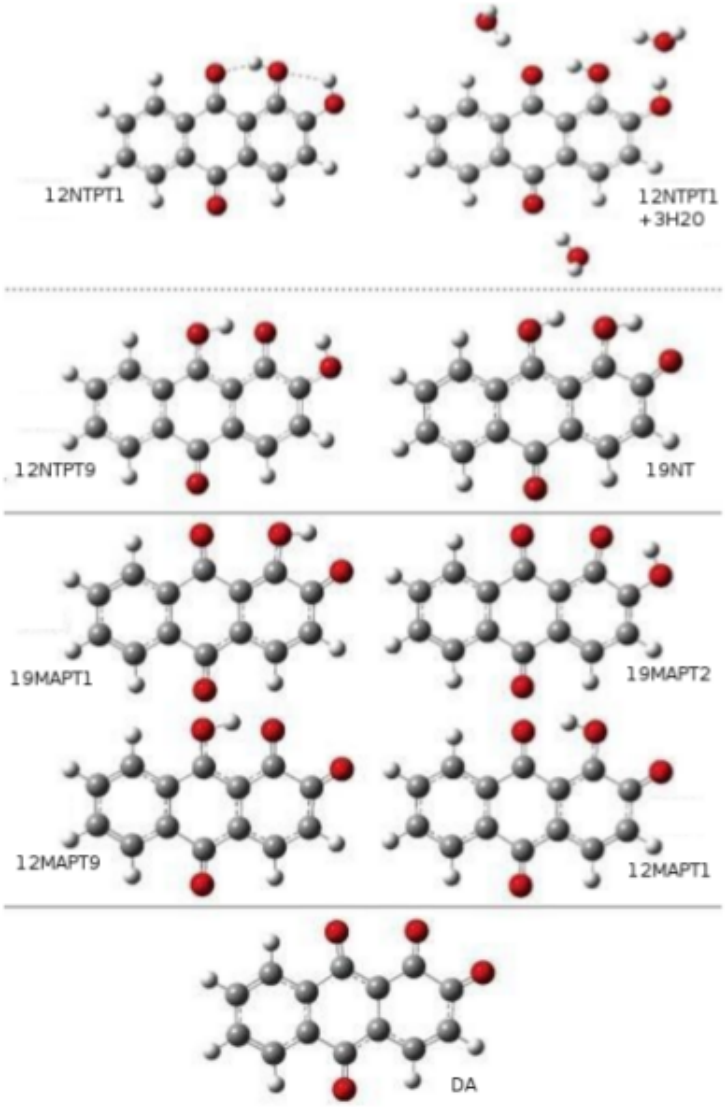

Figure 4.3: The most relevant tautomeric structures of neutral (NT), mono-anionic (MA) and di-anionic (DA) alizarin.

Table 4.1: Relative energies (Δ E_{PT}=E_{PT1}-E_{PT9} [kJ/mol]) of the two proton-transfer (PT1 and PT9) tautomers in the ground state, and absorption wavelengths (λ [nm]) of the $S_1 \leftarrow S_0$ (HOMO-LUMO) electronic transition for free neutral and mono-anionic Alizarin and 1,2Mg/Al-Alizarin complexes in methanol/water solution. DFT/TD-DFT computations with several density functionals and basis sets. Bulk solvent described by the CPCM model, specific solvent effects considered by adding n=(4) water molecules in solvation sphere. All TD-DFT values computed within the non-equilibrium solvation regime.[a]

	Alizarin						1,2Me-Alizarin complex					
	1,2NT			1,2MA			1,2Mg-Aliz$(H_2O)_4$			1,2Al-Aliz$(H_2O)_4$		
Method	Δ E_{PT}	λ_{PT1}	λ_{PT9}	Δ E_{PT}	λ_{PT1}	λ_{PT9}	Δ E_{PT}	λ_{PT1}	λ_{PT9}	Δ E_{PT}	λ_{PT1}	λ_{PT9}
CAM-B3LYP/*aug*-N07D	-25.2	369	463	-21.6	506	588	-10.9	423	533	24.3	377	469
B3LYP/*aug*-N07D	-13.3	434	523	-16.5	619	677	-3.3	511	622	30.8	449	557
PBE0/*aug*-N07D	-19.9	418	508	-16.9	587	640	-2.6	488	599	30.3	430	535
CAM-B3LYP/6-311+G(d,p)	-30.3	368	462	-23.7	501	587	-13.7	423	532	21.9	376	468
B3LYP/6-311+G(d,p)	-23.3	434	522	-18.0	611	674	-5.9	511	621	28.5	448	556
PBE0/6-311+G(d,p)	-22.0	417	506	-15.8	583	643	-5.1	488	598	27.9	429	534
ω-B97XD/6-311+G(d,p)	-30.8	365	459	-25.3	492	581	-14.4	417	525	23.8	373	463
M06-2X/6-311+G(d,p)	-32.1	370	461	-25.6	496	593	-16.1	415	533	19.4	375	463
Exp.		430[b],429[c]	550[b]		540[b]			427.5[d]			479.5[d], 473[c]	

[a] Geometry structures of alizarin and its complexes are depicted in Figures 4.3 and 4.6, respectively.

[b] Experimental data from Ref. (81) measured in methanol solution.

[c] Experimental data from Ref. (53) measured in methanol-water solution.

[d] Experimental data from Ref. (82) measured in dioxan-water solution.

normal coordinate basis vectors of the initial state on those of the final state and vector **K** represents the displacements between the initial and the final state structures. In the present work we have chosen to resort to the vertical gradient model coupled to the Franck-Condon approximation (VG|FC). This is also known in literature as the linear coupling model (LCM) (92) and relies on the observation that the most intense transitions are vertical. The VG model represents a good compromise between computational cost and accuracy, allowing also an analysis of the main vibronic contributions, whenever Duschinsky effects(91) do not play an important role. The vertical approach is well-suited for the simulation of the broad features of the low-resolution spectrum in solution, and its VG approximation is particularly advocated whenever several electronic states and/or molecular systems need to be considered(92; 15; 93). In order to check the validity of the above mentioned assumptions for alizarin, the adiabatic models, namely Adiabatic Hessian (AH) and its approximated variant Adiabatic Shift (AH, see Ref. (93) for a more detailed discussion on the vertical and adiabatic approaches) have been applied to a case study, the lowest electronic transition of the di-deprotonated alizarin (labeled as DA in Figure 4.3), which shows three distinct features in the 450–650 nm range(45; 25) tentatively assigned to the vibronic structure(25). Spectra simulated with the Adiabatic Shift (AS) and Adiabatic Hessian (AH) models, i.e. with the same normal modes and vibrational frequencies in both electronic states or with frequency differences and normal mode mixing taken into account, respectively, are presented in Figure 4.5. Both spectra, show very similar line-shapes, but slightly shifted positions in an absolute energy range. These results suggest that Duschinsky effects do not play a significant role and in this case they can be safely neglected (it is also evident from an analysis of overlap matrix J between the normal modes of the ground and excited electronic states, which is near-diagonal). On the contrary, a shift of the electronic transition origin ($\langle \mathbf{0} \mid \mathbf{0} \rangle$) should be ascribed to the frequency differences between initial and final states, which in turn affect zero point vibrational energies (ZPVE). It should be noted that the spectrum obtained by the most accurate (and computationally expensive) AH|FC model shows the best match with experiment, so agreement between simulated and experimental spectra discussed in

the following sections could be improved by taking into account ZPVE changes. However, results for di-anionic alizarin suggest that since ZPVE corrections are nearly constant (of the order of 0.1 eV), they can be safely neglected in a qualitative analysis of the different effects influencing the overall spectra. Next, comparing the vertical and adiabatic models, we note that the difference between VG|FC and AS|FC is only related to different ways of estimating the shift vector ($\mathbf{K}$) between the equilibium structures in both electronic states: the elements of the "vertical" $\mathbf{K}$ should be considered "effective" displacements, at variance with the correct displacement used in adiabatic methods. When the harmonic approximation is exact, the vertical and adiabatic approaches are equivalent. In all practical cases, they differ and both have strong and weak points. Generally speaking, adiabatic models are better suited for the analysis of the bands closer to the $\langle \mathbf{0} \mid \mathbf{0} \rangle$ origin and more generally reproduce better the fine structure of the spectra, while vertical models describe well the region of the spectrum maximum and give a better account of the most intense bands(93; 94; 95; 96). In the present case, the good agreement between VG and AS spectra confirms the reliability of the harmonic approximation. Finally, we note that the difference between the AH|FC and VG|FC models is mostly related to frequency changes. The latter lead to the shift of the $\langle \mathbf{0} \mid \mathbf{0} \rangle$ transition (in the same way the AS model) and to slightly different relative positions of the vibronic absorption maxima. However, both spectra show very similar overall line-shapes, while correction for zero-point vibrational energy (ZPVE) differences, more accurately taken into account in the AH approach leads to a red-shift smaller than 0.1 eV. In order to emphasize the good agreement between the experimental and simulated VG|FC spectra, in particular considering the relative position of the vibronic maxima, the simulated spectra have been red-shifted by 0.22 eV (52 nm, 32 nm would be required in the case of AH|FC). The same red-shift has been applied to the spectra obtained by simple convolution of the vertical excitation energy (with the same HWHM of 500 cm^{-1} as applied to the VG|FC spectra). Such a comparison, presented in Figure 4.4, clearly shows that inclusion of vibrational contributions is necessary to reproduce correctly the experimental outcomes and can not be obtained by increasing the HWHM used to convolute vertical energy. It is worth noting that agreement on the

relative positions between experimental and simulated spectra can be improved also by mean of hybrid QM/QM' models. Such approaches allow to take into account the vibrational structure of electronic bands (computed at the TD-DFT level), and to correct the absolute values of vertical excitation energies by applying more accurate computational approaches(97) (e.g larger basis sets, or coupled cluster models(98)). On these grounds, application of VG|FC model to simulate the broad spectral features of free alizarin and its Mg(II) and Al(III) complexes is fully validated. We only note that AH approaches should be always considered for a detailed analysis of well resolved experimental spectra and for a preliminary validation of any approximated model, whenever a new system is to be studied.

Furthermore, in order to simulate the electronic spectra in the full UV-vis energy range, the ground-state equilibrium structure and harmonic frequencies have been computed, along with the energy gradient for each relevant excited electronic state, considering that dark states, which do not contribute to the spectra line-shape can be safely discarded. VE computations have been used to identify dipole-allowed electronic transitions with a medium-to-large oscillator strength (f) value, in order to select the excited states on which to focus our attention. The final FC|VG spectra for each system/conformer have been obtained by summing the single-state transitions of all excited electronic states considered. The stick spectra have been convoluted by means of Gaussian functions with half-width at half-maximum (HWHM) equal to 500 cm^{-1}, this value being chosen according to the broad features of the reference experimental absorption spectra(80; 45; 25; 81; 82). Moreover, it has been shown(44) that, in particular for the mono-anionic form, several, probably co-existing, tautomeric forms need to be taken into account in the spectra simulations. Thus, the final spectra have been obtained by adding the single tautomer contributions, with the weight of the i^{th} tautomer (P_i) computed by Boltzmann averaging at 298 K and 1 atm:

$$P_i = \frac{e^{\frac{-\Delta G_i}{Nk_bT}}}{\sum_{j=1}^{n} e^{\frac{-\Delta G_j}{Nk_bT}}} \tag{4.1}$$

where ΔG_i is the relative Gibbs free energy of tautomer i with respect to the most

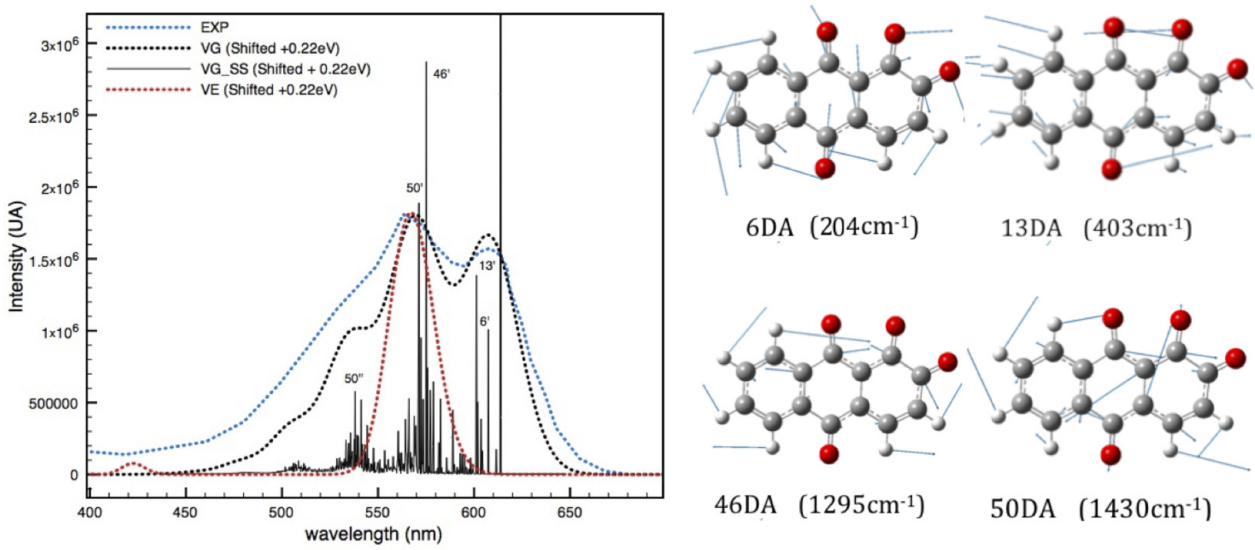

Figure 4.4: Experimental(45; 25) and theoretical electronic spectra of di-anionic alizarin. The spectra were computed at the VG|FC and VE levels, and red-shifted by 0.22 eV. Both theoretical spectra have been convoluted with a HWHM of 500 cm^{-1}. The VG|FC stick spectrum, which shows the single vibrational contributions to the $S_1 \leftarrow S_0$ electronic transition, is also presented. The most intense transitions for each distinct band are indicated by specifying the normal modes excited in the final state, depicted in the right panel, and the associated number of quanta

stable one. N and k_b are the Avogadro and Boltzmann constants, respectively. The ΔG_i computed by the standard harmonic-oscillator rigid-rotor (HORR) model have been sufficient for the purpose of the present work, while the computations with anharmonic-oscillator hindered-rotor approach(99) should be considered for more refined energetic study.

All calculations have been performed with the GAUSSIAN(100) suite of programs.

4.3 Results and discussion

4.3.1 Structure of Alizarin and its metal complexes

Free Alizarin

Formation of alizarin metal complexes, is preceded by the formation of ionic forms of alizarin, thus we start from discussion on the most stable tautomeric forms of neutral, mono- and di-anionic alizarin. All structures are shown in Figure 4.3, while Table 4.2 reports the most important geometry parameters, Gibbs free energy values (ΔG) and Boltzmann populations. All structures correspond to local minima in the ground electronic state in methanol solution described by continuum (C-PCM(83; 84; 85)) models. For neutral alizarin, additional effects due to specific solute-solvent interactions have been considered and structures and properties of alizarin complexes with three explicit water molecules are also presented.

Two tautomeric forms of neutral alizarin differ by the the relative positions of their hydroxyl and carbonyl groups in dihydroxyanthraquinone structure, the 1,2NT and the 1,9NT respectively, with the former more stable by 22.7 kJ/mol (ΔG). Such an energy difference suggests that only a minor fraction of alizarin can be related to the 1,9NT tautomer under experimental conditions. Additionally, there are two possible forms of 9,10 dihydroxyanthraquinone, related to the proton position in the O(11)-H(15)-O(12) hydrogen bond, labelled PT1 and PT9, with the 1,2NT-PT1 significantly more stable (by 19.8 kJ/mol with solvent effects described by CPCM and by 34.5 kJ/mol if ex-

Table 4.2: Ground-state equilibrium structures and relative free energy values for the alizarin tautomeric forms in methanol solution. All computations were done at the CAM-B3LYP/*aug*-N07D//CPCM level. Bond lengths are in $\mathring{A}$, angles in degrees, ΔG in kJ/mol

Bond / Angle	1,2NT				1,9NT	1,9MA		1,2MA		DA
	PT1	PT1(H_2O)$_3$	PT9	PT9(H_2O)$_3$		PT1	PT2	PT9	PT1	
C(9)=O(11)	1.238	1.243	1.295	1.312	1.299	1.227	1.233	1.313	1.245	1.248
C(1)=O(12)	1.342	1.342	1.279	1.287	1.332	1.343	1.273	1.265	1.340	1.256
C(2)=O(13)	1.349	1.340	1.344	1.339	1.270	1.277	1.345	1.250	1.261	1.269
C(10)=O(14)	1.223	1.228	1.223	1.241	1.230	1.236	1.230	1.247	1.239	1.254
O(12)-H(15)	0.997	0.992	1.454	1.410	1.718	-	-	1.456	0.992	-
O(13)-H(16)	0.969	0.989	0.974	0.991	1.819	1.805	0.991	-	-	-
O(11)-H(15)	1.662	1.631	1.046	1.061	0.985	-	-	1.037	1.620	-
O(12)-H(16)	2.138	2.332	2.100	2.417	0.999	0.991	1.810	-	-	-
O(11)-O(12)	2.548	2.530	2.439	2.414	2.577	2.716	2.806	2.431	2.523	2.746
O(12)-O(13)	2.665	2.742	2.670	2.822	2.511	2.521	2.513	2.736	2.696	2.702
C(9)-C(17)-C(1)	119.1	119.3	117.7	118.1	120.9	121.5	120.9	117.9	119.2	120.5
O(11)-C(9)-C(17)	120.7	120.4	120.1	119.9	122.1	123.1	124.2	121.3	121.8	125.9
C(17)-C(1)-O(12)	123.7	122.6	123.2	120.8	123.1	125.3	128.8	121.4	122.1	125.0
C(2)-C(1)-O(12)	116.3	117.3	119.2	121.5	113.1	112	114.4	119.4	115.9	116.7
C(1)-C(2)-O(13)	119.5	122.0	116.6	121.3	115.0	116.1	113.1	119.1	120.8	119.3
O(11)-H(15)-O(12)	146.4	147.7	154.2	154.9	143.5	-	-	154.0	149.5	-
O(12)-H(16)-O(13)	112.6	103.8	115.6	103.7	123.3	126.2	125.0	-	-	-
ΔG_i (kJ/mol)	0.0	0.0	19.8	34.5	22.7	3.8	5.3 (2.2)[a]	21.6 (18.0)[a]	0.0 (0.0)[a]	-

[a] Data taken from reference (44)

plicit solvent molecules are included). Thus, taking into account energetic properties the 1,2NT-PT1 form dominates under experimental conditions, and will be considered in the deprotonation reaction. We only note that the 1,2NT-PT9 form has been observed experimentally(81) and discrepancy between computed ΔG and experimental findings has been ascribed to the sensitivity of proton transfer (PT) processes to environmental effects(81), so that explicit solvent models might be required for a well-balanced description of their energetics(101). However, our results show an opposite effect of explicit solvent. Thus, taking into account that the global minimum on the lowest excited-state potential energy surface (PES) corresponds to the proton-transfer structure, we suggest a more complex process, starting from the formation of 1,2NT-PT9 through an excited-state PT, followed by its relaxation to the ground state and the subsequent photon absorption of this tautomer(64).

An increase of pH leads to the deprotonation of alizarin, with two pK_a values, one in the 6.6–7.5 (pK_{a1}) and the other in the 11.8–12.1 (pK_{a2}) range while, at intermediate pH, the molecule is expected to be found in the mono-anionic form(45; 25). The two different pK_a values suggest that deprotonation goes through two consecutive steps. The geometry parameters listed in Table 4.2 (e.g. the O(11)–H(15) and O(12)–H(16) distances of 1.66 $\mathring{A}$ and 2.14 $\mathring{A}$, respectively) show that, from the two intermolecular hydrogen bonds of 1,2NT, the O(11)$\cdots$H(15)-O(12) one, leading to the six-member ring, is significantly stronger than the O(12)$\cdots$H(16)-O(13) one. This implies that the first deprotonation process is more likely to involve O(13)–H(16) (weaker hydrogen bond) and the removal of H(16). Indeed, the resulting 1,2MA-PT1 structure is the most stable one among all mono-anionic forms, as shown in this work and by the recent study by Préat *et al.*(44). The second deprotonation step leads to the unique di-depronotated structure DA, which is characterised by similar distances between O(11)–O(12) and O(12)–O(13), of 2.746 $\mathring{A}$ and 2.702 $\mathring{A}$, respectively, as expected from the lack of any stabilisation by hydrogen-bonding. Additionally, larger negative charges are located on more distant oxygen atoms (Mulliken charges of -0.81 for both O(11) and O(13), -0.75 for O(12)), but this effect is smaller than suggested in previous experimental works(25). Moreover, the largest increase of electron

density is observed for O(14) (Mulliken charges of -0.86 and -0.62 for di-deprotonated and neutral forms, respectively), so it can be concluded that the negative charge is almost equally distributed over all oxygen atoms.

Mg/Al-Alizarin complexes

The structure of the metal-dye complexes, either 1,2-hydroxyanthraquinone (alizarin) or 1,2,4-hydroxyanthraquinone (1,2,4-HAQ), and the nature of their possible chemical interactions are still under debate(102). However, the formation of di-nuclear chelated complexes shows energetic disadvantages deriving from two adjacent and negatively charged oxygen atoms (48), and shall be only considered for other anthraquinoid resonant structures(48; 103; 104). Thus, we have chosen to study only mono-nuclear bidentate forms, which prevail with respect to the monodentate ones for similar systems (49; 105). Four structures, each one derived from a specific MA conformer, have been considered in the preliminary studies for each metal. It has been shown that both the 1,9MA forms lead to the same 1-hydroxy-9-keto (1,9Mg/Al-Aliz) structure with the H(16) proton bound to the O(13) (as in 1,9MA-PT2), while in case of 1,2MA, two different conformers of 1,2-dihydroxyl (1,2Mg/Al-Aliz) with the H(15) proton bound to O(11) (PT9), or to O(12) (PT1), have been determined. The structures of 1,9- and 1,2-octahedral Mg/Al-Aliz$(H_2O)_4$ complexes are sketched in figure 4.6 while table 4.2 lists the most important geometry parameters and Gibbs free energy values (ΔG). A more detailed study on the effect of Mg coordination by water molecules showed that in all cases (tetrahedral and octahedral coordination) the metal-ligand bond is almost symmetric, so the central C(1)=O(12) bond is shortened, and the two lateral ones elongated with respect to the corresponding MA forms. The bond angles near the complexation site are generally less affected by changes in the coordination structure in 1,9Mg-Aliz than in 1,2Mg-Aliz, while bond angles within the aromatic system are not sensitive to complexation and coordination effects. Moreover, metal coordination by solvent molecules has a negligible effect on the spectral properties of the complex (see Table 4.6), so, only hexa-coordinated Mg-Aliz$(H_2O)_4$ and Al-Aliz$(H_2O)_4$ will be discussed in the following.

Table 4.3: Ground-state equilibrium structures and relative free energy values for the complexed alizarin in solution. All computations were done at the CAM-B3LYP/*aug*-N07D//CPCM level. Bond lengths are in $\mathring{A}$, angles in degrees, ΔG in kJ/mol

	Mg-Aliz$(H_2O)_4$			Al-Aliz$(H_2O)_4$		
Bond / Angle	1,9Mg	1,2Mg-PT1	1,2Mg-PT9	1,9Al	1,2Al-PT1	1,2Al-PT9
C(9)=O(11)	1.255	1.244	1.298	1.259	1.247	1.294
C(1)=O(12)	1.302	1.372	1.298	1.338	1.372	1.323
C(2)=O(13)	1.346	1.308	1.293	1.340	1.331	1.328
C(10)=O(14)	1.220	1.221	1.230	1.223	1.221	1.222
O(12)-H(15)	-	1.013	1.501	-	1.056	1.621
O(12)-Al/Mg	1.957	2.102	2.074	1.833	1.947	1.884
O(13)-H(16)	0.975	-	-	1.012	-	-
O(13)-Al/Mg	-	1.971	2.004	-	1.819	1.828
O(11)-H(15)	-	1.548	1.026	-	1.445	1.001
O(11)-Al/Mg	2.001	-	-	1.873	-	-
O(12)-H(16)	1.965	-	-	1.639	-	-
O(11)-O(12)	2.744	2.479	2.456	2.740	2.422	2.532
O(12)-O(13)	2.578	2.632	2.644	2.427	2.560	2.566
C(9)-C(17)-C(1)	121.1	119.2	118.6	121.4	118.4	120.0
O(11)-C(9)-C(17)	123.1	120.1	120.7	120.6	119.2	120.7
C(17)-C(1)-O(12)	126.9	121.5	122.2	129.0	121.7	123.4
C(2)-C(1)-O(12)	114.9	115.4	117.6	111.4	114.8	115.9
C(1)-C(2)-O(13)	116.2	118.5	116.8	111.7	116.1	115.1
O(11)-H(15)-O(12)	-	150.2	152.3	-	150.8	148.9
O(11)-Al/Mg-O(12)	87.5	-	-	95.3	-	-
O(12)-H(16)-O(13)	118.6	-	-	131.1	-	-
O(12)-Al/Mg-O(13)	-	80.4	80.8	-	85.6	87.5
ΔG_i	0.0	25.2	34.0	0.0	39.1	19.2

4.3.2 Metal coordination effects on the spectra of Alizarin

$S_1 \leftarrow S_0$ transition of mono-anionic Alizarin

It has been suggested(44) that for mono-anionic alizarin, several tautomeric forms can co-exist in an experimental mixture, and contribute to the overall spectrum line-shape. Such effects can be also included in our model, taking into account the relative population of the tautomers. In principle, there are several possibilities to evaluate the composition of a complex molecular mixture. A first option is to simulate fully *ab initio* spectra, with the single contributions estimated from the Boltzmann populations, which in turn are based on more- or less-sophisticated computations of Free Energies (see for example Ref.(99; 106) for definition and application of elaborated theoretical models). Alternatively, the abundances can be estimated from the analysis of some relevant features of the experimental spectra and then used to simulate the overall band shapes(107). It is also possible to estimate relative amounts of sub-components by a procedure involving the fitting of theoretical spectra (varying contributions of single-component ones) to the observed experimental data. In fact, the most reliable conclusions about the molecular system composition can be drawn when both energetic and spectra computations lead to the same results. For mono-anionic alizarin, the fully computational approach, with the ΔG_i in solution computed by standard CPCM model within the harmonic framework, has been applied. Following previous computational studies(44), all mono-anionic forms where the intramolecular hydrogen bond is preserved have been considered (see Fig. 4.3), while structures with the hydroxyl group shifted in other molecular positions have not been taken into account as significantly less stable (≈40 kJ/mol(44)). According to our computations, the most stable structure corresponds to the removal of H(16) (1,2MA-PT1), in line with expectations and previous observations(44; 47). The second most stable tautomeric form is 1,9MA-PT1, followed by 1,9MA-PT2 and 1,2MA-PT9. The 1,9MA-PT1 form is stabilised through hydrogen-bonding creating a five-member ring, and is less stable than 1,2MA-PT1 (with six-member ring) by about 3.8 kJ/mol, so it accounts for about 16% of the total mono-anionic population. Finally, 1,9MA-PT2 is

characterised by the bonding between H(16) and the O(13) carbonyl, a relative energy of about 5.3 kJ/mol, and a population of 9%. These three forms should be considered as participating significantly to the overall spectra, under experimental conditions, while the contribution of 1,2MA-PT9 (less stable by more than 20 kJ/mol) can be safely neglected.

The lowest-energy band of all tautomeric structures of alizarin is related to the HOMO-LUMO transition, and has the same $\pi \rightarrow \pi^*$ character, with essentially similar CT contribution. The $S_1 \leftarrow S_0$ transition leads to some electron density transfer from the catechol part to the leftmost aromatic ring of the molecule and, in particular, the electron density on O(11) increases, while it decreases on O(12) and O(13), as shown in Figure 4.8 for the 1,2NT(PT1) structure. The simulated VG|FC absorption spectrum related to the lowest electronic transition of mono-anionic alizarinates, obtained as a weighted sum of contributions deriving from the 1,9MA-PT1, 1,9MA-PT2 and 1,2MA-PT1 tautomeric forms is compared to its experimental counterpart measured in the 8–10 pH range(45; 25) in Figure 4.7. The single tautomer contributions are also reported, showing the absorption maxima near 455, 445 and 515 nm for 1,9MA-PT1, 1,9MA-PT2 and 1,2MA-PT1, respectively. Experimental λ_{max} is located at about 540 nm. MA4 shows the best match to experiment, supporting that this is the predominant mono-anionic tautomer, in line with the relative energetics. Moreover, taking into account all tautomers allows to improve the agreement with experiment, leading to a very good match between the simulated and observed spectra line-shape and the position of absorption maxima.

UV-Vis spectrum of Alizarin-Mg complexes

Simulated UV-Vis spectra of the 1,9Mg-Aliz and 1,2Mg-Aliz complexes are presented in Figure 4.9 showing in both cases good match with the experimental absorption spectra of Mg-alizarin in dioxane/water solution recorded in the full UV-Vis energy range (200–700 nm)(82). The overall UV-vis spectrum is composed from the transitions to the first 12 excited electronic states, which are listed in the Table 4.4 and described through the most relevant molecular orbitals (MOs). Except for the highest occupied molecular orbital

(HOMO), which is localised mainly in the catechol part of the molecule, all other MOs are delocalised over the whole aromatic system. We also note, that all electronic transitions are localised on the aromatic ring, the molecular orbitals are not extended over the metal ion or solvent molecules (see the ELD plots of the Mg-alizarin complexes displayed in figure 4.9) and the MO shapes essentially match those of the free alizarin. The situation is similar also in the case of Al(III)-alizarin systems, in agreement with previous B3LYP studies(53). So, all electronic transitions have the same character as for the free molecule, mainly $\pi \rightarrow \pi^*$ in line with other theoretical studies performed at the DFT level(48; 53). Furthermore, only the lowest electronic transition shows a partial charge-transfer (CT) character.

The qualitative interpretation of the UV-Vis spectrum leads in a first approximation to a subdivision into two main bands of increasing intensity located in the wavelength range of about 350-500 nm and 200-300 nm, with the latter showing also a small shoulder on the red-side energy wing. First band is related to the $S_1 \leftarrow S_0$ transition and is less intense, but is directly responsible for the final colour of the complex. In variance, the most intense band is composed from several electronic transitions, which can be analyzed in detail based on the simulated results (see Figure 4.10). The possibility to dissect all individual contributions to the overall band-shape allow to identify the most appropriate energy ranges for specific spectrophotometric and fluorimetric measurements(4; 3)(e.g. fluorescence photography under UV light(108; 109)), or laser-assisted removal of overpaints(110), as well as to study UV ageing processes(1; 111). It is interesting to note that a proper account of the vibrational structure of electronic transitions within a static model allows a reliable representation of the overall spectra line-shape including the relative intensities of the observed absorption bands, which is not necessarily the case if simpler models (convolution of vertical excitation energies) are applied. As an example, the $S_1 \leftarrow S_0$ and $S_8 \leftarrow S_0$ contributions to the 1,9Mg-Aliz spectrum show very similar oscillator strengths (see Table 4.4), hence would result in similar intensity bands for spectrum line-shape obtained from convolution of Vertical Energies. It mean, that depending on the choice of the HWHM (large or small), both bands would be broad and not intense, or

narrow and intense, respectively. On the contrary, by taking into account the vibronic structure the total intensity corresponds to the area under line-shape, and not band hight, as highlighted schematically in Figure4.10. Indeed FC|VG computations leads to a broad $S_1 \leftarrow S_0$ band and a narrow $S_8 \leftarrow S_0$ band, in agreement with experimental findings. It has been already demonstrated(112) that the account for the band-shape resulting from the vibrational envelope of single electronic transitions can be important even for qualitative interpretation of experimental data. Thus, due to the relatively low computational cost of FC|VG simulations, it might be recommended to go beyond the simplest VE computations whenever feasible.

Electronic spectra of Mg(II)- and Al(III)-Alizarin complexes: visible energy range

Comparison of the relative free energies between the two possible sets of structures shows a higher stability of the 1,9 complexes for both Mg(II) and Al(III). However, the complexation process of alizarin in alkali solutions obtained by adding Mg(II) or Al(III) salts follows few steps (see Figure 4.2). The deprotonation of neutral alizarin can be considered as a first step, with the relative stability of mono-anionic forms influencing the complex formation. Thus, taking into account the whole picture, that 1,9Mg/Al-Aliz can be formed from mono-deprotonated 19MAPT1 and 19MAPT2 whereas 1,2Mg/Al-Aliz originate from 12MAPT9 and 12MAPT1, and that the 12MAPT1 form is predominant (about 75%), it seems plausible to consider significant amount of the 1,2Mg/Al-Aliz in the experimental mixture. Along the same line, the 1,2Mg-Aliz proton transfer conformer (1,2Mg-PT9) can be safely excluded due to its unfavorable energetics (by about 10 kJ/mol with respect to 1,2Mg-PT1) and the fact that its lowest band absorption wavelength is red-shifted by about 100 nm. The situation is very different for 1,2Al-Aliz; in this case the 1,2Al-PT9 proton transfer conformer is more stable by about 20 kJ/mol and its spectra match well the experimental λ_{max} ($\sim$470 nm) while the $S_1 \leftarrow S_0$ electronic transition energy of 1,2Al-PT1 is blue-shifted by about 100 nm. It should be noted

Table 4.4: Excited state properties of 1,9 and 1,2 Mg-Alizarin complexes in dioxane/water solution, with solvent described by the CPCM model and 4 water molecules in solvation sphere, computed at the TD-CAM-B3LYP/aug-N07D//CPCM level within the non-equilibrium solvation regime. Vertical excitation energies (VE) [eV], absorption wavelengths (λ [nm]), oscillator strengths (f) and dipole moment (μ [Debyee]) are reported along with the most important molecular orbitals (MOs) involved in the transitions.

1,2Mg-Aliz(PT1)						1,9Mg-Aliz					
MOs	VE [eV]	λ [nm]	State	μ^a [D]	f	MOs	VE [eV]	λ [nm]	State	μ^b [D]	f
H-1→L+1	5.45	227	S_{12}	16.74	0.39	H-6→L	5.51	225	S_{12}	20.39	0.00
H-3→L+2	5.39	230	S_{11}	20.11	0.00	H-1→L+2	5.39	230	S_{11}	16.41	0.52
H-6→L	5.35	232	S_{10}	23.43	0.00	H-2→L+1	5.31	233	S_{10}	16.00	0.00
H→L+2	5.31	233	S_9	18.29	0.05	H-1→L+1	5.23	237	S_9	19.27	0.35
H-4→L	4.76	260	S_8	20.52	0.28	H-4→L	4.78	259	S_8	6.47	0.27
H→L+1	4.70	264	S_7	5.35	0.00	H→L+1	4.78	259	S_7	19.06	0.00
H→L+1	4.52	274	S_6	23.75	0.51	H→L+2	4.48	277	S_6	21.56	0.09
H-2→L	4.19	296	S_5	16.39	0.01	H-3→L	4.23	293	S_5	19.37	0.11
H-5→L	4.05	306	S_4	22.31	0.00	H-5→L	4.09	303	S_4	21.31	0.00
H-1→L	3.81	325	S_3	21.16	0.09	H-1→L	3.59	345	S_3	18.70	0.06
H-3→L	3.39	366	S_2	17.41	0.00	H-2→L	3.32	374	S_2	15.84	0.00
H→L	3.00	413	S_1	24.83	0.13	H→L	2.90	428	S_1	19.16	0.23

[a] Ground state Dipole moment = 20.12D

[b] Ground state Dipole moment = 18.99D

that, recently, the 1,2Al-PT1 proton-transfer conformer has been postulated as the one observed experimentally(53). This contradictory conclusion with respect to our analysis is to be ascribed to the different functional used in the other work to compute vertical excitation energies. In fact, as briefly discussed in section 4.2, the electronic energies of the $S_1 \leftarrow S_0$ transition (with a partial CT character), computed at the TD-B3LYP level, are consistently underestimated with respect to the TD-CAM-B3LYP ones. For this reason, we consider our results to be more reliable since the previous computations did not take into account the relative stabilities of the different tautomers in the ground electronic state.

As already metioned, direct comparison between the simulated and experimental spectra of Mg-alizarin complex in dioxane/water solution(82) and in the full UV-vis energy range (200–700 nm) presented in Figure 4.9, shows a good agreement for both the 1,9Mg$(H_2O)_4$ and 1,2Mg$(H_2O)_4$ complexes. Moreover, the much higher intensity of the 1,2Mg spectrum bands at about 270 nm, in line with the red-side shoulder of the experimental band may suggest that, indeed, both complex forms can probably co-exist in solution.

The simulated spectra in the visible energy range for alizarin complexes with Mg(II) and Al(III) are presented in Figure 4.11. For clarity, the spectra of 1,2Mg/Al-Aliz are shown, as the contributions of the 1,9 ones are not changing the qualitative picture. First, it can be noted that the experimentally observed metal complexation effects, that is to say a large blue-shift of the visible band with respect to the mono-anionic free alizarin for Mg and a small one for Al, along with the colour changes from orange (Mg) to red (Al), are well reproduced by simulation. Moreover, our results suggest that the differences in the alizarin spectral properties caused by Mg(II) or Al(III) complexation can be ascribed to the metal effect on the relative stability of the two proton-transfer tautomers in the O(11)-H(15)-O(12) hydrogen bridge.

Considering the band-shape of the $S_1 \leftarrow S_0$ electronic transition of Mg(II) and Al(III) alizarin complexes, 1,2Mg/Al-Aliz shows a structure-less, broad band, similarly to the neutral alizarin, while some vibronic structure (in the same way as the deprotonated

forms) is observed only for 1,9Mg/Al-Aliz. More details are presented in Figure 4.12 and in Table 4.5, taking 1,9Mg-Aliz as an example. In line with the electronic transition localised on the aromatic structure, several vibronic transitions corresponding to in-plane vibrations of the aromatic system (19', 20') contribute to the intensity of the electronic band origin. Moreover, additional bands related to the C=O and O-H group vibrations (82') contribute to the spectra line-shape/broadening. Some changes with respect to the free alizarin, caused by metal complexation, involve additional vibronic bands at about 650 cm^{-1}, with respect to the energy of the $\langle \mathbf{0} \mid \mathbf{0} \rangle$ transition, which are related to the O-Mg-O bonding (49'). Considering both free and complexed alizarin, we can conclude that possible hydrogen bondings, in particular the strongest one O(11)-H(15)-O(12), lead to a band broadening and lack of defined vibronic structure, the latter being most pronounced for the fully deprotonated form. In view of alizarine-based pigments it can be suggested that more pronounced vibronic structure can be expected for bi-dentate binding schemes, and structures without intramolecular hydrogen bond. Moreover, results of the Mg(II)- and Al(III)-alizarin complexes in solution suggests that the presence of the metal does not change the nature of the electronic transitions. However, the spectral properties of both complexes are closely related to the relative stability of proton-transfer tautomers, which in turn is influenced by the presence and electronegativity of the metal ion. Thus, for magnesium-based madder lake, only minor colour modifications with respect to the neutral free dye and related to the metal complexation are observed, while the more positively charged aluminium reverses the stability of the PT tautomers and causes colour change from yellow-orange to red.

4.3.3 Environmental effects on spectra of Alizarin: pH effects

The most relevant environmental effects on the electronic spectrum of free alizarin are related to the lowest electronic transition, which in fact is responsible for the overall molecular colour. Deprotonation has only a limited effect on the nature of the molecular

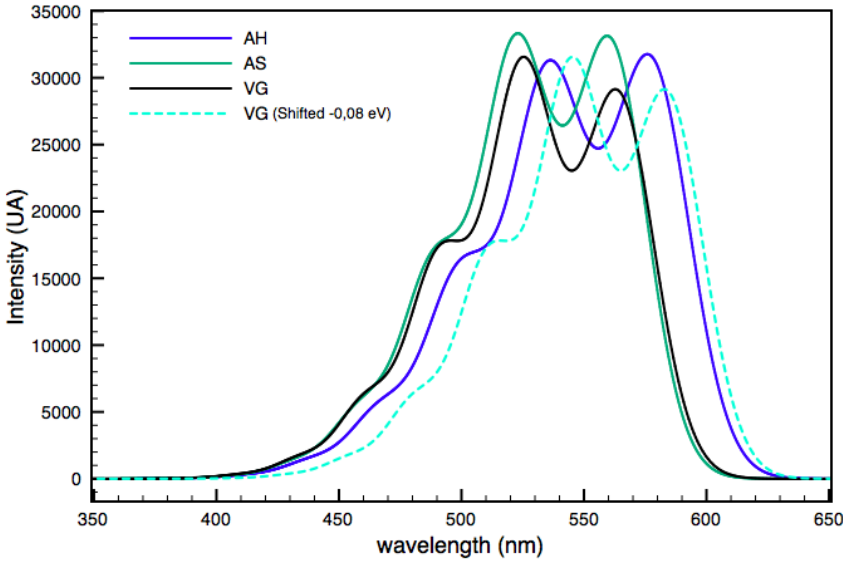

Figure 4.5: Theoretical electronic spectra of $S_1 \leftarrow S_0$ electronic transition for di-deprotonated alizarin computed within vertical and adiabatic approaches: VG|FC, AS|FC, AH|FC, convoluted by HWHM of 500 cm^{-1}.

Table 4.5: Most intense vibrational contributions to the Mg-Alizarin $S_1 \leftarrow S_0$ electronic transition. Energy and intensities of single vibronic contributions for 1,9Mg$(H_2O)_4$-Alizarin complexes in dioxane/water solution are reported, with the solvent described by the CPCM model. The absolute energy of the ($S_1 \leftarrow S_0$) transition and the relative energies of the three most intense transition from fundamental state to the single overtones $\langle \mathbf{0} \mid \mathbf{0} + 1_n \rangle$

Transition	Energy [cm^{-1}]	Intensity
$\langle \mathbf{0} \mid \mathbf{0} \rangle$	21 005	$0.2671*10^7$
1_{19}	218	$0.5268*10^6$
1_{20}	224	$0.8197*10^6$
1_{49}	654	$0.4953*10^6$
1_{82}	1518	$0.6316*10^6$

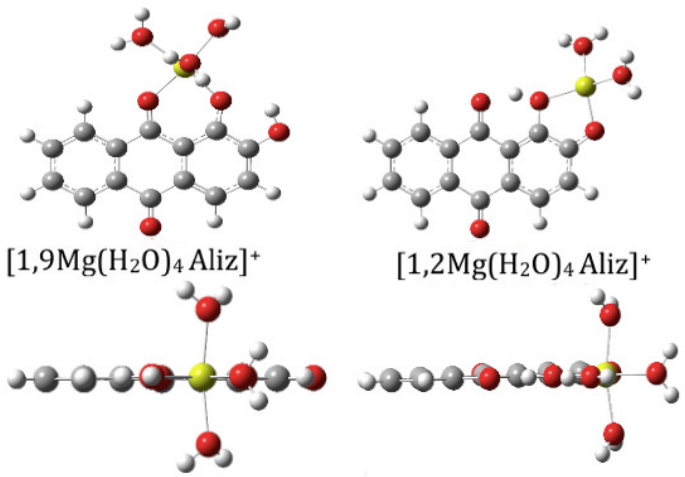

Figure 4.6: Possible metal-ligand equilibrium structures of the Mg/Al-Alizarin complexes in dioxane/water solution (metal replaces one of the hydrogen atoms). The metal binds to the 1-hydroxy and the 9-keto groups and is stabilised in a 6-member ring (1,9Mg/Al-Aliz); the metal binds to the two hydroxyls in positions 1 and 2, leading to a 5-member ring (1,2Mg/Al-Aliz). In all form,s the remaining hydrogen atom creates a bridge with the other chelate ring. Mg-Alizarin complexes were optimized with the solvent described by CPCM model plus 4 water molecules in a solvation sphere. Both parallel and perpendicular (with respect to molecular plane) views are presented.

orbitals, but the orbital energies change significantly. Passing from neutral to di-anionic alizarin, the HOMO-LUMO gap and in consequence the vertical excitation energy decreases (see Table 4.6), and this effect is responsible for the net red-shift of the visible band. However, in addition to the shift in band position, deprotonation can affect also the spectra line-shape and absorbtion intensities, and such effects can not be easily accounted for by standard electronic structure computations. Experimental(45) and computed, vibrationally-resolved electronic spectra in the 350–700 nm range are compared in Figure 4.13. Experimental data refer to spectra measured at different pH conditions, so to neutral, mono-anionic and di-anionic forms, with absorption bands changing from a weak structure-less transition for neutral alizarin to a more intense band with multiple intense absorption maxima for the di-depronotated species. The normalized experimental spectra have been reported, thus the simulated spectra, for which molar absorption coefficients (in $dm^3mol^{-1}cm^{-1}$) are directly computed have been scaled by an uniform factor, so to preserve the relative computed intensities between tautomeric forms.

It is evident that the simulated spectra reproduce qualitatively the bathochromic effect, spectra line-shape modifications and intensity changes observed upon deprotonation. In the case of DA, it has been postulated(25), that vibronic progressions are responsible for the band-shape. However, it is often non trivial to judge if the rich line-shape observed experimentally is related to the vibronic structure or shall be rather ascribed to different conformers(14). Vibronic computations lead to a realistic spectra line-shape, thus allowing to confront and verify each hypothesis, and to analyse the band-shape tuning by the environment (pH range).

It can be noted that several vibrations give significant contributions to the band-shape of the $S_1 \leftarrow S_0$ transition. These are in-plane, low-frequency vibrations of the overall aromatic system, which are essentially present in the whole pH range, and remain equally important despite environmental changes. Additionally, some higher-frequency vibrations, namely stretchings and bendings of the C-OH and C=O groups contribute to the overall spectra line-shape. For neutral and mono-anionic forms, such vibronic transitions lead to the band broadening, whereas specific vibronic contributions become

marked for the di-anionic form. In the latter case, it has been postulated, on the basis of the energy gap between the absorption maxima, that the vibronic structure is mainly due to the C=O stretching vibrations(44), while the present study suggests a more delocalised character of the most involved vibrational contributions 46DA and 50DA, reported in Figure 4.4. Finally we note that the simulated spectra reported here and obtained by applying in all cases the same Gaussian broadening function with a HWHM of 500 cm^{-1}, reproduce qualitatively all experimental observations.

We note that absolute positions of the $S_1 \leftarrow S_0$ transitions for both proton transfer conformers of neutral 1,2NT alizarin are shifted by approximately 50 nm with respect to experiment. This discrepancy can be ascribed to the sensitivity of proton transfer (PT) processes to environmental effects(81; 101), as well as to the effects of the choice of functional. We have tested both effects; Figure 4.14 shows that from the the computations performed with B3LYP, CAM-B3LYP and ωB97XD, with or without inclusion of few explicit solvent molecules, neither match the position absorption maxima, but all reproduce correctly the band shape. Moreover, it has been shown recently that the proton-transfer dynamic effects, which are beyond current static model, are responsible for the band broadening and a larger red-shift(76).

4.4 Conclusions

An integrated computational approach has been applied to study structures and electronic properties of free alizarin and its Mg(II) and Al(III) complexes, in solution and under different pH conditions, with an emphasis on the simulation of optical spectra line-shapes directly comparable with their experimental counterparts. The present study demonstrates that environmental and/or complexation effects are qualitatively well reproduced by simulations, underlying the ability to dissect the role of several, concomitant effects in tuning optical properties. It is noteworthy that even structure-less broad electronic bands observed in UV-Vis spectra in solution hide a complex set of vibronic transitions, which are directly responsible for the spectra line-shape. The description of such effects

Table 4.6: Properties of the $S_1 \leftarrow S_0$ (HOMO-LUMO) electronic transition of free alizarin (in ethanol/water solution), Mg-Alizarin$(H_2O)_4$ complexes and Al-Alizarin$(H_2O)_4$ complexes (in dioxane/water solution). Bulk solvent (ethanol/dioxane) described by the CPCM model, specific solvent effects considered by adding n=(4) water molecules in a metal coordination sphere. Vertical excitation energies (VE) [eV], absorption wavelengths λ [nm]), oscillator strengths (f) and dipole moment (μ [Debyee]) are reported. All values are computed at the TD-CAM-B3LYP/*aug*-N07D//CPCM level within the non-equilibrium solvation regime.

Form	VE [eV]	λ [nm]	μ	f
1,2NT(PT1)	3.36	369	5.2	0.20
1,2NT(PT9)	2.67	463	1.1	0.30
1,9MA(PT1)	2.78	446	11.5	0.25
1,9MA(PT2)	2.82	440	9.5	0.27
1,2MA(PT1)	2.45	506	15.0	0.21
1,2MA(PT9)	2.10	588	9.7	0.27
DA	2.37	523	19.2	0.44
1,9Mg	2.90	428	19.2	0.23
1,2Mg(PT1)	3.00	413	24.8	0.13
1,2Mg(PT9)	2.33	533	25.9	0.21
1,9Al	2.79	445	29.4	0.15
1,2Al(PT1)	3.24	383	26.7	0.10
1,2Al(PT9)	2.75	451	30.4	0.15

requires a proper account of the vibrational effects also to describe correctly the ratio in band intensity and respective broadening of the electronic transitions, in particular when they show similar oscillator strengths. The band shapes not only contribute to the correct interpretation of experimental findings, allowing more confident assignments of the electronic transitions, but provide also important improvements with respect to the purely electronic picture, being responsible for the colour perceived by the human eye. The latter aspect is particularly relevant for the computational studies of pigments, including the ones used in painting or textile colouration over the years. Realistic computational studies including stereo-electronic, dynamic, and environmental effects already stand as very powerful tools to analyse the composition of original works of arts, and the effects that occurred over the years affecting both the material composition and their chromatic properties. In the next step, a support base linked with the dye through metal ligand shall be considered in a model following lines recently explored by some of us for similar systems(52).

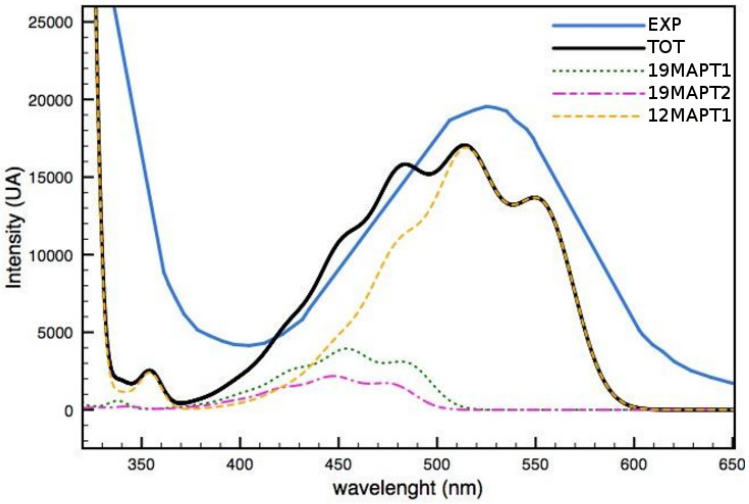

Figure 4.7: Experimental(45; 25) and theoretical electronic spectra of band **I** (*vide infra*) for mono-deprotonated alizarin. Simulated total spectrum (TOT) and its components: weighted contributions from three tautomers (1,9MA-PT1, 1,9MA-PT2 and 1,2MA-PT1.

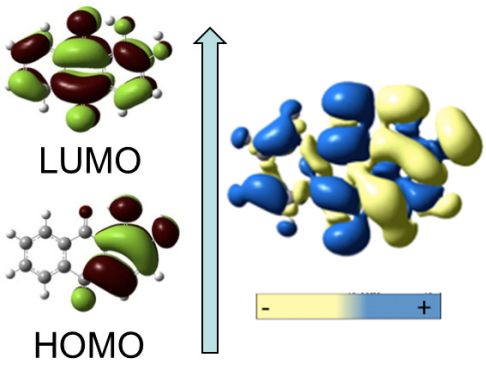

Figure 4.8: Frontier molecular orbitals and changes in electronic density (ELD) during the HOMO→LUMO transition. The regions, which have lost electron density as a result of transition are shown in bright yellow, whereas the darker blue regions gained electron density. ELD densities have been evaluated with an isovalue threshold of 0.0004.

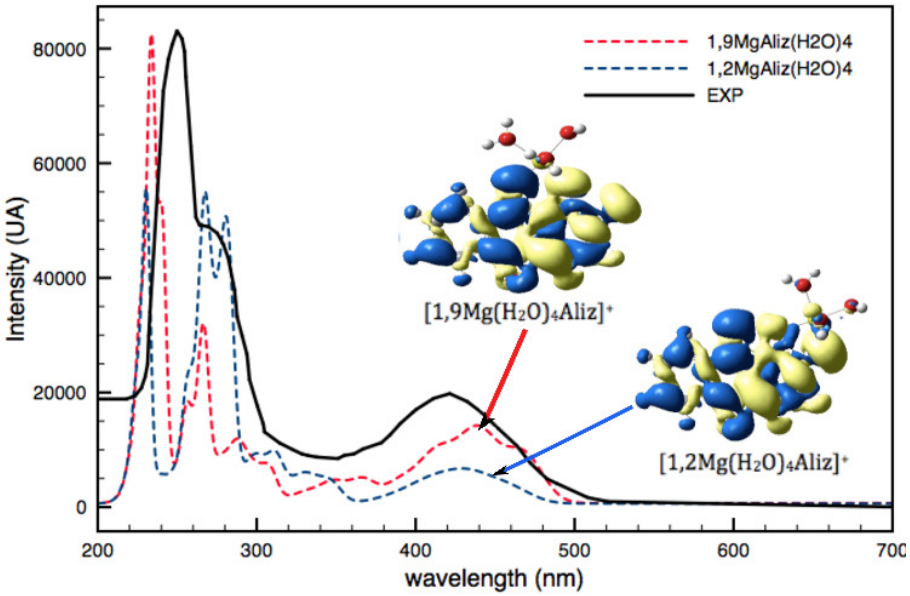

Figure 4.9: Vibrationally resolved electronic spectra of complexed alizarin (1,9Mg (red) and 1,2Mg (blue) forms) in dioxane/water solution, considering 4 explicit H_2O molecules. Experimental spectra were taken from Ref. (82). For band **I** which corresponds to the $S_1 \leftarrow S_0$ (HOMO→LUMO) transition, changes in electronic density (ELD) are also reported. The regions, which have lost electron density as a result of the transition, are shown in bright yellow, whereas the darker blue regions gained electron density. ELD densities were evaluated with an isovalue threshold of 0.0004.

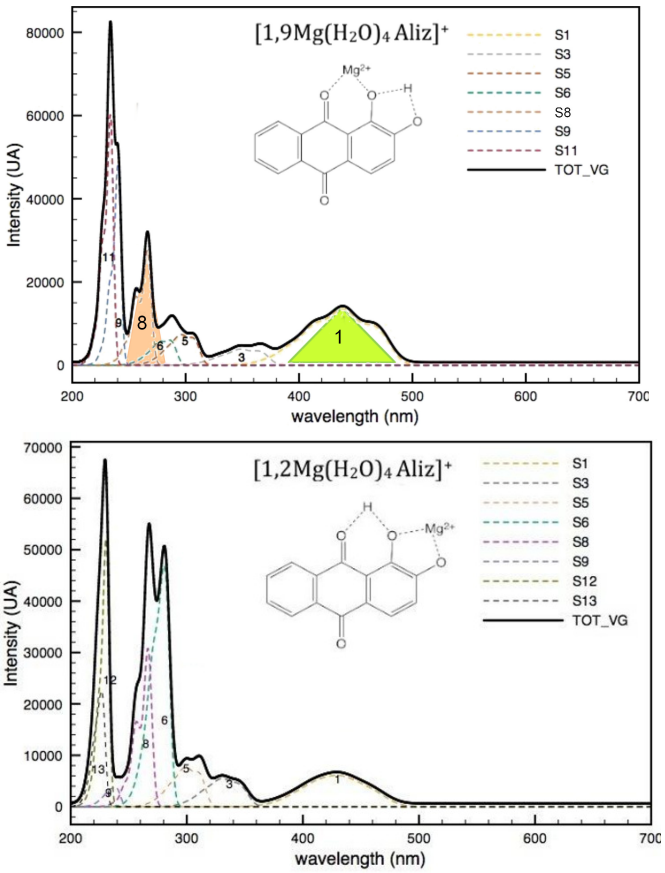

Figure 4.10: Total simulated VG|FC spectra for Alizarin Mg-complexes in dioxane-water solution, along with their single-state contributions. 1,9Mg-Aliz (upper panel) and 1,2Mg-Aliz (lower panel).

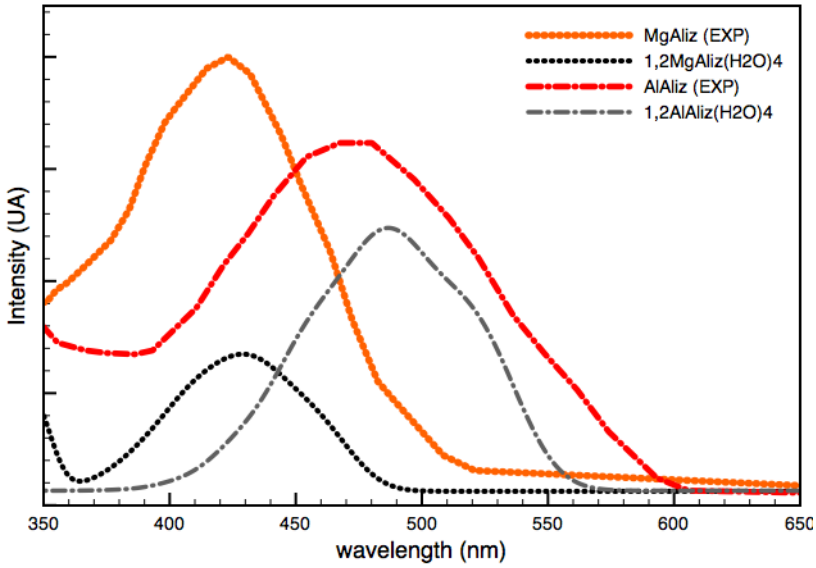

Figure 4.11: Electronic spectra line-shapes of lowest-energy band for Mg- and Al-alizarin complexes (1,2Mg (orange, dots) and 1,2Al (red, dot-dash)) in dioxane/water solution, simulated by considering 4 explicit H_2O molecules and dioxane modeled with CPCM. Experimental spectra were taken from Ref. (82)

.

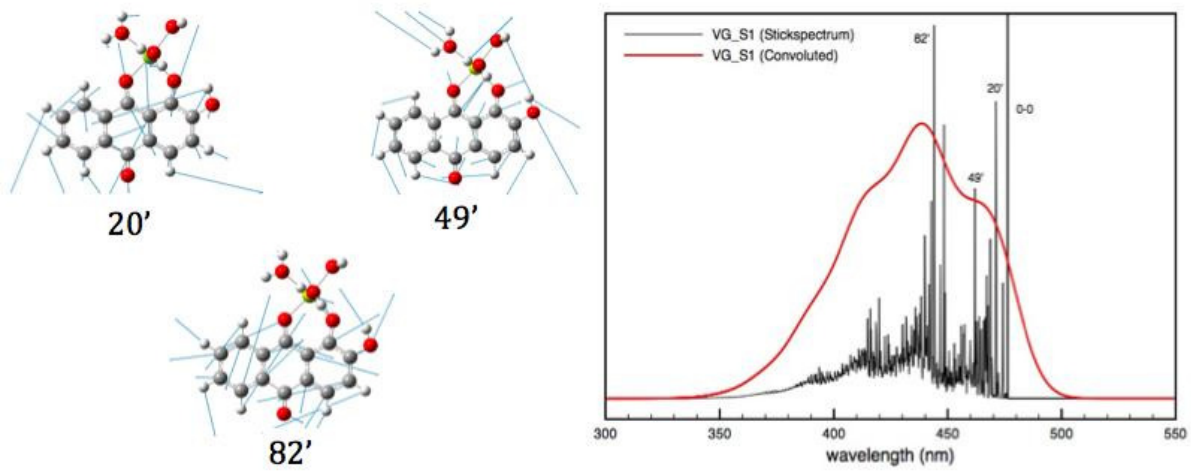

Figure 4.12: Vibronic contributions to the spectra band shape of the 1,9Mg$(H_2O)_4$ alizarin complex.

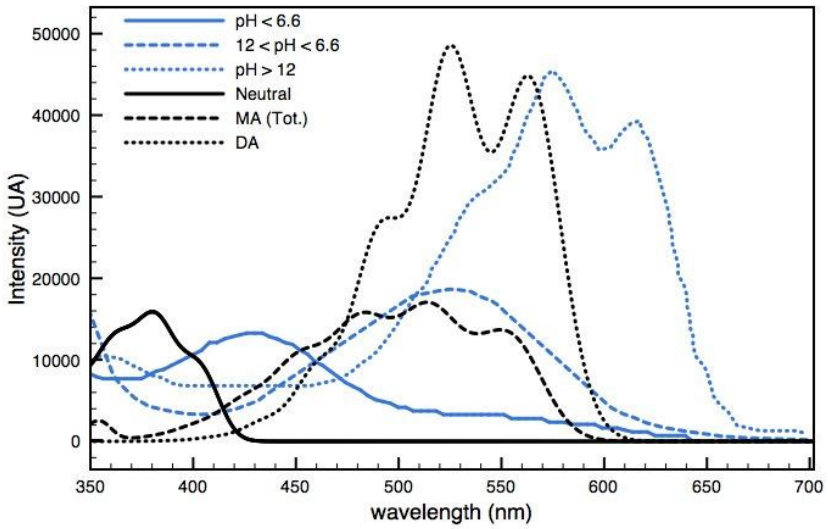

Figure 4.13: Experimental(45) (blue lines) and theoretical (black lines) electronic spectra of neutral, mono-anionic and di-anionic alizarin. The pH-induced red-shift of the visible band observed experimentally is clearly reproduced by the simulations.

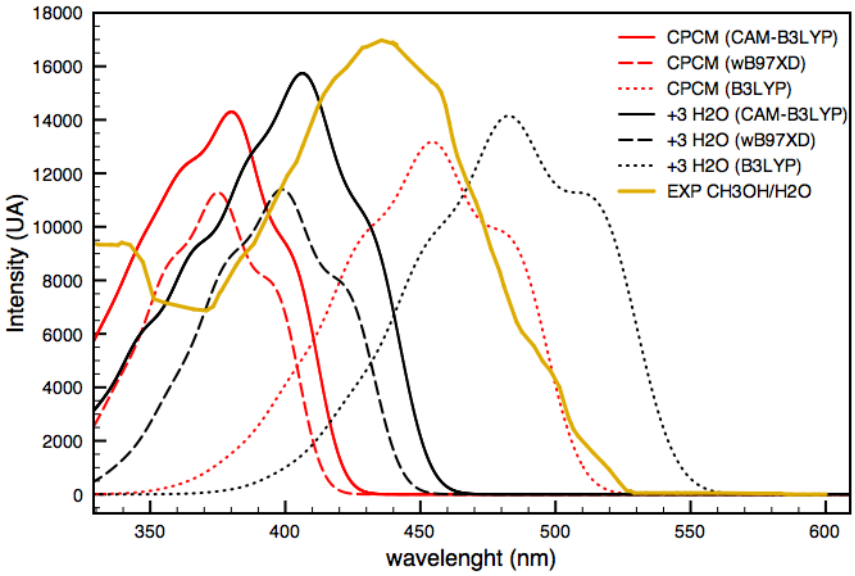

Figure 4.14: Experimental(81) and simulated electronic spectra of the neutral form of free alizarin computed with B3LYP, CAM-B3LYP and ωB97XD functionals and aug-N07D basis set. Simulated VG spectra of 1,2NT(PT1) in methanol solution (CH_3OH) described by CPCM model and by CPCM plus 3 explicit water molecules in the first solvation shell.

Bibliography

[1] Brunetti, B. G.; Sgamellotti, A.; Clark, A. J. *Acc. Chem. Res.* **2010**, *43*(6), 693–694.

[2] Fantacci, S.; Amat, A.; Sgamellotti, A. June **2010**, *43*(6), 802–813.

[3] Rosi, F.; Miliani, C.; Clementi, C.; Kahrim, K.; Presciutti, F.; Vagnini, M.; Manuali, V.; Daveri, A.; Cartechini, L.; Brunetti, B. G.; Sgamellotti, A. SEP **2010**, *100*(3), 613–624.

[4] Miliani, C.; .; Romani, A.; Favaro, G. *Spectrochim. Acta A*. **1998**, *54*, 581–588.

[5] Creagh, D. C. *Radiat. Phys. Chem.* **2005**, *74*(6), 426 – 442.

[6] Adriaens, A. *Spectrochim. Acta B* **2005**, *60*(12), 1503 – 1516.

[7] Murcia-Mascarós, S.; Domingo, C.; Sánchez-Cortés, S.; Cañamares, M. V.; García-Ramos, J. V. *J. Raman Spectrosc.* **2005**, *36*, 420.

[8] Brai, M.; Camaiti, M.; Casieri, C.; De-Luca, F.; Fantazzini, P. *Magn. Reson. Imaging* **2007**, *25*(4), 461 – 465.

[9] Szostek, B.; Orska-Gawrys, J.; Surowiec, I.; Trojanowicz, M. *J. Chromatogr.* **2003**, *A*, 179–192.

[10] Duran, A.; Herrera, L. K.; de Haro, M. C. J.; Justo, A.; Perez-Rodriguez, J. L. *Talanta* **2008**, *76*(1), 183 – 188.

[11] Jaquemin, D.; Préat, J.; Wathelet, V.; Perpète, E. A. *J. Chem. Phys.* **2006**, (124), 074104.

[12] Tilocca, A.; Fois, E. *J. Phys. Chem. C* **2009**, *113*, 8683–8687.

[13] Amat, A.; Clementi, C.; De-Angelis, F.; Sgamellotti, A.; Fantacci, S. *J. Phys. Chem. A* **2009**, *113*, 15118–15126.

[14] Barone, V.; Baiardi, A.; Biczysko, M.; Bloino, J.; Cappelli, C.; Lipparini, F. *Phys. Chem. Chem. Phys.* **2012**, *14*, 12404–12422.

[15] Barone, V.; Bloino, J.; Biczysko, M.; Santoro, F. *J. Chem. Theory Comput.* **2009**, *5*, 540–554.

[16] Barone, V., Ed. *Computational Strategies for Spectroscopy, from Small Molecules to Nano Systems.;* John Wiley & Sons, Inc. Hoboken: New Jersey, 2011.

[17] Clary, D. C. *Science* **2006**, *314*, 265–266.

[18] Pedone, A.; Biczysko, M.; Barone, V. *ChemPhysChem* **2010**, *11*, 1812–1832.

[19] Barone, V.; Polimeno, A. *Chem. Soc. Rev.* **2007**, *36*, 1724.

[20] Jaquemin, D.; Préat, J.; Wathelet, V.; Fontaine, M.; Perpète, E. A. *J. Am. Chem. Soc.* **2006**, *128*, 2072–2083.

[21] Grimme, S. *Rev. Comput. Chem.* **2004**, *20*, 153.

[22] Prampolini, G.; Bellina, F.; Biczysko, M.; Cappelli, C.; Carta, L.; Lessi, M.; Pucci, A.; Rugger, G.; Barone, V. *Chem. Eur. J.* **2013**, *19*, 1996–2004.

[23] Bremond, E.; Alberto, M. E.; Russo, N.; Ricci, G.; Ciofini, I.; Adamo, C. *Phys. Chem. Chem. Phys.* **2013**, *15*, 10019–10027.

[24] Bloino, J.; Biczysko, M.; Santoro, F.; Barone, V. *J. Chem. Theory Comput.* **2010**, *6*, 1256–1274.

[25] Miliani, C.; Romani, A.; Favaro, G. *J. Phys. Org. Chem.* **2000**, *13*, 141–150.

[26] Jacquemin, D.; Bremond, E.; Ciofini, I.; Adamo, C. *J. Phys. Chem. Lett.* **2012**, *3*(4), 468–471.

[27] De-Santis, D.; Moresi, M. *Ind. Crop. Prod.* **2007**, *26*(2), 151 – 162.

[28] de Armas, R. S.; San-Miguel, M.; Oviedo, J.; Sanz, J. F. *Comp. Theor. Chem.* **2011**, *975*, 99–105.

[29] Huber, R.; Moser, J. E.; Gräetzel, M.; J.Wachtveitl. *J. Phys. Chem. B* **2002**, *106*, 6494.

[30] de Armas, R. S.; Lopez, J. O.; San-Miguel, M.; Sanz, J. F.; Ordejòn, P.; Pruneda, M. *J. Chem. Theory Comput.* **2010**, *6*, 2856–2865.

[31] Deng, P.; Fei, J.; Zhang, J.; Feng, Y. *Food Chem.* **2011**, *124*, 1231–1237.

[32] Deng, P.; Fei, J.; Feng, Y. *J. Electroanal. Chem.* **2010**, *648*, 85:91.

[33] Blömeke, P.; Poginsky, B.; Shmutte, B.; Marquardt, C.; Westendorf, H. *Mutat. Res.* **1992**, *265*, 263.

[34] Kaur, P.; Chandel, M.; Kumar, S.; Kumar, N.; Singh, B.; Kaur, S. *Food Chem. Toxicol.* **2010**, *48*, 320–325.

[35] Şahinaa, İ.; Nakiboğlu, N. *Anal. Chim. Acta* **2006**, *572*, 253–258.

[36] Amin, A. S. *J. Pharmaceut. Biomed.* **2002**, *29*, 729–736.

[37] DelMedico, A.; Fielder, S.; Lever, A.; Pietro, W. *Inorg. Chem.* **1994**, *33*(6), 1507.

[38] Del-Medico, A.; Auburn, P. R.; Dodsworth, E. S.; Lever, A. B. P.; Pietro, W. J. *Inorg. Chem.* **1994**, *33*(8), 1583–1584.

[39] Kapel, M.; Selby, D. W. *Talanta* **1969**, *16*, 915.

[40] Bilgic, D.; Karaderi, S.; Bapli, I. *Rev. Anal. Chem.* **2007**, *26*, 99–108.

[41] Chen, K.; Leona, M.; Vo-Dinh, K. C.; Yan, F.; Wabuyele, M.; Vo-Dinh, T. *J. Raman Spectrosc.* **2006**, *37*, 520–527.

[42] Clementi, C.; Nowik, W.; Romani, A.; Cibin, F.; Favaro, G. *Anal. Chim. Acta* **2007**, *596*(1), 46–54.

[43] Ferreiro, M.; Rodríguez-Otero, J. *J. Mol. Struct. THEOCHEM* **2001**, *542*, 63–77.

[44] Préat, J.; Laurent, A. D.; Michaux, C.; Perpète, E. A.; Jacquemin, D. *J. Mol. Struct.* **2009**, *901*, 24–30.

[45] Savko, M.; Kascakova, S.; Gbur, P.; Miskovsky, P.; Ulicny, J. *J. Mol. Struct. THEOCHEM* **2007**, *823*, 78–86.

[46] Sasirekha, V.; Umadevi, M.; Ramakrishnan, R. *Spectrochim. Acta A.* **2008**, *69*, 148–155.

[47] Komiha, N.; Kabbaj, O. K.; Chraibi, M. *J. Mol. Struct. THEOCHEM* **2002**, *594*(3), 135 – 145.

[48] Fain, V. Y.; Zaitsev, B. E.; Ryabov, M. A. *Russ. J. Coord. Chem.* **2004**, *30*(5), 365–370.

[49] Doskocz, M.; Kubas, K.; Frackowiak, A.; Gancarz, R. *Polyhedron* **2009**, *28*(11), 2201 – 2205.

[50] Bakola-Christianopoulou, M. N. *Polyhedron* **1984**, *3*(6), 729–734.

[51] Giustetto, R.; Wahyudi, O. *Micropor. Mesopor. Mat.* **2011**, *142*(1), 221 – 235.

[52] Pedone, A.; Bloino, J.; Barone, V. *J. Phys. Chem. C* **2012**, *116*(33), 17807–17818.

[53] Say-Liang-Fat, S.; Cornard, J. P. *Polyhedron* **2011**, *30*, 2326–2332.

[54] Grazia, C.; Clementi, C.; Miliani, C.; Romani, A. *Photochem. Photobiol. Sci.* **2011**, *10*, 1249–1254.

[55] Soubayrol, P.; Dana, G. *Magn. Reson. Chem.* **1996**, *34*, 638–645.

[56] Brewer, D. G.; Page, J. A. *Can. J. Chemistry* **1963**, *41*, 1695 –1702.

[57] Hohenberg, P.; Kohn, W. Nov **1964**, *136*(3B), B864–B871.

[58] Kohn, W.; Sham, L. J. Nov **1965**, *140*(4A), A1133–A1138.

[59] Scalmani, G.; Frish, M. J.; Menucci, B.; Tomasi, J.; Cammi, R.; Barone, V. *J. Phys. Chem.* **2006**, *124*, 094107.

[60] Yanai, T.; Tew, D. P.; Handy, N. C. *Chem. Phys. Lett.* **2004**, *393*(1-3), 51 – 57.

[61] Barone, V.; Bloino, J.; Biczysko, M. *Phys. Chem. Chem. Phys.* **2010**, *12*, 1092–1101.

[62] Puzzarini, C.; Biczysko, M.; Barone, V. *J. Chem. Theory Comput.* **2011**, *7*(11), 3702–3710.

[63] Jaquemin, D.; Perpète, E. A.; Scuseria, G. E.; Ciofini, I.; Adamo, C. *J. Chem. Theory Comput.* **2008**, *4*, 123–135.

[64] Jaquemin, D.; Brémond, E.; Planchat, A.; Ciofini, I.; Adamo, C. *J. Chem. Teory Comput.* **2011**, *7*(6), 1882–1892.

[65] Barone, V.; Biczysko, M.; Bloino, J.; Borkowska-Panek, M.; Carnimeo, I.; Panek, P. *Int. J. Quantum Chem.* **2012**, *112*, 2185–2200.

[66] Double and triple-ζ basis sets of n07 and sns families are available for download.

[67] Barone, V.; Cimino, P.; Stendardo, E. *J. Chem. Theory Comput.* **2008**, *4*, 751.

[68] Barone, V.; Cimino, P. *Chem. Phys. Lett.* **2008**, *454*, 139.

[69] Chai, J.-D.; Head-Gordon, M. *J. Chem. Phys.* **2008**, *128*, 084106/1–15.

[70] Chai, J.-D.; Head-Gordon, M. *Phys. Chem. Chem. Phys.* **2008**, *10*, 6615–6620.

[71] Zhao, Y.; Schults, N. E.; Truhlar, D. G. *J. Chem. Theory Comput.* **2006**, *2*, 364–382.

[72] Zhao, Y.; Truhlar, D. G. *Theor. Chim. Acta* **2008**, *120*, 215–241.

[73] Becke, D. *J. Chem. Phys.* **1993**, *98*, 5648–5652.

[74] Adamo, C.; Barone, V. *J. Chem. Phys.* **1999**, *110*, 6158–6170.

[75] Mangiatordi, G. F.; BrÃÂ©mond, E.; Adamo, C. *J. Chem. Theory Comput.* **2012**, *8*(9), 3082–3088.

[76] Douma, D. H.; M'Passi-Mabiala, B.; Gebauer, R. *J. Chem. Phys.* **2012**, *137*(15), 154314.

[77] Peach, M. J. G.; Helgaker, T.; Salek, P.; Keal, T. W.; Lutnaes, O. B.; Tozer, D. J.; Handy, N. C. *Phys. Chem. Chem. Phys.* **2006**, *8*, 558–562.

[78] Isegawa, M.; Peverati, R.; Truhlar, D. G. *J. Chem. Phys.* **2012**, *137*(24), 244104.

[79] Charaf-Eddin, A.; Planchat, A.; Mennucci, B.; Adamo, C.; Jacquemin, D. *J. Chem. Theory Comput.* **2013**, *9*(6), 2749–2760.

[80] Wouters, J.; Rosario-Chirinos, N. *J. Am. Inst. Conserv.* **1992**, *31*(2), 237–255.

[81] Le-Person, A.; Cornard, J. P.; Say-Liang-Fat, S. *Chem. Phys. Lett.* **2011**, *517*, 41–45.

[82] Serap, K.; Dilek, B. *Rev. Anal. Chem.* **2008**, *27*, 251–261.

[83] Barone, V.; Cossi, M. *J. Phys. Chem. A* **1998**, *102*(11), 1995–2001.

[84] Cossi, M.; Rega, N.; Scalmani, G.; Barone, V. *J. Comput. Chem.* **2003**, *24*(6), 669–681.

[85] Tomasi, J.; Mennucci, B.; Cammi, R. *Chem. Rev.* **2005**, *105*, 2999–3094.

[86] Cossi, M.; Barone, V. *J. Chem. Phys.* **2001**, *115*, 4708–4717.

[87] Cammi, R.; Corni, S.; Menucci, B.; Tomasi, J. *J. Chem. Phys.* **2005**, *122*, 104513.

[88] Corni, S.; Cammi, R.; Menucci, B.; Tomasi, J. *J. Chem. Phys.* **2005**, *123*, 134512.

[89] Improta, R.; Barone, V.; Scalmani, G.; Frisch, M. J. *J. Chem. Phys.* **2006**, *125*(5), 054103.

[90] Marenich, A. V.; Cramer, C. J.; Truhlar, D. G.; Guido, C. A.; Mennucci, B.; Scalmani, G.; Frisch, M. J. *Chem. Sci.* **2011**, *2*, 2143–2161.

[91] Duschinsky, F. *Acta Physicochimica URSS* **1937**, *7*, 551.

[92] Macak, P.; Luo, Y.; Ågren, H. *Chem. Phys. Lett.* **2000**, *330*, 447–456.

[93] Biczysko, M.; Bloino, J.; Santoro, F.; Barone, V. In *Computational Strategies for Spectroscopy. From Small molecules to nano-systems*; Barone, V., Ed.; John Wiley & Sons, Inc., 2011; pages 361–443.

[94] Jankowiak, H.-C.; Stuber, J. L.; Berger, R. December **2007**, *127*, 234101.

[95] Hazra, A.; Chang, H. H.; Nooijen, M. *J. Chem. Phys.* **2004**, *121*, 2125–2136.

[96] Hazra, A.; Nooijen, M. *Phys. Chem. Chem. Phys.* **2005**, *7*, 1759–1771.

[97] Bloino, J.; Biczysko, M.; Crescenzi, O.; Barone, V. June **2008**, *128*(24), 244105.

[98] Caricato, M.; Mennucci, B.; Scalmani, G.; Trucks, G. W.; Frisch, M. J. *J. Chem. Phys.* **2010**, *132*, 084102.

[99] Bloino, J.; Biczysko, M.; Barone, V. *J. Chem. Theory Comput.* **2012**, *8*(3), 1015–1036.

[100] Frisch, M. J.; Trucks, G. W.; Schlegel, H. B.; Scuseria, G. E.; Robb, M. A.; Cheeseman, J. R.; Scalmani, G.; Barone, V.; Mennucci, B.; Petersson, G. A.; Nakatsuji, H.; Caricato, M.; Li, X.; Hratchian, H. P.; Izmaylov, A. F.; Bloino, J.; Zheng, G.; Sonnenberg, J. L.; Hada, M.; Ehara, M.; Toyota, K.; Fukuda, R.; Hasegawa, J.; Ishida, M.; Nakajima, T.; Honda, Y.; Kitao, O.; Nakai, H.; Vreven, T.; Montgomery, J. A.; Jr.; Peralta, J. E.; Ogliaro, F.; Bearpark, M.; Heyd, J. J.; Brothers, E.; Kudin, K. N.; Staroverov, V. N.; Kobayashi, R.; Normand, J.; Raghavachari, K.; Rendell, A.; Burant, J. C.; Iyengar, S. S.; Tomasi, J.; Cossi, M.; Rega, N.; Millam, J. M.; Klene, M.; Knox, J. E.; Cross, J. B.; Bakken, V.; Adamo, C.; Jaramillo, J.;

Gomperts, R.; Stratmann, R. E.; Yazyev, O.; Austin, A. J.; Cammi, R.; Pomelli, C.; Ochterski, J. W.; Martin, R. L.; Morokuma, K.; Zakrzewski, V. G.; Voth, G. A.; Salvador, P.; Dannenberg, J. J.; Dapprich, S.; Daniels, A. D.; Farkas, Ö.; Foresman, J. B.; Ortiz, J. V.; Cioslowski, J.; Fox, D. J. *GAUSSIAN09 (Revision C.01)* **Gaussian, Inc., Wallingford, CT, 2009**.

[101] Abkowicz-Bienko, A.; Biczysko, M.; Latajka, Z. *Comput. Chem.* **2000**, *24*(3-4), 303 – 309.

[102] Grazia, C.; Clementi, C.; Miliani, C.; Romani, A. *Photochem. Photobiol. Sci.* **2011**, *10*, 1249–1254.

[103] Fain, V. Y.; Zaitsev, B. E.; Ryabov, M. A. *Koord. Khim.* **2003**, *29*(5), 395.

[104] Fain, V. Y.; Zaitsev, B. E.; Ryabov, M. A. *Koord. Khim.* **2004**, *30*(5), 385.

[105] André, E.; Lapouge, C.; Cornard, J. P. *J. Phys. Chem. A* **2008**, *112*, 9829–9834.

[106] Barone, V.; Biczysko, M.; Bloino, J.; Puzzarini, C. *Phys. Chem. Chem. Phys.* **2013**, *15*, 1358–1363.

[107] Biczysko, M.; Bloino, J.; Carnimeo, I.; Panek, P.; Barone, V. *J. Mol. Struct.* **2012**, *1009*, 74–82.

[108] Daniilia, S.; Bikiaris, D.; Burgio, L.; Gavala, P.; Clark, R.; Chryssoulakis, Y. OCT **2002**, *33*(10), 807–814.

[109] Bicchieri, M.; Ronconi, S.; Romano, F.; Pappalardo, L.; Corsi, M.; Cristoforetti, G.; Legnaioli, S.; Palleschi, V.; Salvetti, A.; Tognoni, E. *Spectrochimica Acta Part B: Atomic Spectroscopy* **2002**, *57*(7), 1235 – 1249.

[110] Pouli, P.; Selimis, A.; Georgiou, S.; Fotakis, C. *Acc. Chem. Res.* **2010**, *43*(6), 771–781.

[111] Marengo, E.; Liparota, M. C.; Robotti, E.; Bobba, M. *Vibrational Spectroscopy* **2006**, *40*(2), 225 – 234.

[112] Neugebauer, J.; Baerends, E. J.; Nooijen, M.; Autschbach, J. *J. Chem. Phys.* **2005**, *122*(23), 234305.

CHAPTER 5

IN SILICO DESIGNED NEW TIOPHENE-BASED MECHANOCROMICAL MATERIAL

In this chapter we present a virtual screening that was capable to aid the experimental investigation to select a derivative with the desired optimal spectral features in terms of aggregachromic features and characterized by the best spectral properties and luminescence response. The best candidate was finally syntesized and dispersed into a polyethylene matrix achieving an *in silico designed* mechanocromic material. Besides the applications of this novel type of materials, we want to underline here that the integration of computational and experimental techniques reported in the following of this chapter defines an efficient protocol that can be generally applied to make a selection among a similar molecular candidates, which constitute the essential responsive part of a supramolecular device.

5.1 Introduction

Recent progress in material engineering and in the design of nanohybrid compounds has been inspired in the past decades by the growing interest in the new soft *smart* materials which are endowed with specific optical properties that can be tuned and controlled by external stimuli such as light, heat, mechanical stress, etc (1; 2; 3; 4). This type of smart devices can be designed for many different applications, such as camouflage systems, anti-counterfeiting, attoreactor sensors and other important applications such as informational displays or white emitting vesicles. Such type of intelligent materials are based essentially on the assembly of different units each of them performing a specific function; for example a compound able to respond to a wide variety of stimuli can be inserted within polymeric matrices (either in interfacial regions or in more complex supramolecular architectures) in order to obtain platform characterized by an high tunability (5). Among this *mechanoresponsive* materials, thanks to the wide areas of possible applications, particular attention has been recently (6; 7) devoted to a class of compounds called *mechanoresponsive* whose color (in absorptions and/or fluorescence emission) changes upon the application of any type of mechanical stress. In this regards organic chromophores, usually characterized by an extended π-conjugated structure, shows large photoresponse in a spectral region that can be easily tuned from the visible to the near-infrared by an appropriate and selective molecular design. But it is important to take into account also the possibility of forming molecular aggregates that adds complexity to the problem but providing, at the same time, a wealth of exciting opportunities. In fact with respect to the isolated chromophores the corresponding molecular aggregates can display entirely new features and are also sensitive to the medium properties, leading to the development of new aggregachromic materials (6; 7; 8). In any case, the most important part (that is the responsive part) of a mechanochromic material is the organic chormophore that can be either chemically linked onto the polymeric support or blended to it. In the latter case, some general criteria must be satisfed by the dye (7): as the rigid rodlike shape or the presence of electron-withdrawing (EW) or electron-donating (ED) groups in the aromatic

core of the dye. The choice of the best candidate among a set of similar molecules, to use as chromphore in technological applications, may be rather difficult if based only on the chemical intuition, since an accurate prediction of the spectral features (including Stokes shift or line shapes) can become very cumbersome. In variance, the availability of reliable and predictive computational methods described in the first part of this Ph.D thesis, can be very beneficial, since the results of an in silico screening can effectively guide the synthetic work, with clear benefits in terms of cost and time. For instance, when dealing with mechanochromic materials, it is crucial to select those chromophoric units that posses some of the following characteristics: a well oriented transition dipole, a large Stokes shift (for high-emission efficiency), optical behaviour depending on the aggregation extent, and, in the particular case of anti-counterfeiting needs they must posses a strong absorption in the near-UV region and emission in the visible range (7).

From a practical point of view, once a basic molecular candidate possessing this required features has been spotted through experimental investigations, an in silico screening can proceed in order to predict the desiderd properties on a larger set of homologues that differ from the parent chromophore by a small number of substituents groups. Once one or more targets have been identified by calculation to posses the desired quality the experimental efforts can be concentrated only on them. Clearly such a conceptual procedure can be applied only if the computational predictions are reliable and appropriate approaches are therefore required allowing the direct simulation of the spectroscopic signals but retaining, at the same time, a reasonable computational cost. We have underlined in the introductory part of this thesis that this requests appears to be satisfied by the DFT-based methods granted the DFT functional is carefully chosen. The same advances has been discussed also for the simulation of the spectral features where now not only the vertical absorption and emission transition can be reliably obtained but also the whole spectral line-shapes can be simulated (9; 10).

5.1.1 The choice of the best compounds

Generally speaking, organic fluorophores featuring heteroaromatics as the main π-conjugated backbones usually display increased polarizability, stability and also thermal and chemical robustness required for the fabrication of plastic materials. In particular, thiophene-based π-conjugated molecules have recently attracted great interest owing to their remarkable electrical and optical features (11). Starting from this observations, synthetic effort was focused on the preparation of novel thienyl-substituited 1,4-bis(ethynyl)benzenes where donor and acceptor groups are localized on the two terminal thiophene part (See fig. 5.1). In fact this class of dyes is characterized by a rigid, rodlike, highly conjugated molecular structure highly functionalizable by the addition of different peripheral electron withdrawing (EW) or electron donating (ED) groups. Moreover, the high electron delocalization of such compounds, favoured by the presence of the central benzenic part and the two lateral thiophene groups, should in principle give rise to bright absorption/emission in the UV/Vis range, coupled to the strong sensitivity to the nature of the push/pull substituent. This fact is consistent with the hypotesis that different pairs of groups linked in the molecular skeleton could be able to sensitively shift the absorption and/or emission maximum wavelength (λ_{max}) toward a different spectral regions.

In the design protocol applied here the quantum mechanical methods are employed for the in silico screening of UV/Vis absorption and emission spectra characterizing a series of derivatives of the compound in fig. 5.1, based on the same aromatic backbone but bearing substituent groups of different electron donating and electron accepting capability. Once the most promising compound is selected, it is effectively synthesized and characterized by measuring its absorption and emission spectra in solution. Next, experimental spectra can be compared with the computed ones to assess the quality of the predictions. Eventually, the target chromophore is dispersed in linear low-density polyethylene (LLDPE) matrix, and optical properties of the resulting mechanochromic material are then investigated. In the following of this presentation we will mainly focus on the computational part of the work, a complete and more exhaustive description of the experimental procedures (i.e.

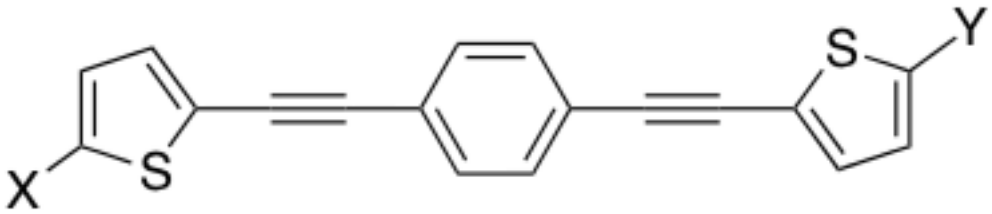

Figure 5.1: General structure of the thienyl-substituted 1,4-bis(ethynyl)benzenes, the donor and the acceptor groups are labelled as X and Y and are responsible for the shift of the absorption and emission wavelength, the capability of X/Y pairs in tuning optical properties of the chromophoric moiety is investigated through the computational screening in order to select the best one to be effectively synthesized in laboratory.

synthesis of dyes, dispersion into a polimeric dye etc) can be found in the corresponding publication (See Appendix).

5.2 Computational details

All the calculations were performed at the DFT level (12; 13) by exploiting the CAM-B3LYP functional (14) and the aug-N07D basis set (15; 16). This functional has already been shown to give overall good performance for a broad range of excited electronic states, moreover such a combination of functional and basis set has been chosen according to previous works in the field (17; 18; 19) assessing its accuracy at treating electronic excitation phenomena. Vertical excitation energies (VE) and excited state optimizations were calculated within the time-dependent (TD)-DFT formalism (20). To perform computations of vibrationally resolved one-photon absorption and one-photon emission electronic spectra, two different approaches, i.e. the Vertical Gradient (VG) and the Adiabatic Shift (AS) models, have been applied to simulate spectra. In all calculations the Franck-Condon

(FC) approximation (i.e. the assumption that the electric dipole remains constant during the transition) has been applied. This assumption is generally valid for fully allowed transitions, such as the ones considered in this work. The simulated stick spectra have been convoluted by means of Gaussian functions with half-width at half-maximum (HWHM) of 750 cm-1. This value has been chosen according to the broad features of reference experimental absorption spectra. The ground state frequencies and normal modes were obtained analytically, whereas excited state frequencies and normal modes were obtained by numerical differentiation of TDDFT gradients. Calculations in tetrahydrofuran (THF) solution were obtained by exploiting the C-PCM (Conductor-like Polarizable Continuum Model) (21; 22; 23) within the electronic nonequilibrium solvation regime in the linear response scheme (20; 24; 25; 26; 27; 28). The molecule-shaped cavity surrounding the solute molecule was made of interlocking spheres centered on heavy atoms: the default set of sphere radii implemented in the Gaussian 09 code was exploited. All QM calculations were performed using a locally modified version of the Gaussian 09 program (29).

5.3 Computational screening of push-pull substituents

As the effect on the general spectral features of the dye composed of selected combination push/pull substituents is not easily predictable based only on chemical intuition an extened virtual screening taking into account several possible candidates and their combinations into push-pull pairs has been set up. As it has been discussed in previous chapters, among the available computational protocols, the popular VE approach gives the most basic information on the optical properties of chromophores. In variance, for the simulation of electronic spectra line-shapes, the vibrationally resolved electronic spectra simulations with methods such as VG, AS, and AH are mandatory in order to correctly interpret the experimental findings, as demonstrated previously. Considering that spectra simulations are our ultimate goal, the study starts from the validation of the computational model employed in this work (i.e. choice of the best DFT functional/basis set, VG and AS approximation and solvation model) which has been performed on both phenyl-

and thiopene-based π-conjugated chromophores, by comparing the computed spectra with their experimental counterparts. It was found that both VG and AS models can be confidently applied to simulate broad spectral features.

5.3.1 First validation

A first validation of the proposed approach, has been focused on verifying its capability to describe spectrum of similar known chromophore in solution. This has been done by performing calculations on a p-diethinylbenzene derivative (labeled as M1, see Figure 5.2) in THF solution whose experimental absorption spectrum had previously been reported in the literature. Such a compound was chosen due to the para-ethynylphenyl group, which constitutes part of the central skeleton of the screened systems, and in particular as it contains the π-delocalized unit which should be the key player at determining the absorption/emission properties of the analogues studied in this work. In fig. 5.2, the experimental (30) and computed spectra of M1 are compared, for the latter exploiting the different methodologies (i.e. VE, VG and AS approaches, with or without the account of solvent effects). In general, the account for solvation effects in the calculations improves the agreement between calculations and experiments. The difference between calculated and experimental absorption maxima (λ) is notably decreased moving from vacuo to THF solution for the VE method (λ_{vac} = 26 nm and λ_{thf}= 11 nm), while both the position of the absorption maxima and spectra line shape are improved for VG one. For such a reason, here and in the following analysis, solvent effects will always been introduced in the computational model. More in detail, both the VE, VG and AS approaches give a very good prediction of the experimental absorption spectrum as far as the spectral range is concerned, although, as expected, the VG/AS methods definitely overcome the VE due to the inclusion of the vibronic effects. Additionally again both VG and AS approaches lead to very similar results, so can be considered essentially equivalent for the purpose of current study. On the whole, results for p-diethinylbenzene give a first assessment of the adequacy of the chosen computational model (DFT functional/basis set, VG/AS and

solvation model)

In order to confirm the transferability of the adopted computational models to the class of target molecules considered in the present work, prior to the analysis of simulated VG and AS spectra, all different theoretical models (including also AH) were also validated for the lowest electronic transition of a reference compound. This has been identified in the simplest homologue of the series, 1,4-bis(thiophen-2-ylethynyl)benzene (named 1j and presented in fig 5.3). As far as adiabatic approaches are concerned, the spectra simulated within AS and AH models are presented in Figure 5.4, allowing us to discuss the possible influence of frequency changes and normal mode rotation between initial and final states. Both spectra show very similar line-shapes, but slightly shifted positions, namely about 10 nm for both absorption and emission. More important, the abovementioned shift has the same sign for absorption and emission (being in both cases the AS maximum wavelength lower than the one computed with the AH approximation), so that the predicted Stokes shift remains almost unaltered. These results suggest that the Duschinsky effects do not play significant role and in this case can be safely neglected by adopting the less expensive AS approximation. Next, before comparing the vertical and adiabatic models, it should be noted that the difference between VG and AS is solely related to the approximation used to estimate the shift along the normal modes of the two involved electronic states: while in adiabatic methods the true shift is computed, an *effective* shift is used in the vertical approach. When the harmonic approximation is exact, the vertical and adiabatic approaches are equivalent, and in the present case the good agreement between VG and AS spectra confirms the reliability of such an approach. It may be worth noticing that the difference between AH and VG is again related mainly to frequency changes. These lead to the shift of the 0-0 transition (in analogy to the AS model) and to slightly different relative positions of vibronic absorption maxima. However, both spectra show very similar overall line-shapes

On these grounds, application of both VG and AS models to simulate broad spectral features of chromophores considered in this work is fully validated. Finally, in Figure 5.4 are also reported the absorption/emission peaks resulting from the application of the

	Absorption (λ_{nm}^{max})				Emission (λ_{nm}^{max})			
	VE	VG	AS	Exp	VE	VG	AS	Exp
1a	354	350	350	348	427	392	395	403
1b	376	374	373	368	462	420	424	bb[a]
1c	359	362	364	352	433	395	398	bb[b]
1d	377	374	373	372	463	430	435	468
1e	353	350	349	348	426	392	395	395

[a]Broad band (bb) from 420 to 570nm.

[b]Broad band from 395 to 460nm.

Table 5.1: Computed and experimental maximum absorption and emission wavelengths (λ^{max}) of compounds 1b-e.

low level vertical excitation (VE) model. It appears that, besides the loss of information concerning the band shape, the maximum absorption wavelength is well reproduced with respect to higher-level techniques, whereas a larger error is found for the emission. Moreover, since absorption and emission VE errors have opposite sign, an overestimation of the Stokes shift is to be expected in this case. A final validation of the reliability of the computational protocol in the specific context of the thiophene-based chromophores was performed for compounds **1a-e** (fig. 5.5) when the measured absorption and emission spectra in THF where compared to their VE, VG and AS counterparts with respect to the transition energies (table 5.1) and whole spectra (figure 5.5) simulated in the same solvent emploing the C-PCM model.

From the table 5.1 we can see that the VE approach is able to reproduce the absorption maxima well and with an average error between calculated and experimental values of about 6 nm. Even more important is the fact that the calculations are able to correcly reproduce the experimental trend found for the class of chromophores moving from one to the other (i.e. **1a**, **1e**, **1c**, **1b**, **1d**). In addition the MO plots shows that in all cases the most intense transition is due to an HOMO-LUMO excitation involving the frontier

orbitals all of π character, so that the transition of interest (i.e. the visible one) can be classified as $\pi \rightarrow \pi^*$.

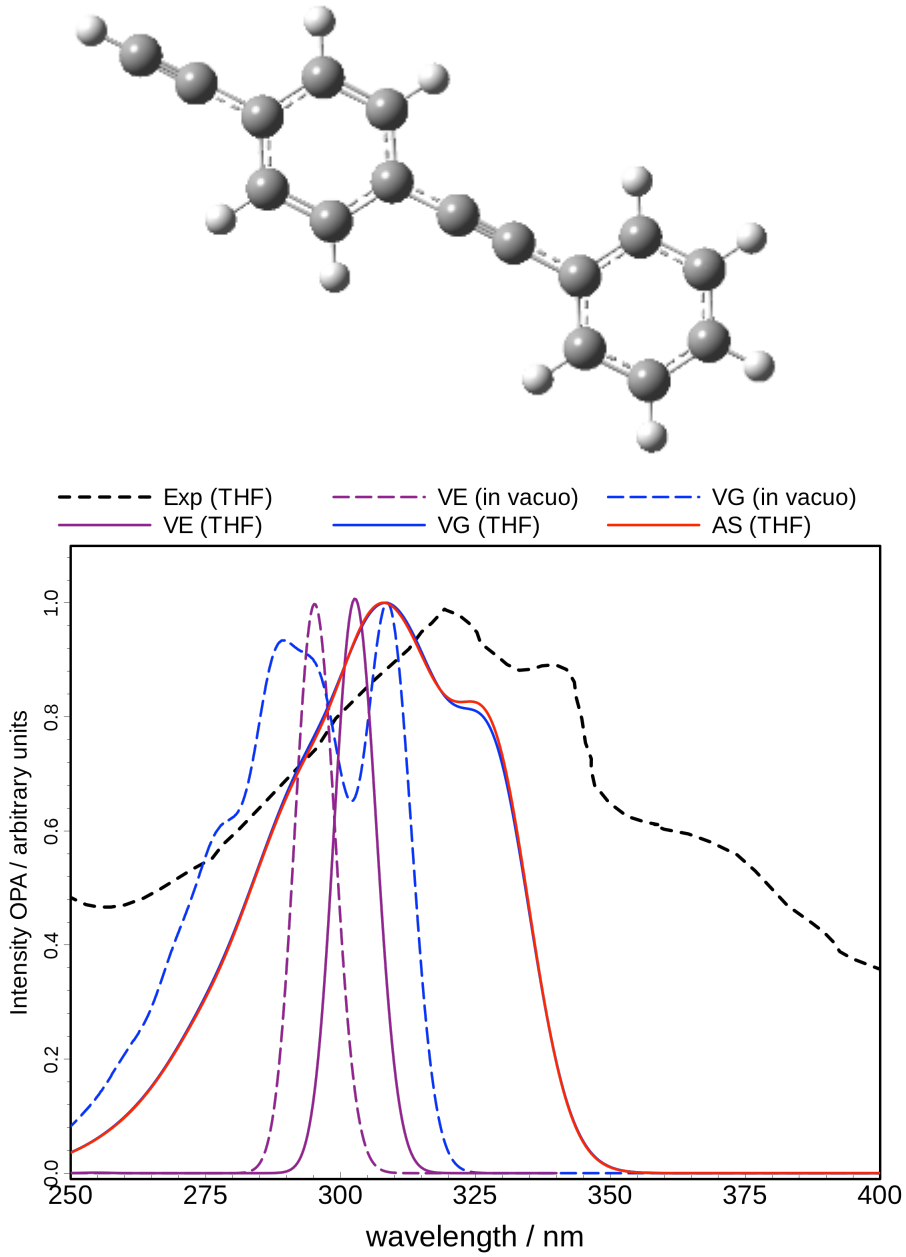

Figure 5.2: Absorption spectra computed for the M1 molecule (see upper panel). Experimental spectrum is reported with a black dashed line for comparison (30). All theoretical spectra both in vacuo (dashed lines) and in THF solution (solid lines) were obtained by exploiting the VE (purple lines), VG (blue lines) and AS (red line) approaches, convoluted with a Gaussian function with 750 cm^{-1} HWHM.

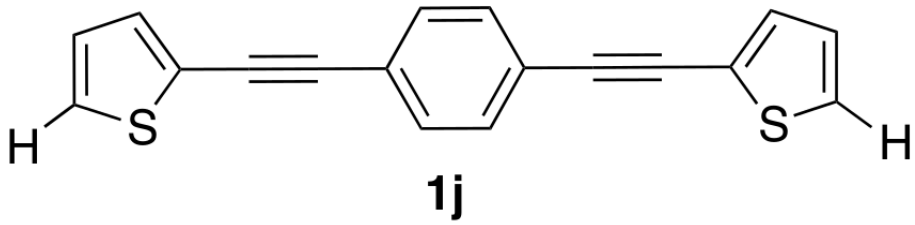

1j

Figure 5.3

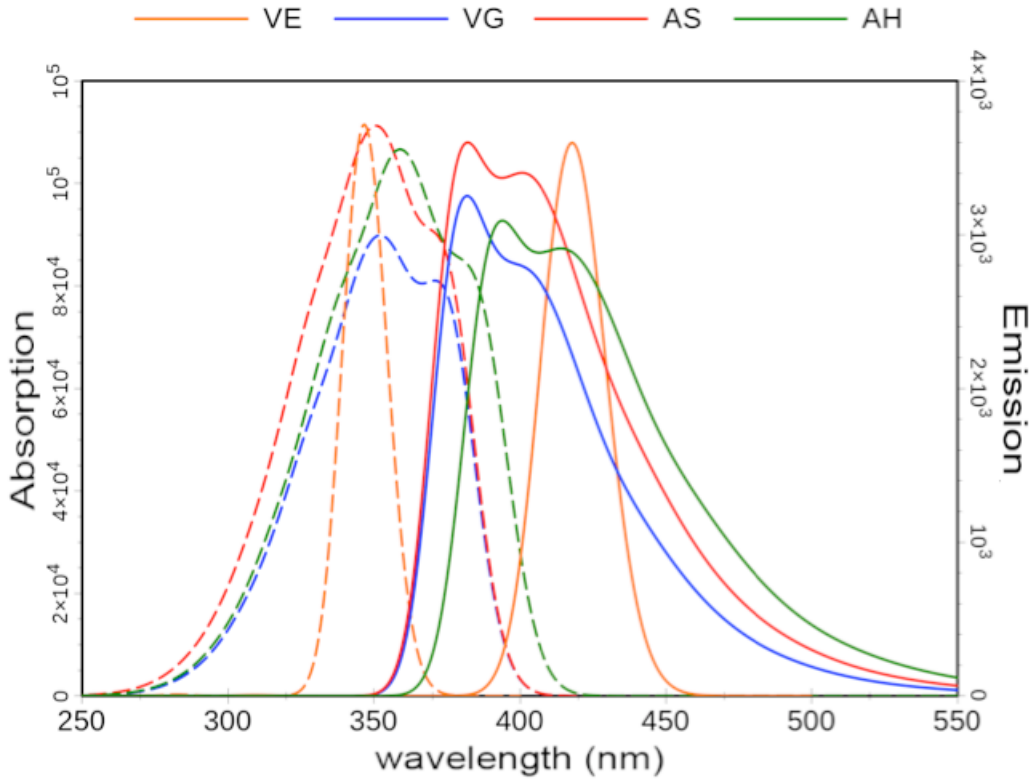

Figure 5.4: Absorption (dashed lines) and emission (solid lines) spectra, computed on reference compound 1j using different theoretical models: Vertical Energy (VE, orange lines), Vertical Gradient (VG, blue lines), Adiabatic shift (AS, red lines) and Adiabatic Hessian (AH, green lines). All spectra are convoluted with a Gaussian function of 750 cm^{-1} of half width at half maximum (HWHM). Absorption intensity: molar absorption coefficient in $dm^3mol^{-1}cm^{-1}$, emission intensity in μJ $mol^{-1}s^{-1}$.

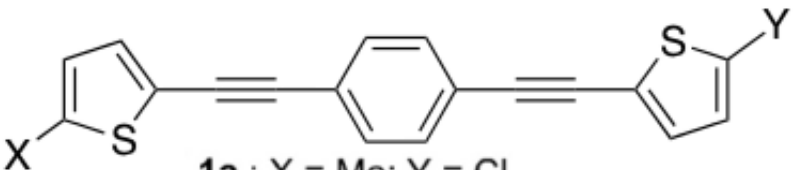

1a : X = Me; Y = Cl
1b : X = COMe; Y = OMe
1c : X = Me; Y = OMe
1d : X = MeO; Y = CHO
1e : X = Me; Y = Me

Figure 5.5

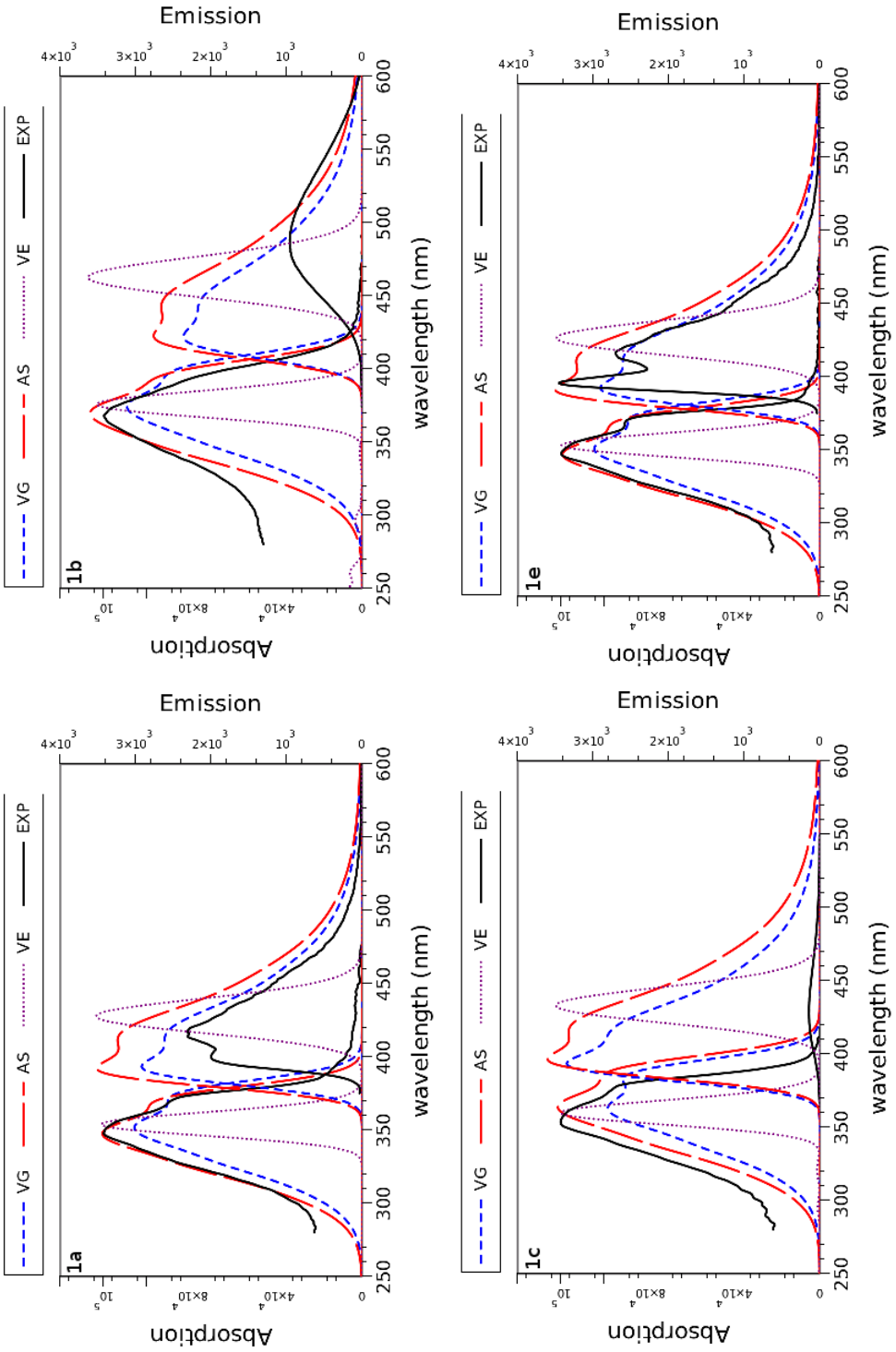

Figure 5.6: Computed and experimental spectra are shown for compound 1a, 1b, 1c and 1e. Experimental spectra are reported with a black solid line. Dashed, solid, and dotted lines are employed for spectra computed in the VE (purple), VG (blue) and AS (red) approximation respectively. For absorption intensity the molar absorption coefficient is expressed in $dm^3 mol^{-1}$ cm^{-1} whereas emission intensity are expressed in μJ mol^{-1} s^{-1}.

Moving to emission, as already found in the preliminary tests the VE approach gives less accurate results and is therefore less effective to make realiable predictions on fluorescence. For instance in compounds **1a** and **1e** a larger average error between experimental results and calculations is obtained, particularly around 20nm. Furthermore, the absence in the VE approach of any reliable treatment of the line-shape makes the comparison and the assignment of the experimental and calculated absorption maxima very difficult. This fact is most evident for the emission band of the compunds **1b** and **1c** in which the broad shape of the experimental band makes a precise assignment of the maximum emission wavelength rather questionable and difficult to explain. For such reasons, a simple check on vertical excitation energies has been followed by more refined calculation with VG and AS approaches. Absorption and emission spectra computed with different approaches are compared to their experimental counterpart in fig. 5.6 for compounds **1a**, **1b**, **1c** and **1e** and similar results are obtained for the other homologue. Inspection of fig. 5.6 confirms the ability of both VG and AS approaches to give a maximum absorption wavelength in excellent agreement with the experimental results also describing, at the same time, very accurately the experimental line-shapes. More important is the fact that the improvement with respect to the simpler VE method is most evident for emission than for absorption. In fact, the increase in accuracy of the vibronic approaches is more visible for **1a** and **1e** chromophores, for which the separation between the two most intense peaks is now evident and very well reproduced, and the accuracy of the predicted maximum wavelength is increased, with respect to VE computed values by roughly a factor of 2. It is important to see that the emission bands obtained experimentally for the compounds **1b** and **1c** are rather broad and do not present a clear pattern and vibronic structure. This fact renders the comparison between experimental and simulated counterparts very difficult. Broadly speaking, as far as **1b** and **1c** are concerned VG and AS (but also the VE) spectra falls within the wide spectral region (395-460nm) of the experimental emission. Another very important fact is that the emission maxima obtained with VG and AS approaches are also in agreement with the trend found experimentally in luminescence, that is the order found is **1e** < **1c** < **1a** < **1b** < **1d**. This important result suggest that

the virtual screening of the absorption properties of this class of novel chromophores can be performed at the VE level. It can be concluded that although the computational cost of the vibronic VG/AS fluorescence spectra is certainly balanced by the gain in accuracy and reliability, the large number of molecular targets to be investigated suggest that we should perform an initial preliminary screening at the VE level also with respect to the emission calculations. Thereafter, a restricted set of homologues will be selected based on the VE results and considered for further more accurate calculation with the higher level AS approach. Finally, from practical point of view the target compound will be effectively synthesized and will be thus chosen within this second restricted set.

5.4 Performing virtual screening

In addition to some substituents already considered in the previous set **1a-1e** as the CHO group, several new chromophores homologues of **1**, characterized by a strong electron withdrawing 2-methylenemalonic unit, were included in the new screening set. As a matter of fact, this latter type of substituent should be characterized by both a large Stokes shift, generally associated with highly luminescent dyes, and an increased capability to aggregate, owing to the augmented polarity and the pronounced rodlike shape (31; 32). The presence of different push and pull substituents may also drive the transition dipole moment along the molecular axis, thus conferring to the molecule some anisotropic potentialities (33). Our VE screening is summarized in table 5.2, and for each homologue of the target set, the position of the absorption and emission peaks and the computed Stokes shifts are reported.

It appears that different pairs of X and Y substituents highly influence the resulting absorption and emission positions. The homologue characterized by X = Y = H (labeled **1j**) is reported in the first row and can be taken as a reference to evaluate the direction of the computed shifts, In this respect, all X/Y pairs shift toward larger values, that is, lower energy regions of the spectrum, both in absorption and in emission. In the former case, as far as pull substituents are concerned, the maximum shift (around 90 nm with respect

X	Y	Absorption (nm)	Emission (nm)	Stokes Shift (nm)
H	H	347	418	71
	CHO	377	463	86
	CH=($C_9H_4O_2$)	434	534	100
OH	CH=$C(CN)_2$	426	527	101
	CH=C(CN)(COOH)	418	520	102
	COOH	370	454	84
	CHO	370	461	91
	CH=($C_9H_4O_2$)	433	529	96
SH	CH=$C(CN)_2$	419	520	101
	CH=C(CN)(COOH)	412	516	104
	COOH	364	454	90
	CHO	388	491	103
	CH=($C_9H_4O_2$)	442	562	120
NH_2	CH=$C(CN)_2$	436	567	131
	CH=C(CN)(COOH)	428	558	130
	COOH	382	479	97

Table 5.2: VE screening results: predicted maximum absorption/emission wavelenghts and Stokes shifts.

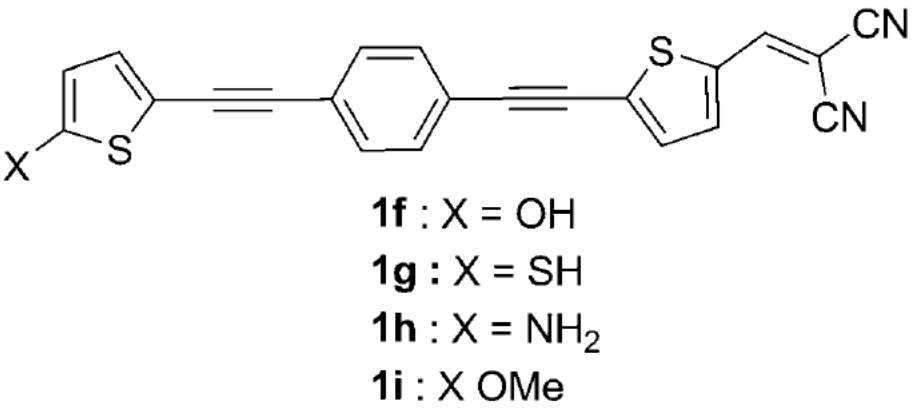

Figure 5.7

to the 1j compound) is observed for Y = (CH=($C_9H_4O_2$)), whereas the minimum one of about 30 nm is registered when aldehydic or carboxylic groups are employed. Also the red-shifts due to the X push substituents appears for a fixed Y, rather regular with the order NH_2>OH≈SH. The predicted red-shift in emission with respect to **1j** is even more marked, being as large as 100 nm. In other words the substitution of hydrogen atoms whit other groups systematically increases the Stokes shift. It may be worth noting that, at variance with the absorption, no regular trend can be spotted on Y substitution for a given X group. For instance, the red-shift caused by the CH=($C_9H_4O_2$) and CH=$C(CN)_2$ Y substituents is 111 and 102 nm, respectively, when combined with X = SH and 144 and 149 nm, respectively, when combined with X = NH_2. Generally speaking, this results indicate the absence of a clear trend and rule out the possibility of a simple rationalization of the results based only on push/pull effects, thereby highlighting the important role that an *in silico* screening can play toward improved rational molecular design.

5.4.1 Restricted screening

Based on the former VE screening, a new restricted set was selected by considering that the largest Stokes shift is registered for chromophores substituited with Y = CH=$C(CN)_2$. Absorption and emission spectra have been therefore simulated at the AS level for this

pull groups in combination with all three considered push ones, giving rise to target compounds **1f**, **1g** and **1h** with X = OH, SH and NH_2 respectively (see fig. 5.7). The AS computed spectra, presented in figure 5.8, clearly show that the final target cannot be identified among the considered homologues solely based only the VE results. In fact, despite the fact that **1h** seems to be the most promising one (Table 5.1) owing to the largest Stokes shift computed at the VE level and the similar transition intensity found for all the compounds, the absorption and emission spectra reported in figure 5.8 shows that althought **1h** exhibits the largest spectral window between absorption and emission maxima, at the same time much lower absorption and, even more important for our study, emission intensity are to be expected.

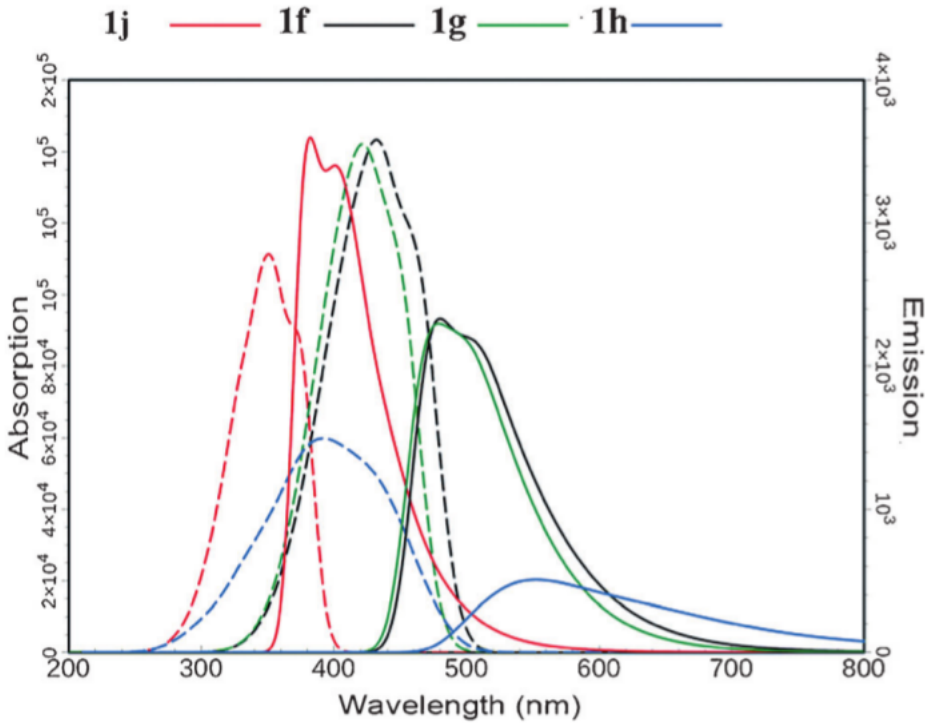

Figure 5.8: Absorption (dashed line) and emission (solid lines) spectra of the restricted screening set 1fâ1h, reported along with the reference compound 1j. All spectra have been simulated within the AS approach and convoluted with a 750 cm^{-1} half width at half-maximum (HWHM) Gaussian function.

For such reason the **1f** and **1g** chromophores, showing large Stokes shift and at the same time good absorption and emission features, are particularly suitable for the applicative purpose explained in the start of this section. Between the latter two systems **1g** where X = SH may show some disadvantages related to the significant change of the steric position of the SH group upon the electronic excitation. Therefore, the **1f** could be suggested as the best candidate for further development. However because we had to take into account the necessity of modulating the interaction between the dye molecule and its miscibility within the polimeric matrix, compound **1i**, where the hydroxyl push substituent is replaced by a methoxy group was finally chosen as the target chromophore to be effectively prepared in the laboratory. Absorption and emission band were then re-computed according to this final susbstitution: the resulting spectra are then reported in fig 5.9 together with the ones obtained for homologue **1f**. It is worth mentioning that in this case, both absorption and emission spectra were computed at the AS level to enforce the prediction and improve the comparison with the experimental band.

After the synthesis and the experimental characterization of compound **1i** the resulting band maxima were found at 422 nm in absorption and at 512 nm in emission. The agreement between the theoretical prediction and the experiment is very good, both for position of the absorption and emission bands as well as for their intensities. Moreover, the use of the AS method allowed us to predict a line shape, which is also in good agreement with the measured experimental spectra. Finally, in line with the validation results, the overall reproduction of the absorption spectrum is better than the one found for emission, which results in a slightly underestimated Stokes shift. However, all in all, the computed screening indicated a target molecule with the desired characteristics.

Figure 5.10 illustrate the behaviour found in emission of a LLDPE film containing 0.02 and 0.1 wt% of **1i** compound, in our case the film passes after drawing from the OFF state to ON state, such that occurring in light switches. The selected dye when dispersed into linear low-density polyethylene showed emission features depending on the dye-aggregation extent, that is, a remarkable quenching of luminescence occurs at the highest concentration. Once a mechanical stress was applied, the dye promptly restored

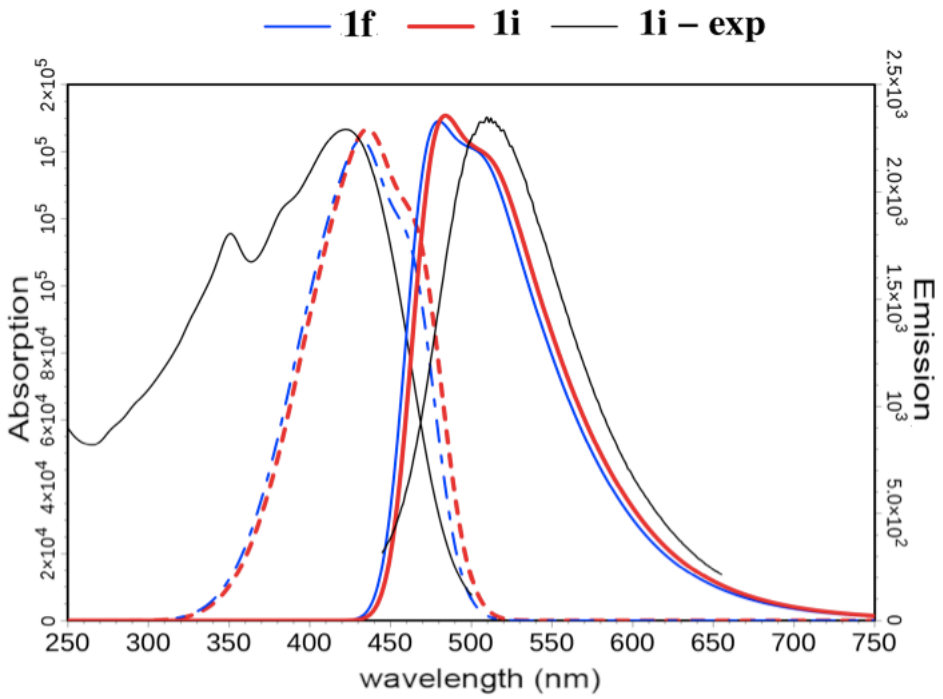

Figure 5.9: Experimental (black solid lines) and computed (dashed and solid lines for absorption and emission, respectively) spectra of the final target compound 1i . Computed spectra for 1f are reported for comparison. All spectra simulated within the AS approach and convoluted with a Gaussian function of 750 cm^{-1} HWHM.

its bright green emission thanks to the rupture of its supramolecular structure provided by the polimer-matrix orientation displaying distinct mechanochromic behaviour.

5.5 Conclusions

Finally it can be underlined that the results presented in this chapter clear demonstrate the agreement between the computational screening and the experimental results along with the predictive advantages of the computational chemistry. The selection of the best candidate for the preparation of mechanochromic devices was indeed a fundamental issue, especially in the presence of a rather large set of possible chromophores. The present study also demonstrates, from a computational point of view, that experimental effects

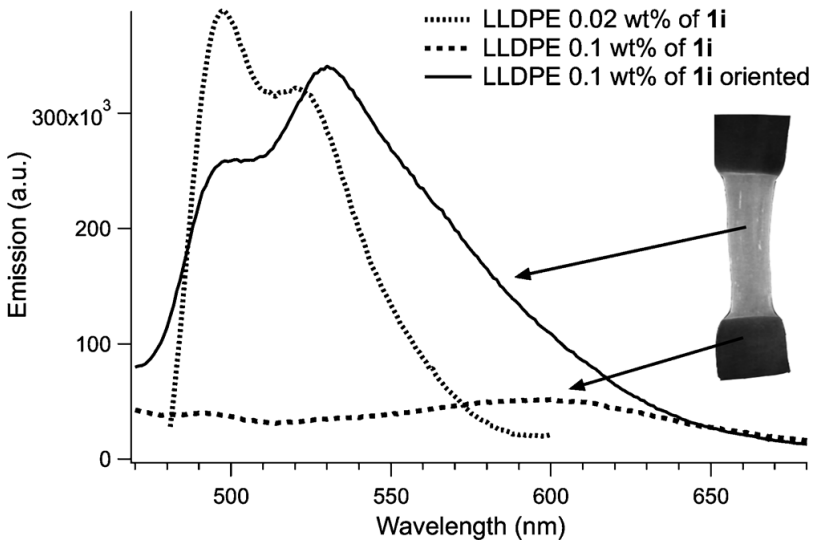

Figure 5.10: Emission of a LLDPE film containing 0.02 and 0.1 wt% 1i before and after orientation. Inset: digital image of the oriented film under irradiation at 366 nm

(e.g. solvation, and vibronic effects) are well reproduced by our simulations, which underlies the ability of such an approach to dissect the role of several, concomitant effects in tuning optical properties. The effective combination on the experimental design and the parallel computational screening allowed the selection of the best molecular chromophore in terms of highly anisotropic features, aggregachromic properties and bright luminescence. Thereafter, a smart material was created by assembling the chromophoric unit within a polimeric matrix. A further step forward that can be realized regarding the computational screening could be to take into account, at reliable level of accuracy, the interactions of the polimeric matrix with the chromophore, thus extending the predictions to the whole mechanochromic material.

Bibliography

[1] Zhang, X.; Rehm, S.; Safont-Sempere, M. M.; W´ourthner, F. *Nat. Chem.* **2009**, *1*, 623–629.

[2] Sagara, Y.; Kato, T. *Nat. Chem.* **2009**, *1*, 605–610.

[3] Sagara, Y.; Kato, T. *Angew. Chem.* **2011**, *123*, 9294–9298.

[4] Anzenbacher, P.; Li, F.; Palacios, M. A. *Angew. Chem.* **2012**, *124*, 2395.

[5] Bredas, J. L.; Marder, S. R.; Reichmanis, E. *Chem. Mater.* **2011**, *23*, 309–309.

[6] Pucci, A.; Bizzarri, R.; Ruggeri, G. *Soft. Mater.* **2011**, *7*, 3689–3700.

[7] Pucci, A.; Ruggeri, G. *J, Mater. Chem.* **2011**, *21*, 8282–8291.

[8] Weder, C. *J. Mater. Chem.* **2011**, *21*, 8235–8236.

[9] Barone, V.; Bloino, J.; Biczysko, M.; Santoro, F. *J. Chem. Theory Comput.* **2009**, *5*, 540–554.

[10] Bloino, J.; Biczysko, M.; Santoro, F.; Barone, V. *J. Chem. Theory Comput.* **2010**, *6*, 1256–1274.

[11] Usui, M.; Fukumoto, H.; Yamamoto, T. *Bull. Chem. Soc. Jpn.* **2010**, *83*, 1397.

[12] Hohenberg, P.; Kohn, W. Nov **1964**, *136*(3B), B864–B871.

[13] Kohn, W.; Sham, L. J. Nov **1965**, *140*(4A), A1133–A1138.

[14] Yanai, T.; Tew, D. P.; Handy, N. C. *Chem. Phys. Lett.* **2004**, *393*(1-3), 51 – 57.

[15] Barone, V.; Biczysko, M.; Bloino, J.; Borkowska-Panek, M.; Carnimeo, I.; Panek, P. *Int. J. Quantum Chem.* **2011**, page DOI:10.1002/qua.23224.

[16] Double and triple-ζ basis sets of n07 family, are available for download.

[17] Bloino, J.; Biczysko, M.; Santoro, F.; Barone, V. April **2010**, *6*(4), 1256–1274.

[18] Barone, V.; Bloino, J.; Biczysko, M. *Phys. Chem. Chem. Phys.* **2010**, *12*, 1092–1101.

[19] Jacquemin, D.; Bremond, E.; Planchat, A.; Ciofini, I.; Adamo, C. *J. Chem. Teory Comput.* **2011**, *7*(6), 1882–1892.

[20] Scalmani, G.; Frish, M. J.; Menucci, B.; Tomasi, J.; Cammi, R.; Barone, V. *J. Phys. Chem.* **2006**, *124*, 094107.

[21] Barone, V.; Cossi, M. *J. Phys. Chem. A* **1998**, *102*(11), 1995–2001.

[22] Cossi, M.; Rega, N.; Scalmani, G.; Barone, V. *J. Comput. Chem.* **2003**, *24*(6), 669–681.

[23] Tomasi, J.; Mennucci, B.; Cammi, R. *Chem. Rev.* **2005**, *105*, 2999–3094.

[24] Cossi, M.; Barone, V. *J. Chem. Phys.* **2001**, *115*, 4708–4717.

[25] Cammi, R.; Corni, S.; Menucci, B.; Tomasi, J. *J. Chem. Phys.* **2005**, *122*, 104513.

[26] Corni, S.; Cammi, R.; Menucci, B.; Tomasi, J. *J. Chem. Phys.* **2005**, *123*, 134512.

[27] Improta, R.; Barone, V.; Scalmani, G.; Frisch, M. J. *J. Chem. Phys.* **2006**, *125*(5), 054103.

[28] Marenich, A. V.; Cramer, C. J.; Trulhar, D. G.; Guido, C. A.; Mennucci, B.; Scalmani, G.; Frisch, M. *J. Chem. Sci.* **2011**, *2*, 2143–2161.

[29] Frisch, M. J.; Trucks, G. W.; Schlegel, H. B.; Scuseria, G. E.; Robb, M. A.; Cheeseman, J. R.; Scalmani, G.; Barone, V.; Mennucci, B.; Petersson, G. A.; Nakatsuji, H.; Caricato, M.; Li, X.; Hratchian, H. P.; Izmaylov, A. F.; Bloino, J.; Zheng, G.; Sonnenberg, J. L.; Hada, M.; Ehara, M.; Toyota, K.; Fukuda, R.; Hasegawa, J.; Ishida, M.; Nakajima, T.; Honda, Y.; Kitao, O.; Nakai, H.; Vreven, T.; Montgomery, J. A.; Jr.; Peralta, J. E.; Ogliaro, F.; Bearpark, M.; Heyd, J. J.; Brothers, E.; Kudin, K. N.; Staroverov, V. N.; Kobayashi, R.; Normand, J.; Raghavachari, K.; Rendell, A.;

Burant, J. C.; Iyengar, S. S.; Tomasi, J.; Cossi, M.; Rega, N.; Millam, J. M.; Klene, M.; Knox, J. E.; Cross, J. B.; Bakken, V.; Adamo, C.; Jaramillo, J.; Gomperts, R.; Stratmann, R. E.; Yazyev, O.; Austin, A. J.; Cammi, R.; Pomelli, C.; Ochterski, J. W.; Martin, R. L.; Morokuma, K.; Zakrzewski, V. G.; Voth, G. A.; Salvador, P.; Dannenberg, J. J.; Dapprich, S.; Daniels, A. D.; Farkas, Ö.; Foresman, J. B.; Ortiz, J. V.; Cioslowski, J.; Fox, D. J. *GAUSSIAN09 (Revision C.01)* **Gaussian, Inc., Wallingford, CT, 2009**.

[30] X., Z.; M., Y.; G., X.; X., L.; P., Y. *Macromol. Rapid Commun.* **2001**, *22*, 358–362.

[31] Tirelli, N.; Amabile, S.; Cellai, C.; Pucci, A.; Regoli, L.; anf F. Ciardelli, G. R. *Macromolecules* **2001**, *34*, 2129–2137.

[32] Pucci, A.; Tirelli, N.; Ruggeri, G.; Ciardelli, F. *Macromol. Chem. Phys.* **2005**, *206*, 102.

[33] Pucci, A.; Cappelli, C.; Bronco, S.; Ruggeri, G. *J. Phys. Chem. B* **2006**, *110*, 3127–3134.

Part III

Conclusions and perspectives

CHAPTER 6

CONCLUSIONS AND PERSPECTIVES

In this Ph.D thesis we have discussed and presented how computational chemistry, in particular computational spectroscopy, can stand as a well suited tool for interpreting and predicting experimental outcomes. In the first chapter we have discussed the computational chemistry models available nowadays to the chemical community, focusing on the DFT-based methods which are well suited for the studies of the medium-to-large systems such as the ones studied here. In the second chapter we have briefly presented the computational methodologies employed to carry out calculations, focusing on the theory underlying the computations of the vibrationally resolved electronic spectra, the key point of this thesis. In the next chapters, presented methodologies have been applied to study optical properties for chromophores of biological, technological and cultural heritage interest. In the 3^{rd} chapter the problems related to the proper choice of the DFT functional are discussed in more detail, and computational benchmarks of different ones are presented along with methodological aspects and examples on spectra computations for some coumarin derivatives; the aim of this chapter was to select the best performing functional to be employed (after further restricted validation) in the following chapters 4 and 5. In the 4^{th} chapter a computational study on the environmental and coordination

effects on the electronic spectra of organic pigments; that is a computational study on Alizarin and Alizarin-Mg/Al complexes is presented. In particular, it has been possible to describe electronic and structural characteristics of free alizarin in different environmental (pH) conditions, showing that observed changes of the spectra line-shapes are well reproduced by simulations. Then such studies are extended to Mg/Al-coordinated alizarin, taking into account solvation, and coordination effects, which all influence the final perceived colour. In the 5^{th} chapter we have presented a general procedure for a selection of the best candidate among a rather large set of homologues via the *computational screening*, that is, calculating their optical properties in order to select the best one with the final desired characteristics. The application of such a computational scheme resulted to be very beneficial since the selection of the best target can be very difficult if the prediction were based only on the chemical intuition. Our computational protocol has facilitated design and synthesis of a mechanocromic material with the final desired properties. The theoretical models and examples presented in this Ph.D. thesis point out the reliability and applicability of current state-of-the art computational protocols in both interpreting and in predicting the optical properties of medium-to-large systems. Nowadays the number of realistic applications aided by advanced computations is growing very fast and studies presented here can be seen as examples how *in silico* support can be very beneficial for studies of molecular systems of direct technological interest.

APPENDIX

List of pubblications related to this thesis

- *Luciano Carta, Malgorzata Biczysko, Julien Bloino, Daniele Licari, Vincenzo Barone*
  Environmental and complexation effects on the structures and spectroscopic signatures of organic pigments relevant to cultural heritage: the case of alizarin and alizarin Mg(II) Al (III) complexes
  Physical Chemistry Chemical Physics, Volume 16, pages 2897-2911 - (2 December 2013)

- *Dr. Giacomo Prampolini, Prof. Fabio Bellina, Dr. Malgorzata Biczysko, Dr. Chiara Cappelli, Luciano Carta, Dr. Marco Lessi, Dr. Andrea Pucci, Prof. Giacomo Ruggeri, Prof. Vincenzo Barone*
  Computational Design, Synthesis, and Mechanochromic Properties of New Thiophene-Based π-Conjugated Chromophores
  Chemistry - A European Journal, Volume 19, Issue 6, pages 1996-2004 - (4 February 2013)

LIST OF TABLES

Acknowledgments

Official Acknowledgments:

The autor want to acknowledges all people that has partecipated to the realization of all the works here presented. First of all the supervisor Prof. Vincenzo Barone, then Dr. Malgorzata Biczysko for the help to write this thesis, Prof. Fabio Bellina, Dr. Andrea Pucci, Dr. Marco Lessi e al Prof. Giacomo Ruggeri for the realization of the experimental part of the work presented in chapter 5. Dr. Giacomo Prampolini and Dr. Chiara Cappelli for the help in the planning of the computational part of the POLOPTEL project (chapter 5). All the other persons that helps me in the realization of all the works and to the writing of this final thesis are acknowledged.

Ringraziamenti ufficiali:

L'autore vuole ringraziare in generale tutti coloro che hanno contribuito direttamente ed indirettamente alla realizzazione di questo lunghissimo elaborato. In primo luogo al supervisore Prof. Vincenzo Barone, alla Dr. Malgorzata Biczysko per aver continuamente riletto il testo della tesi ed avermi consigliato di apportare di volta in volta le correzioni. Al Prof. Fabio Bellina, al Dr. Andrea Pucci, Dr. Marco Lessi e al Prof. Giacomo Ruggeri va un ringraziamento per la realizzazione della parte sperimentale dei lavori presentati nel Capitolo 5. Un particolare ringraziamento va anche al Dr. Giacomo Prampolini e alla Dr.ssa Chiara Cappelli per avermi aiutato alla stesura del piano di lavoro per il progetto POLOPTEL del Capitolo 5. Inoltre desidera ringraziare tutti coloro che hanno partecipato, direttamente o indirettamente, alla stesura di questa tesi finale.

Finished to write at January 22, 2014